TRIBOLOGICAL STUDIES OF SURFACE TEXTURING FOR APPLICATION IN AIR-CONDITIONING AND REFRIGERATION COMPRESSORS

BY

SURYA PRATAP MISHRA

THESIS

Submitted in partial fulfillment of the requirements
for the degree of Master of Science in Mechanical Engineering
in the Graduate College of the
University of Illinois at Urbana-Champaign, 2011

Urbana, Illinois

Adviser:

Professor Andreas A. Polycarpou

ABSTRACT

Operating conditions such as load and speed of compressors are getting more aggressive to improve efficiency. Also, protection from beneficial surface layers, such as ferrous chlorides, on the critical interfaces is compromised as the refrigerants industry is moving from traditional (CFC/HFC) to environmentally friendly refrigerants. Thus, there is a need to have a closer look at the critical tribo-contacts and devise ways to make them more robust and wear-resistant.

In this work, first of its kind studies were done to evaluate the possibility of using surface texturing for realistic gray cast iron compressor surfaces. Three types of micro-dimple patterns (40 μm diameter and 10 μm depth, 60 μm diameter and 7.5 μm depth, 60 μm diameter and 4 μm depth) with two area densities of 5% and 20% were created on the pin surfaces by the method of laser surface texturing. The results of the controlled tribological experiments with the texture patterns were compared against untextured surfaces under starved lubrication conditions. Under identical conditions of load, the untextured pins failed while all the textured pins operated successfully. In addition, the textured pins survived the entire duration of three hours in durability type studies highlighting their long term usefulness. Selected tests were also done at different sliding speeds, lubricant types and refrigerants and the usefulness of surface texturing at aggressive conditions was realized. For the wear and durability experiments, the beneficial effect of the micro-dimples could be attributed to the lubricant storage ability. A trade-off between the effect of the material pile-ups or bulges around the micro-dimples and the lubricant storage volume of the micro-dimples determined the difference

in performance between the texture patterns. In addition, step loading scuffing experiments were done using the texture patterns and the scuffing resistance was found to primarily depend on the lubricant storage ability of the micro-dimples.

Even though surface texturing was found to have a positive effect, such behavior needs to be evaluated under specific lubricants and refrigerants, to fully understand the complex phenomena driving the improved performance. Overall, the research work done in this thesis developed new information about the application of surface texturing for air-conditioning and refrigeration compressor applications. It was demonstrated successfully that texturing could be applied to compressor surfaces operating under realistic conditions such as starved lubrication and provide significant tribological benefits.

ACKNOWLEDGEMENTS

Professor Andreas A. Polycarpou is a kind of adviser who will challenge you immensely but will always help you learn and be there to guide if you falter and need support. I could not have asked for more. It has been a real pleasure working on my Masters thesis under his guidance. His contribution to the successful completion of this thesis is foremost and I offer my sincere gratitude for this co-operation. I am indebted to him for his sincere advices on numerous instances which have helped me to make correct decisions.

The Tribology and Microtribodynamics Laboratory has been an integral part of my graduate studies since I joined it in January 2010. I met some wonderful people and made friends for life. I would like to thank each and every one of them who have been very welcoming and friendly. In particular I would like to thank Emerson Escobar Nunez, former PhD student, for training me on the UHPT and being ever so patient with me and Seung Min Yeo, current PhD student, for being a very good friend and colleague. Seung Min and I shared the office and discussed about different things, both research and otherwise. I deeply acknowledge his help in some of the SEM and nanoindentation measurements. I must also thank other members of my research group – Melih, Sujana, Antonis, Jungkyu and Wasim – in no particular order, in providing an intellectually stimulating yet friendly and congenial atmosphere.

My sincere thanks to Department of Mechanical Science and Engineering for the Teaching Assistantships I received during the first year of my graduate studies and Air Conditioning and Refrigeration Center (ACRC) and FMC Technologies Inc. Fellowship

for taking care of the financial needs during the second year of my graduate studies. This enabled me to concentrate thoroughly on the research. The materials characterization and analyses were done at the Center of Microanalysis of Materials, University of Illinois at Urbana Champaign, which is partially supported by the U.S Department of Energy under grant DEFG02-91-ER45439.

Last, but not the least, I would like to offer my sincere gratitude to my family back in India, who have always supported and believed in me. Without their unconditional love and support, I would not have been what I am today. Living so far away from home is always a challenge and they have been instrumental in making sure I am happy and able to concentrate on my work without any worries.

To my wonderful family

TABLE OF CONTENTS

CHAPTER 1: INTRODUCTION 1

1.1 Background on air-conditioning and refrigeration compressors 1

1.2 Motivation for current work 12

1.3 Thesis Organization and Outline 14

CHAPTER 2: REVIEW OF SURFACE TEXTURING AND CHARACTERIZATION OF TEXTURED SAMPLES USED IN THIS WORK 16

2.1 Introduction 16

2.2 Techniques for surface texturing 17

2.3 Tribological benefits from surface texturing 23

2.4 Specimen materials and surface texturing used in this work 35

CHAPTER 3: WEAR EXPERIMENTS IN THE PRESENCE OF REFRIGERANT ENVIRONMENT 47

3.1 Objective 47

3.2 Experimental Procedure 47

3.3 Wear experiments 53

3.4 Durability (or Life) experiments 85

3.5 Wear analysis 90

3.6 SEM/EDS studies 109

3.7 Summary and Conclusions 117

CHAPTER 4: SCUFFING EXPERIMENTS IN THE PRESENCE OF REFRIGERANT ENVIRONMENT 120

4.1 Objective 120

4.2 Experimental Procedure 121

4.3 Results and Discussions 123

4.4 Summary and Conclusions 141

CHAPTER 5: CONCLUSION AND FUTURE WORK 143

5.1 Summary of Thesis 143

5.2 Primary Conclusions 146

5.3 Future Work 149

BIBLIOGRAPHY 152

APPENDIX A: PRELIMINARY EXPERIMENTS WITH POLISHED TEXTURE PATTERNS 158

APPENDIX B: PRELIMINARY STUDIES ON POLYMERIC COATINGS AT ELEVATED TEMPERATURES FOR COMPRESSOR APPLICATIONS 163

CHAPTER 1: INTRODUCTION

1.1 Background on air-conditioning and refrigeration compressors

1.1.1 Air-conditioning and refrigeration compressors

Compressors are one of the most important parts of the refrigeration and air-conditioning cycles. They compress the low-pressure gas (refrigerant) into high temperature, high pressure gas from where it moves into the condenser and gets cooled. Further, the refrigerant gas flows into the expansion valve and evaporator and finally back to the compressor to complete the cycle. There are various types of compressors used in air-conditioning and refrigeration systems such as swash-plate, scroll, rotary and vane.

In swash-plate type compressors (Figure 1.1), an inclined swash-plate connected to the drive shaft moves the pistons back and forth compressing the refrigerant. Critical tribo-contacts occur between the steel shoes (shown in Figure 1.1) and the swash-plate and are prone to failure. This is particularly significant during start-stop operation when the contact is in starved lubrication regime with greater metal-to-metal contact.

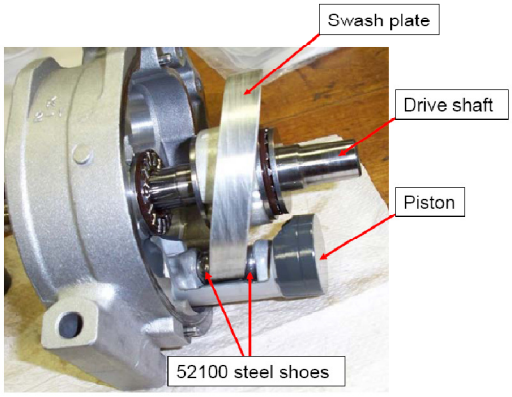

Figure 1.1: Cut-away swash plate type compressor showing important tribo-components [1]

A scroll compressor (Figure 1.2) consists of two circular involute scrolls which are out of phase by 180°. One of the involutes is stationary and is called the *Fixed Scroll* while the other is rotating and is called the *Orbiting Scroll*. The main advantage of such a compressor is the fewer number of moving parts which bring down the failure modes and lead to reduction in noise and vibration. The main disadvantage is related to the number of cycles of involutes spirals needed to compress the refrigerant to the desired pressure.

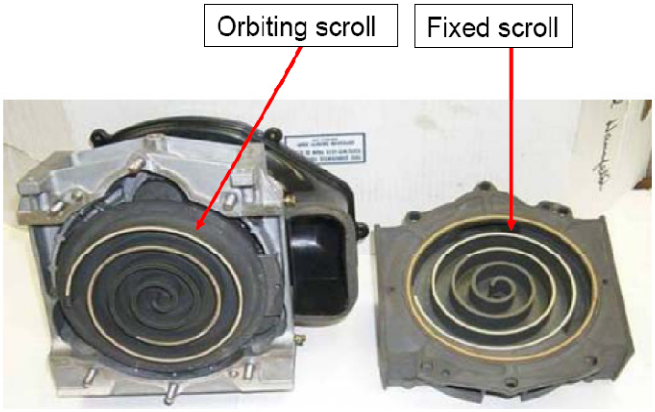

Figure 1.2: Opened scroll type compressor with some of its components shown [1]

Similar critical sliding tribo-contacts (Figure 1.3) also exist in other type of compressors such as Vane type and Piston type compressors. This means that tribological studies done on these kinds of compressors can be generally applied.

Figure 1.3: Wrist pin/connecting rod interface in a piston type compressor [2]

1.1.2 Refrigerants in air-conditioning and refrigeration compressors

In very early times, the most common refrigerants included anything that worked and was available. Ammonia, propane (R-290), water (R-718), carbon tetrachloride (R-10) were common and comprised the first generation of refrigerants [3]. The second generation of refrigerants was marked by a shift to fluoro-chemicals on ground of safety and durability. While chlorofluorocarbons (CFCs) and hydrochlorofluorocarbons (HCFCs) were the dominant ones, ammonia still continued to be the popular refrigerant for large industrial systems [3]. The third generation of refrigerants focused on stratospheric ozone protection. CFCs contained ozone depleting compounds and their use was banned according to the Montreal Protocol [3]. Hydrofluorocarbon (HFC) based refrigerants such as R-134a and R-404a replaced the traditional CFCs and HCFCs, and are widely used for air-conditioning and refrigeration applications today [1]. The fourth generation of refrigerants has a focus on global warming [3]. In the 1997 Kyoto Agreement, HFCs were pointed out to be ones with high global warming potential (GWP) and their use was regulated [1]. Thus, in recent years the thrust has been on environmentally friendly refrigerants and there is a great interest to pursue natural refrigerants such as water, air, isobutane (R-600a), ammonia and CO_2 (R-744) [4]. The automotive industry is currently pursuing three candidates to replace R-134a in mobile applications. These candidate refrigerants are carbon dioxide (R-744) and R-1234yf in direct expansion systems and R-152a in indirect systems [3]. Table 1.1 gives a comparison of the ODP, GWP and atmospheric lifetime of different refrigerants.

Table 1.1: Ozone depletion potential, global warming potential and atmospheric lifetime for different refrigerants [1]

Refrigerant	ODP	GWP	Atmospheric lifetime (years)
R-12	1	7100	102
R-22	0.05	4100	13.3
R-134a	0	1430	14.6
R-744 (CO_2)	0	1	>500
R-1234yf	0	4	11

R-744 is an attractive choice as a natural refrigerant. It is non-flammable and non-toxic unlike hydrocarbons and ammonia. R-744 has zero ozone depletion potential (ODP) and negligible global warming potential compared to CFCs and HCFCs [4]. R-744 can be easily obtained from industrial processes and recycled and implemented as a refrigerant. Even when small quantities of R-744 are released to the environment (for example: during maintenance and repair of the air-conditioning and refrigeration systems), the effect on global warming will be negligible compared to the release of industrial CO_2 from cars and plants and other high GWP refrigerants like R-134a and R-404a [5]. In addition to the potential in mobile air-conditioning applications, many studies are being conducted on R-744 for stationary applications as well. The use of R-744 is also increasing, especially in Europe, for commercial applications [3]. However, the major roadblock in the implementation of R-744 is the requirement of high operating pressures, which necessitates significant re-design of bearings, seals etc. Figure 1.4 shows a typical pressure-enthalpy thermodynamic cycle of R-744. Operating pressures range from 3 MPa (435 psi) at the low pressure side to 12 MPa (1740 psi) at the high pressure side [4]. These

conditions of pressure are approximately 5 to 6 times higher than in conventional refrigerants such as R-134a.

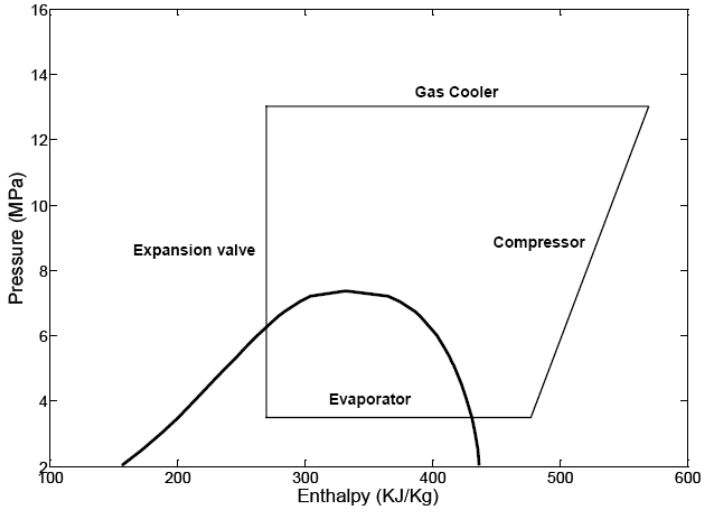

Figure 1.4: Typical thermodynamic operating conditions of R-744 based air-conditioning system

New alternative refrigerants are being currently researched to optimize performance and environmental impact. One such refrigerant is R-1234yf ($CF_3CF{=}CH_2$), jointly developed by Honeywell and DuPont [1], and referred to as "yf." The ODP of this refrigerant is zero while the GWP is negligible compared to refrigerants such as R-134a and is slightly higher than R-744 (Table 1.1). However, the main advantage of this refrigerant compared to R-744 is that the working pressures are similar to that of traditional refrigerants like R-134a and thus can be used as a direct replacement without the need for significant re-engineering of the system. However, there are concerns regarding the flammability and cost of R-1234yf. Thus, its production requires stringent process control [3].

1.1.3 Lubricants in air-conditioning and refrigeration compressors

In typical air-conditioning and refrigeration compressors, the main duties of the lubricant are [6]:

a) Reducing friction between sliding interfaces
b) Preventing welding/scuffing between contact surfaces during periods of starved lubrication, start-ups and shut-downs
c) Transferring heat from components such as bearings, pistons etc
d) Sealing gaps between high and low pressure regions such as pistons, valves etc. and
e) Preventing corrosion

The most important function of the lubricant is the reduction in friction and wear, which is mainly dependent on its viscosity. The variation of friction coefficient in lubricated contacts with a dimensionless parameter, called the Sommerfeld number (S), is described by the Stribeck curve (Figure 1.5). The Stribeck curve provides information on three lubrication regimes:

1) *Boundary Lubrication Regime:* There is significant asperity interaction in this regime as only a thin layer of lubricant exists between the sliding interfaces. Such regimes are found at low Sommerfeld numbers, typically at lower sliding speeds or lower lubricant viscosity.
2) *Mixed Lubrication Regime:* Under this regime, the number of contacting asperities gets reduced and there is a partial film separating the sliding interfaces. This regime typically occurs at intermediate Sommerfeld numbers.

3) *Hydrodynamic/Elasto-hydrodynamic Regime:* In this regime, the film thickness is thicker than the combined root mean square roughness of the two sliding interfaces. There is complete separation of the two surfaces, which means this is the most ideal lubrication regime for the compressor to operate.

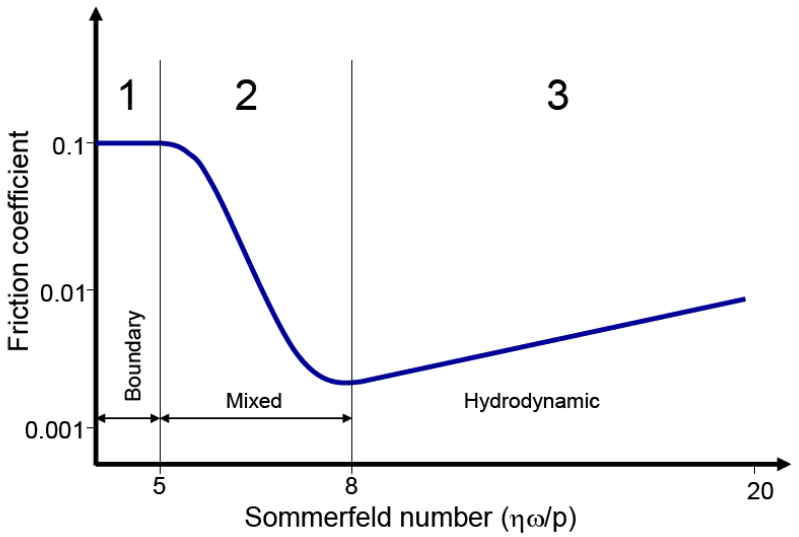

Figure 1.5: A typical Stribeck curve showing variation of friction coefficient in lubricated contacts [1]

For air-conditioning and refrigeration systems, it is also important to understand the lubricant-refrigerant relationship particularly in terms of solubility, viscosity and miscibility [6]. When the lubricant is exposed to refrigerant vapors, it absorbs some amount of refrigerant which depends on the type of lubricant, refrigerant, temperature and pressure. This can be critical because due to the low viscosity of the refrigerant, the overall viscosity of the lubricant-refrigerant solution is reduced relative to the base oil. For example, when the lubricant absorbs about 10% of refrigerant, the viscosity is reduced to less than half of the base oil [6]. When liquid lubricant and liquid refrigerant are mixed together, they could exist as a single liquid or two separate liquids with the denser one at the bottom. This again depends on the type of lubricant, refrigerant,

percentage composition and the temperature of the liquids. For example, Ammonia does not mix with lubricants except in small amounts while R-22 is miscible over the complete range [6]. Miscibility is a key issue as it has been reported that incomplete miscibility of R-744 with commonly used lubricants in the vapor compression cycle affects the way the lubricant is transported out of the refrigeration circuit [7]. Also, it has been shown that the presence of lubricant reduces the thermodynamic coefficient of performance [8]. Thus, the critical role of the lubricant in the air-conditioning and refrigeration systems cannot be overemphasized.

Different types of lubricants are used for compressor applications. Typically for inexpensive compressors, such as piston-type in home appliances, mineral oils are used as the lubricants. These could be *Yellow Oils* which have a Napthenic (cyclo-paraffins) structure and made up of cyclic or ring molecules or *White Oils* which have Paraffin structure with molecules made of straight carbon chains with some branched chains [6]. Mineral oils have a wide range of viscosities and performance is further improved by specialized additives.

However, as the compressor operating conditions get more aggressive in pursuit of higher efficiency, there is greater stress on the contacting elements inside the compressor. Thus, new lubricants are designed to be able to withstand such conditions and ensure that no failure occurs. Synthetic lubricants are increasingly being used; most common among them being Polyalkylene glycol (PAG) and Polyolester (POE). Figure 1.6 shows their chemical structure. PAG lubricants are polymer chains of ethylene and propylene oxides. Its chemical structure can be modified such that large number of viscosities can be achieved. The polarity of PAGs can also be altered to make them

soluble in different types of media [9]. In POE lubricants, the presence of an active ester group provides mobility at lower temperature, decreases volatility at higher temperature and improves absorption on metallic surfaces.

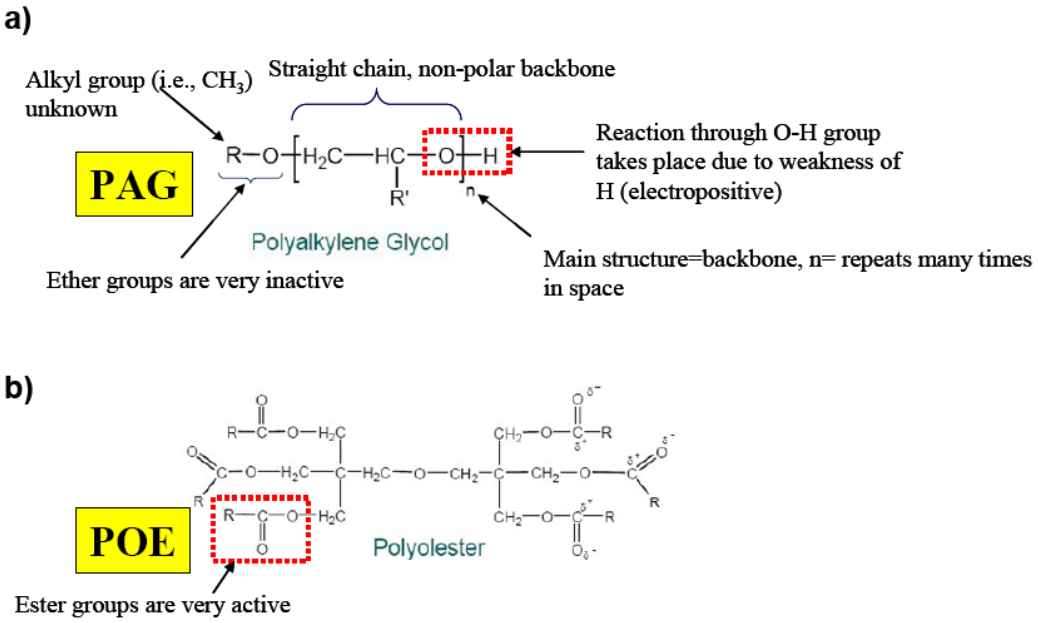

Figure 1.6: Chemical structure of (a) PAG and (b) POE lubricant [1]

1.1.4 Common (typical) compressor materials

Materials such as Al390-T6, gray cast iron and Mn-Si brass are commonly used materials for critical tribo-pairs in air-conditioning and refrigeration compressors. Al390-T6 and Mn-Si brass are usually found in automotive air-conditioning compressors while gray cast iron is used in industrial scroll compressors [4]. Table 1.2 shows the typical chemical composition of these three materials.

Table 1.2: Chemical composition of common compressor materials [4]

Element	Chemical percentage by weight (wt%)		
	Al390-T6	Gray cast iron	Mn-Si brass
Al	76.00	-	0.01
C	-	3.20-3.70	-
Cu	3.00-4.00	-	60.40
Fe	1.00	Balanced	0.23
Mg	0.40-1.00	-	-
Mn	0.50	0.70-0.80	2.43
Pb	-	-	1.24
Si	16.00-18.50	2.20-2.55	0.86
Zn	1.00	-	35.58

Al390-T6 contains a high percentage of silicon (16-18%) which provides good wear resistance. The primary and eutectic silicon particles are embedded in the Al matrix, with the eutectic particles being more uniform. Figure 1.7 shows a surface cross-section SEM image of Al390-T6. The primary silicon particles are responsible for improving the strength of the alloy.

Gray cast irons have graphite flakes with sharp edges surrounded by the pearlite matrix as shown in Figure 1.8. Cementite and ferrite appear as light and dark lamellar structures respectively. The addition of silicon promotes the formation of the graphite flakes.

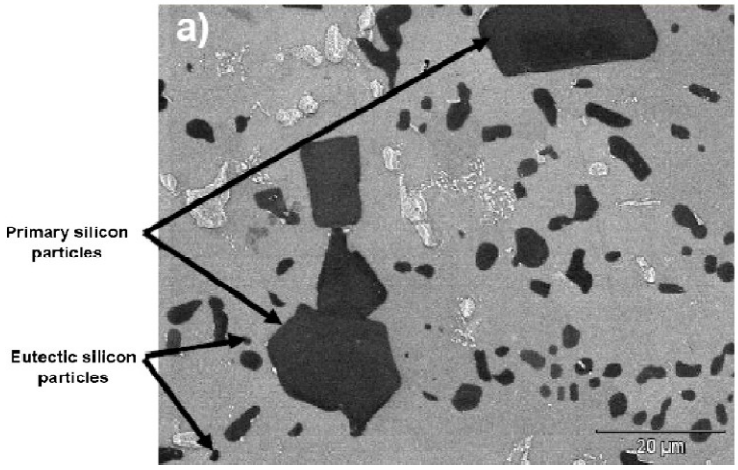

Figure 1.7: Surface cross-section SEM image of untested Al390-T6 [4]

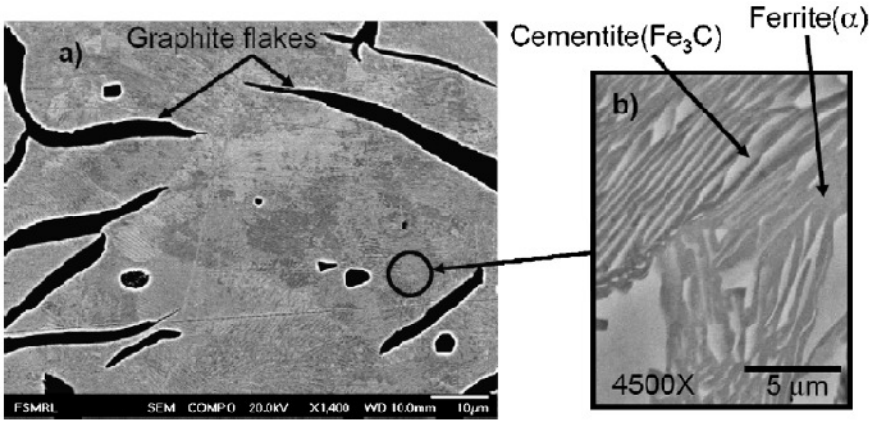

Figure 1.8: Surface cross-section SEM image of untested gray cast iron [4]

Mn-Si brass consists of a copper rich α soft phase and a manganese silicide phase (Mn_5Si_3). Silicon increases the wear resistance of the alloy by forming hard Mn_5Si_3 and improves its performance during plastic deformation. Primary and small Mn_5Si_3 particles can be seen in Figure 1.9 along with lead (Pb).

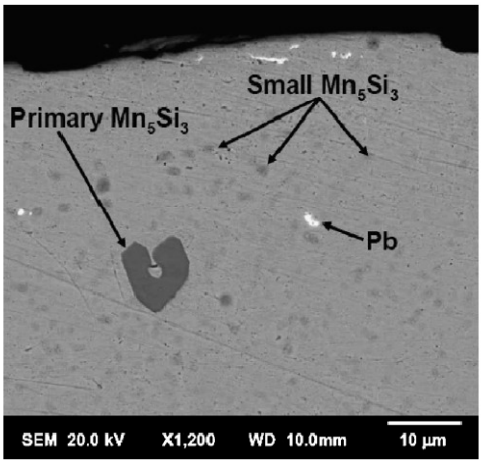

Figure 1.9: Surface cross-section SEM image of untested Mn-Si brass [4]

Nunez et al. [4] conducted scuffing studies on the above described materials against SAE 52100 steel shoes under realistic compressor operating conditions in the presence of environmentally friendly R-744 refrigerant. They observed that the scuffing performance of Mn-Si brass and gray cast iron was similar, although gray cast iron had a higher strength than Mn-Si brass. However, the performance of both materials was better than that of Al390-T6. While gray cast iron and Al390-T6 exhibited sudden scuffing failure, the failure in Mn-Si brass was gradual which could be advantageous in actual applications.

1.2 Motivation for current work

Environmental concerns have forced the refrigeration industry to move from CFC to HFC and more recently low GWP refrigerants like R-744 (CO_2) and newly developed R-1234yf. The immediate impact of such a change is the load limits on critical interfaces within the compressors. Chlorine in CFC refrigerant causes the formation of beneficial ferrous chloride protective layers on iron surfaces [10]. In addition, operating conditions

such as load and speed of the compressors are getting more aggressive to improve efficiency. Thus, there is a need to have a closer look at the interfaces and devise methods to make them more robust and wear-resistant. Currently, much of the attention is focused on lubricants [11], and protective surface coatings. Hard coatings such as WC/C [10], DLC [12], WC/C + DLC and TiAlN + WC/C [2] have been successfully applied and shown to be beneficial under dry sliding conditions in the presence of refrigerants such as R-134a, R-744 etc. Research has also been done on PEEK/PTFE-based soft polymeric coatings [13-15]. These coatings are particularly useful to further the development of oil-less compressors in the future. However, currently most of the compressors use oil for lubrication and will probably continue to do so in the future until robust materials/ coatings that can perform under a wide range of conditions are established. In addition, the state of lubrication in many critical compressor components is unknown and usually is in the boundary/mixed regime [12]. Thus there is a need to also investigate solutions other than the "traditional" approaches of protective coatings and explore innovative surface engineering solutions such as surface texturing.

Surface texturing has been widely used for friction and wear reduction applications such as cylindrical face rings, piston rings, hydrodynamic bearings etc. [16-18]. It involves creation of regular micro-sized features on the surface which serve various functions under different lubrication regimes. Typically, in the form of micro-dimples, textured surfaces have been proven beneficial in not only lubricated contacts but also in dry sliding conditions. In the boundary/mixed lubrication regime, the micro-dimples serve as lubricant reservoirs and provide lubricant at the interface. However, despite its popularity, the effect of surface texturing has not been studied on compressor surfaces

under realistic operating conditions, till date. The objective of the current work is to explore the idea of surface texturing as a surface engineering approach to improve the tribological performance of compressor surfaces in the presence of environmentally friendly refrigerants, particularly in the boundary/mixed lubrication regime.

1.3 Thesis Organization and Outline

As mentioned above, to our knowledge, surface texturing has not been applied for tribological performance improvement under realistic compressor operating conditions and this study is a first of its kind. Thus, it is essential to have a basic understanding of the surface texturing technology. State-of-the-art in surface texturing technology for tribological applications is presented in Chapter 2. Different techniques to produce such micro-features on the surface of a material are presented along with a literature review of the tribological benefits of surface texturing under different lubrication regimes. In the later part of the chapter, detailed characterization of the textured patterns to be used in this study is also provided. Surface profile measurements, optical images and high magnification SEM images are also provided.

R-744 (CO_2) is a natural refrigerant and is environmentally friendly which makes it an attractive choice. Compared to the currently used R-134a (ODP = 0 and GWP = 1430), its GWP is 1 while ODP is 0. Chapter 3 deals with constant load type wear experiments done on the texture patterns primarily in the presence of R-744. Boundary/mixed/starved lubrication type of experiments was conducted using an Ultra High Pressure Tribometer. Surface profile measurements of the textured pins and the counter disks were done before and after the tests, to quantify the surface changes. To

have a better understanding of the tribological behavior, SEM and EDS analyses were also performed on the tested specimens. Currently, R-134a is widely used as the refrigerant of choice, for mobile applications. It is an HFC-based refrigerant and its use has been regulated by the Kyoto Protocol. There is a growing sense of urgency to replace such high GWP refrigerants with environmentally friendly refrigerants. In that respect, the newly developed refrigerant R-1234yf is being touted as a direct replacement for R-134a. Chapter 3 also deals with some tribological studies done in the presence of R-134a and R-1234yf to compare the performance of these two refrigerants and provide some insights into the benefits of surface texturing in current and future systems.

Scuffing is an important issue for compressor manufacturers. It is an instantaneous failure which renders the device non-functional. In Chapter 4 studies done on the High Pressure Tribometer to understand the scuffing performance of textured pins compared to untextured pins under starved lubrication conditions are presented. The major conclusions from this thesis research work and the directions for future work are presented in Chapter 5.

CHAPTER 2: REVIEW OF SURFACE TEXTURING AND CHARACTERIZATION OF TEXTURED SAMPLES USED IN THIS WORK

2.1 Introduction

The idea of using textured surfaces for improving tribological performance is not new. Cylinder liner honing has been used since many years with the understanding that such a surface modification helps in preserving lubricants at the interface, which in turn helps reduce wear. Surface texturing, as is understood today, involves the creation of regular micro-sized features on the surface of a material. In recent years, surface texturing has received a lot of attention for achieving tribological improvements.

The size and geometry of the micro-sized features varies depending on the application, the processing techniques and materials. Typical sizes range from few microns to hundreds of microns. Some of the geometries include circle, square, oval, grooves etc. In the literature, the most common type of geometry found is in the form of circular/spherical micro-dimples due to their easy fabrication and lower costs [19]. For a micro-dimpled surface (Figure 2.1), the three significant geometrical parameters are the diameter of the dimple (d), the depth of the dimple (h) and the area density (A) [16, 18-20]. The area density is, simply put, the percentage of the surface area covered by the dimples.

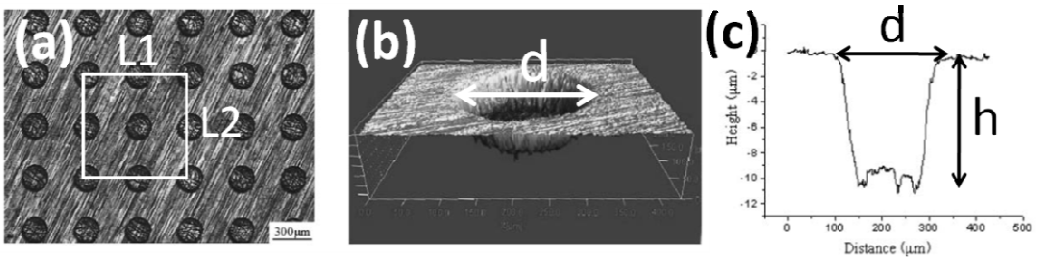

Figure 2.1: (a) Textured surface showing an array of micro-dimples (b) 3-D surface topography measurements of an individual micro-dimple and (c) 2-D line scan of an individual micro-dimple [19]

From Figure 2.1 (a), it can be calculated by finding the area of the marked rectangle and finding the number of full dimples lying within that area, which in this case are 4. So, the area density will be given by:

$$A = \frac{4x\left(\frac{\pi}{4}d^2\right)}{L1xL2} X\ 100$$

In the next sections, the different techniques for manufacturing such micro-sized features on the surface as well as the motivation for using such a surface engineering approach in different lubrication regimes will be discussed.

2.2 Techniques for surface texturing

It is challenging to produce regular repeatable micro-structures on a material surface and so naturally, a lot of research is focused on the processing techniques. Several types of processing techniques are being currently used to produce these micro-dimples. The techniques are fundamentally different and bring with them some advantages and some limitations. To be commercially viable, it is essential that the adopted processing technique works well for a wide variety of materials and it is possible to produce repeatable micro-structures at low cost. Some of the technologies currently in use are described below.

2.2.1 Laser surface texturing (LST)

Laser surface texturing (LST) is the most popular and widely used method to create micro-dimples on the surface of a material. It is extremely fast, easily controllable and can be used on a range of materials such as metals, ceramics, polymers etc. [17]. Also,

the shape, size, area density and depth of the micro-dimples can be easily manipulated by changing the laser parameters [17]. The laser texturing process involves sublimation, melting and vaporization of the material on the surface resulting in a micro-dimple. In metals, the laser processing presents challenging problems of high thermal conductivity with low melt temperatures. Thus, laser processing of metals is always accompanied by heat affected zones and appearance of melt specimen [21], such as material pile-ups around the micro-dimples in laser surface texturing process. However, by appropriately selecting the laser parameters such as pulse energy, number of pulses and mode, the shape and dimensions can be controlled, including minimizing the "collateral" damage [17].

Laser texturing is popular because of its versatility of use. It can be used to create different shapes and sizes with ease. By using a galvometric scanner, for example, the laser beam can be tilted and can be used to create tilted surfaces with a large depth [22]. Also, the roughness of the textured surfaces can be controlled by using a laser polishing process [22].

2.2.2 Vibromechanical texturing (VMT)

The Vibromechanical Texturing (VMT) method developed by Greco et al. [23] builds upon the traditional turning process by substituting the traditional tool holder with a piezo-actuated flexural structure called micro-positioning stage (MPS). In the conventional turning process the work piece rotates while the cutting tool scans across its length with certain depth of cut and feed. However, in this modified process an additional controlled motion is provided to the tool, radially into the work piece, typically sinusoidal

oscillations. Figure 2.2 show the MPS along with an image of the textures produced using this process.

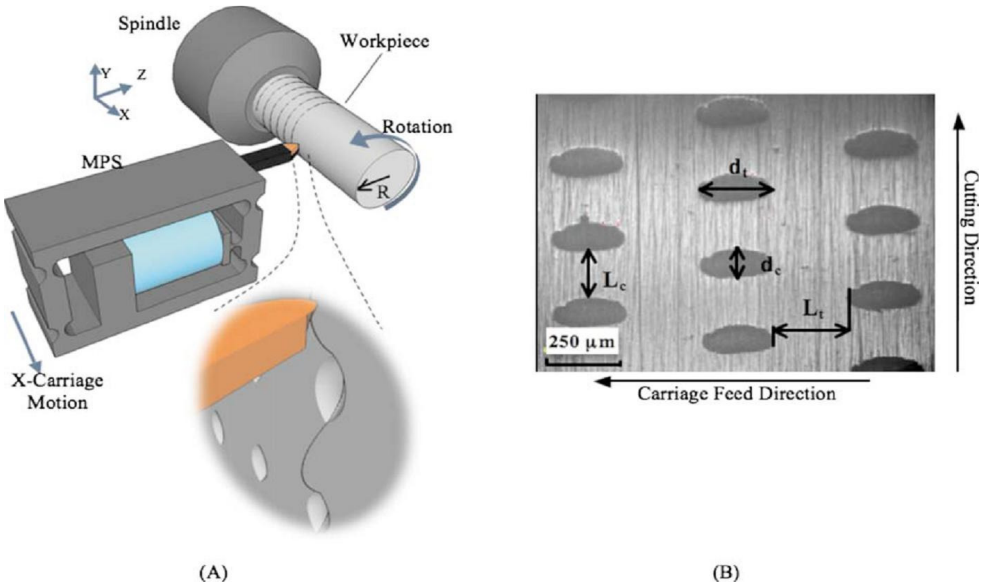

Figure 2.2: Schematic of the MPS and textures created using VMT method [23]

Greco et al. [23] have shown that such a method can be successfully applied to a wide variety of materials including aluminum and hardened steel. VMT was used to create micro-dimples in three different configurations – outer diameter, flat/end surface and inner diameter. In such a method, it is critical that appropriate tool is chosen, since the condition of the tool tip is significant to achieve uniform micro size dimples. The dimples were typically associated with material pile-up on one side, which were easily removed by light polishing using a fine grit abrasive cloth. The positive points of such a texturing method is its low cost, fast processing time, versatility in using different materials and configurations.

2.2.3 Diamond embossing

The diamond embossing technique has its roots in the photolithography and anisotropic techniques which can be used to micro-pattern materials like silicon. However, instead of using the process to create the final surface, Jacobson et al. [24] used it to prepare an embossing tool. They carried out anisotropic etching of silicon to create square pyramidal or rectangular roof-top structures out of silicon, which were coated with a thin film of diamond using the HFCVD (Hot Filament Chemical Vapor Deposition) process. A nickel backing was applied to the thin diamond coating to provide structural support. The remaining silicon was etched away to expose the array of micro diamond indenters. Figure 2.3(a) shows the processing steps involved in creating the micro-indenters. Figure 2.3(b) shows an array of diamond micro-indenter and Figure 2.3(c) shows the mechanical pressing method to create the micro-textures using the micro-indenters. Steel balls and steel flat were successfully textured by pressing them statically onto the embossing tool surface. To increase the fraction of indented surface, repeated indentations may be made with small controlled displacement of the tool.

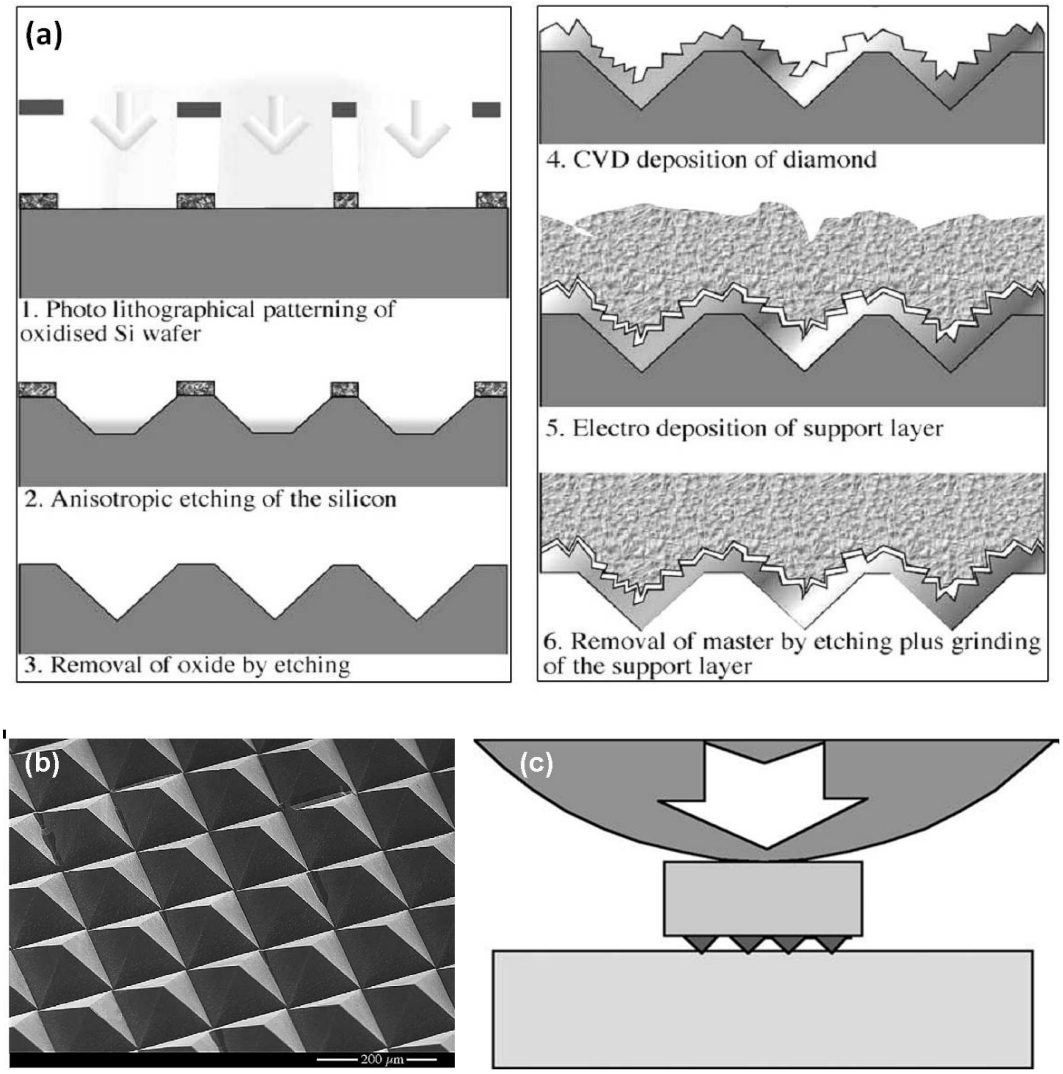

Figure 2.3: (a) Processing steps, (b) Array of diamond micro indenter and (c) Mechanical pressing process used in the diamond embossing technique [24]

2.2.4 Micro casting

Cannon and King [25] have developed a casting based micro-fabrication strategy to create regular micro-structures on the surface of a material. Figure 2.4 shows the typical process steps. They have shown that metals can be reliably cast into different types of structures such as ridges, holes or pillars. Flexibility of the mould is one of the biggest advantages of this process, enabling micro-casting on even curved surfaces.

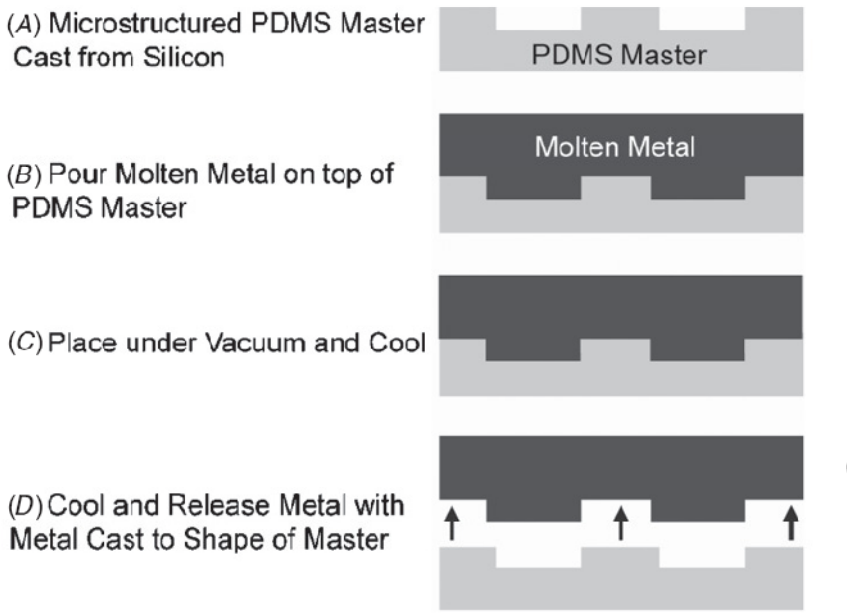

Figure 2.4: Process of micro casting metal [25]

The same researchers successfully created aluminum molds with integrated micro-structures. The aluminum was cast from curved micro structured ceramic molds which were cast from curved micro structured rubber. The micro structures on the aluminum molds had an aspect ratio of 1:1 and a size range of 25-50 µm. They were able to show that such a process can be successfully applied with excellent repetition fidelity and that different shape of micro-features such as circles, squares and triangles can be easily molded [26]. Thus this newer technology has potential for application on a large scale with reduced costs.

2.2.5 Other techniques

Apart from the techniques described above, some researchers have used other techniques to create micro-sized features. Rapoport et al. [27] showed the use of pulsed arcs sustained in the space between a thin electrode and the sample to create micro-

dimples. The principle involved applying a sufficiently high voltage (6kV) to break down the air gap (0.25-0.5 mm) between the electrode and the sample. The vertical motion (Z) of the thin electrode and the horizontal (XY) motion of the substrate was computer controlled for accurate positioning.

2.3 Tribological benefits from surface texturing

By using the innovative approach of surface texturing, significant friction reductions have been realized in different mechanical systems such as piston rings, cylinder liners, mechanical face seals etc. The three important geometrical parameters of these micro-dimples are the diameter, depth and area density. Many researchers are working to find suitable optimal dimensions to maximize the benefits from texturing. These micro-dimples on the surface help in improving the tribological behavior by:

1. Boosting the hydrodynamic pressure under full film lubrication
2. Acting as lubricant reservoirs under boundary/mixed or starved lubrication
3. Trapping wear debris under dry sliding condition

2.3.1 Benefits in full film lubrication

In 1966, Hamilton et al. [28] first provided a scientific understanding of the effect of surface texturing in the form of micro-asperities that acted as micro-hydrodynamic bearings in lubricated contacts. This area of research remained fairly dormant until 1996 when Etsion and Burstein [29] presented a model to highlight significant performance improvements of a mechanical face seal with evenly distributed spherical micro-dimples. This work was followed by an experimental work by Etsion et al. [30] where laser surface

textured seal rings were tested showing that an optimum dimple depth over diameter exists to maximize the film stiffness and PV limit.

Following this, more extensive theoretical modeling and experimental studies were done by Etsion et al. [31]. The modeling was based on solving Reynold's equation for the hydrodynamic pressure distribution and good agreement between theory and experiments were presented. Dramatic friction reduction up to 65% (Figure 2.5) was shown for actual seals tested in water [32].

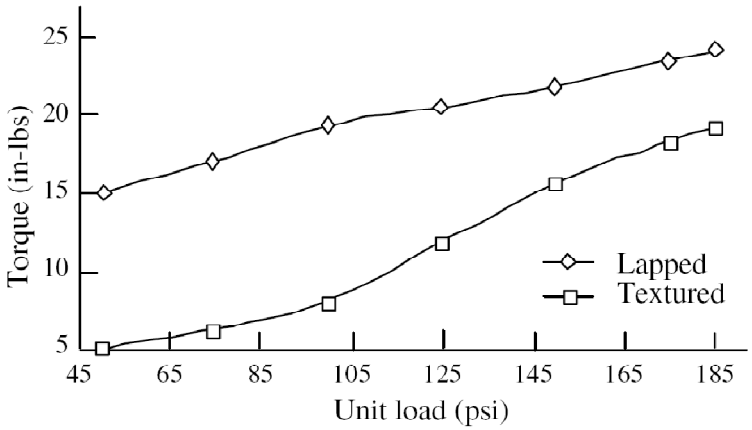

Figure 2.5: Comparison of the friction torque versus face load for textured and untextured SiC/SiC seals in water [32]

However, as can be seen in Figure 2.5, the benefit in terms of friction torque reduction is reduced at higher seal pressures, corresponding to higher face loads. To overcome this issue, another concept known as "partial texturing" evolved. This involved texturing only a portion of the seal corresponding to the high pressure side effectively creating a converging seal gap in the direction of pressure drop [33]. Figure 2.6 shows the pictures of two seals, one with full texturing and one with partial texturing.

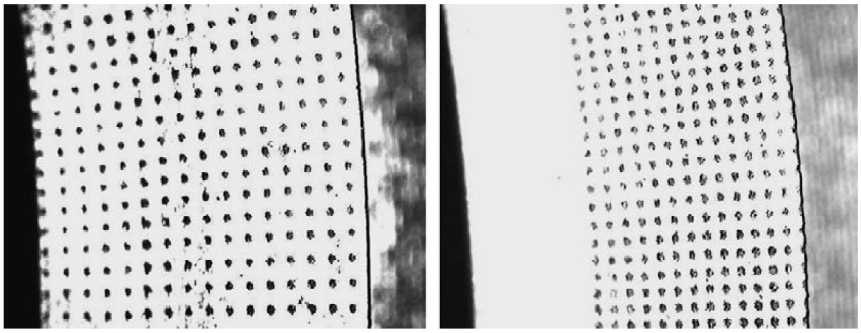

Figure 2.6: Two seal ring faces with same width showing full texturing and partial texturing [16]

The concept of generating load bearing capacity in a partial textured surface is shown in Figure 2.7. The textured portion of the slider provides larger clearance than the non-textured portion, effectively acting as a stepped slider.

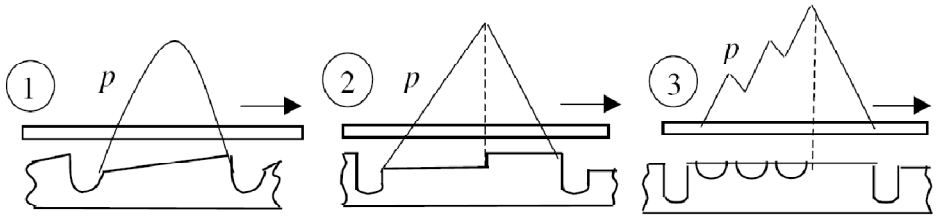

Figure 2.7: Typical pressure distribution in (1) plane slider (2) stepped slider and (3) surface textured parallel slider [33]

The application of surface texturing has also been explored in other mechanical systems such as piston ring-cylinder liner systems. Ronen et al. [34] studied the role of surface texturing and realized that significant hydrodynamic effects can be generated even with nominally parallel surfaces with textures. An optimum value of the micro-dimple diameter over depth ratio was also found that minimized the friction force. It was found that friction reduction of 30% or more could be realized by the use of surface texturing over the entire area of the piston rings. The theoretical results were later experimentally verified by Ryk et al. [35]. Further, the effect of partial texturing was

explored by Kligerman et al. [18] who developed an analytical model to study the potential of partial laser texturing in reducing friction between a piston ring and cylinder liner. They demonstrated the advantages of partial texturing over full texturing and identified optimum texturing fraction for a wide range of ring width and operating conditions. The minimum average friction force for the optimum partial textured rings was found to be 30-55% lower than that of optimum full textured rings. The results were experimentally verified Ryk et al. [36] who realized friction reduction up to 25% using partial textured piston ring compared to an untextured ring.

In addition to the theoretical approach and subsequent experimental verification for real life applications, researchers have also studied the effect of surface texturing on a more fundamental level to understand the mechanism of friction reduction as well as to optimize the texturing parameters. Nakano et al. [37] applied different types of micro-textures on the surface of cast iron and studied their effect on the tribological properties of cast iron. Texturing on cast iron blocks was done by milling or shot blasting to create groove patterns, mesh patterns and dimples. The groove patterns and mesh patterns produced by milling had a width of 500 µm and depth of 45-50 µm while for the shot blasted patterns, the width of the grooves and the diameter of the dimples were 60 µm and the depth was 6-10 µm. Before initiating the test, a flat configuration between the sliding interfaces was achieved by polishing them with 320-4000 grit abrasive paper. A commercially available lubricant for sliding guideways of machine tools was supplied drop wise to the interface at the rate of 150 µL/min. They found that for the groove and mesh patterns, the friction coefficient was higher than that of the flat surface. This is because the lubricating oil flowed through the grooves leading to a thin lubricant film

resulting in boundary lubricated conditions. On the other hand, the dimple patterns were able to hold lubricant and cause an increase in the hydrodynamic pressure. Thus the lubricant film became thicker resulting in an improved load carrying capacity. Their studies highlighted the need for having isolated micro-pockets of lubricant reservoirs to get benefits from the hydrodynamic effects. They also reported that texturing led to reduction in fluctuations of the friction coefficient compared to flat specimens with no texture.

The significance of the texture geometrical parameters on friction reduction was explored by Yan et al. [19] by orthogonal experiments. They created the dimples using an electrolytic etching process which resulted in no heat affected layer, residual stresses, cracks etc. and so the surface did not require further polishing. Micro-dimples with diameter 50-300 µm, depth 5-20 µm and area density 5-20% were created on chromium coated ductile cast iron and tested at four different combinations of load and speed, under submerged conditions in a CD15W-40 engine oil. The range analysis suggested that micro-dimple pattern with diameter of 100-200 µm, depth of 5-10 µm and area density of 5% were optimal for low friction at the test conditions. A maximum friction reduction of 77.6% was realized at a load of 1 MPa and speed of 0.5 m/s, compared to the untextured surface. Range analysis and analysis of variance (ANOVA) suggested that the dimple area density was the most important parameter influencing the friction coefficient, followed by the dimple depth and diameter at the load-speed conditions used. The authors however note that the order of influence could change at different load-speed conditions.

2.3.2 Benefits in boundary/mixed or starved lubrication

For cases where micro-dimples act as micro hydrodynamic bearings theoretical modeling can be done to optimize the texturing parameters for the specific operating conditions. However, most of the work done with texturing in the boundary/mixed or starved lubrication regime is experimental in nature. This is because the involved phenomena are quite complex and can only be described analytically in limited cases [33]. A trial and error approach based on physical understanding is used to optimize the texturing dimensions, especially for the dry sliding or starved lubrication cases where theoretical modeling does not exist. In such cases, the tribological benefits are due to the lubricant storage and wear debris trapping ability of the micro-dimples.

Yi et al. [38] showed that the maximum PV value of mechanical face seals can be increased by applying texturing. P is the pressure of the medium in the seal cavity and V is the velocity between the contacting surfaces. The surface of T8 steel disks were textured using a Nd:YAG laser to produce micro-dimples of diameter 200 μm, depth 8-10 μm and area density of 10%. Laser texturing resulted in material ridges around the micro-dimples and was removed by polishing for 3 min using a diamond paste of size 500 nm. Before the test, the disk was smeared with base oil and spun on a centrifuge to achieve a thin oil film on the surface. From the tests, the maximum PV value of the textured seals was observed to increase by 2.5 times compared to the untextured seals. The reason for the improvement was attributed to the lubricant retention and wear debris trapping ability of the micro-dimples. The authors noted that the lubricating effect is highly dependent on the oil content during the friction process and proposed that as the

lubricant film at the interface breaks down, oil accumulated inside the micro-dimples reaches the interface on account of free energy reduction.

Wakuda et al. [39] studied the effect of texturing on friction reduction between silicon nitride plate and cylindrical steel pins under boundary lubricated conditions to simulate the cylindrical line contact in a cam/follower combination. Texturing on the ceramic plate was done by both abrasive jet machining (AJM) and excimer laser beam machining (LBM) which resulted in two different shapes of the micro-dimples. The micro-dimples had a diameter of 40-120 µm, depth of 5 µm and area density of 7.5-30%. Unlike in metals, the area around micro-dimples created in the ceramic samples remained smooth and no deburring process was required. The tests were carried out at 490 N load, corresponding to a contact pressure of 0.78 GPa, and the sliding speed was varied from 0.012 to 1.2 m/s. No significant friction reduction was observed for micro-dimples with 40 µm diameter because the scale of the micro-dimples was too small to act as lubricant reservoirs. At a micro-dimple diameter of 80 µm, friction reduction was observed for 7.5 and 15% area density, while friction increased for 30% area density. This was because as the area density increased, the actual contact surface decreased leading to higher contact pressures. In comparison, dramatic friction reductions were obtained for micro-dimples with 120 µm diameter and 7.5 and 15% area density while slight friction reduction was also obtained for 30% area density. It was also shown that the micro-dimple shape was not a critical factor in friction reduction which depended mainly on the texture size parameters such as diameter, depth and area density. For cylindrical line contact sliding condition, the dimple size relative to the contact width is an important factor in

determining the effect of texturing on friction reduction. Under the tested conditions, a micro-dimple diameter of 100 μm and area density of 5-20% is recommended.

Borghi et al. [40] studied the friction behavior between 100Cr6 steel pin and textured 30NiCrMo12 nitriding steel using one drop of oil at the contact. For normal loads larger than 3 N, which corresponded to contact pressure of 3 MPa, 75% reduction in friction was observed compared to untextured surfaces. Long sliding tests successfully demonstrated the ability of the textures to maintain the low friction coefficient for longer periods of time.

2.3.3 Effect on transitions in lubrication regime

To fully realize the potential of surface texturing in improving the tribological performance of lubricated sliding interfaces, it is important to evaluate and understand the impact of texturing on the transitions in lubrication regimes. Hupp and Hart [41] studied the effect of the texture geometry on the movement of the stribeck curve. The micro-dimples were created by the process of photolithography combined with electroless nickel plating and was tested using a triborheometer in the presence of a weakly viscoelastic interfacial lubricant. Figure 2.8 shows the effect different texture geometries have on the stribeck curve, presented as a variation of friction coefficient, C_f with Gumbel number, G_u ($G_u = \eta\Omega/\sigma$) where η is lubricant viscosity, Ω is angular velocity and σ is normal stress.

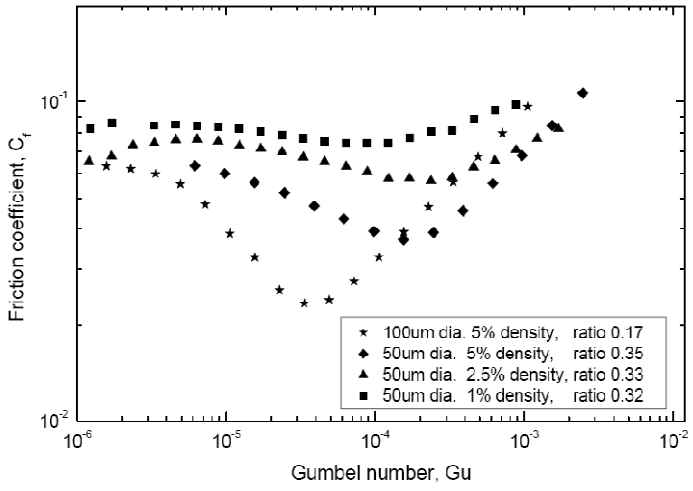

Figure 2.8: Stribeck curve for different texture patterns tested with a weakly viscoelastic lubricant on a triborheometer [41]

From Figure 2.8, as the micro-dimple diameter is kept constant and the area density is changed, there is a vertical shift in the stribeck curve. However, when the texture is changed, both vertical and horizontal shift of the stribeck curve is observed.

A more comprehensive experimental study was done by Kovalchenko et al. [42] who conducted tests at sliding speeds in the range of 0.015-0.75 m/s and nominal contact pressures from 0.16-1.6 MPa. Two oils with different viscosities were used and results of the textured specimens were compared to that of standard polished and ground specimens on a Stribeck curve. Figure 2.9 shows the friction behavior of the textured and untextured specimens in a Stribeck curve format.

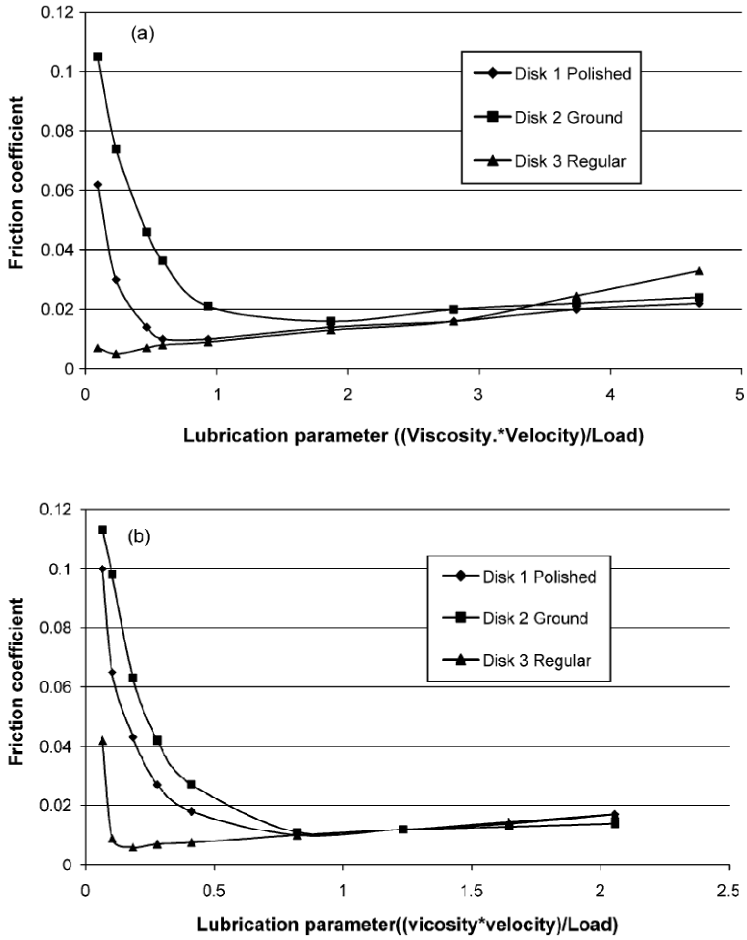

Figure 2.9: Friction behavior of the textured and untextured specimens in (a) high viscosity lubricant and (b) low viscosity lubricant [42]

From Figure 2.9 it can be seen that for the high viscosity oil, the transition from boundary to a mixed and finally to hydrodynamic lubrication regime occurs at low speeds and high loads for the polished disks compared to the ground disks. For the textured specimens, no clear transition was observed perhaps because hydrodynamic regime existed all through the testing conditions. However, for the low viscosity oil, clear transitions were observed for the textured specimens. Compared to the untextured disks, textured specimens displayed the transition in lubrication regimes at lower speeds and

higher loads. Thus, the effect of the texturing is that the Stribeck curve moves down and to the left enabling a transition of lubrication regime at lower speeds and higher loads.

2.3.4 Effect on seizure or scuffing resistance of sliding interfaces

Seizure of sliding interfaces occurs suddenly and renders the devices non-functional. So, it is imperative that seizure failure of sliding interfaces be researched to extend life-times of sliding pairs, which includes research on surface texturing. Koszela et al. [43] investigated the effect of surface texturing on the seizure resistance between bronze CuSn10P and 42CrMo4 steel. An oil drop was added just before starting the tests to lubricate the surfaces. The seizure test was carried out at a normal load of 2700 N, corresponding contact pressure being 27 MPa, and stopped when the friction coefficient reached a limit value of 0.15. In comparison to the untextured specimens, lifetimes for the textured specimens were found to increase by 5 times. The best sample with the longest time to seizure had comparatively deep micro-dimples of 100 μm and an area density of 26%. The worst cases were for samples with area density greater than 50% and low micro-dimple depths.

Galda et al. [44] studied the effect of the shape such as spherical, short drop and long drop dimples and distribution of the micro-dimples on the seizure resistance of lubricated interfaces. Tests were conducted at a sliding speed of 0.27-0.55 m/s and a step loading which corresponded to a nominal pressure of 3 MPa per 15 minutes, starting with 9 MPa. The authors report that even for the smallest speed of 0.27 m/s, the textured samples improved the seizure resistance compared to the untextured samples and the seizure resistance also improved for higher speeds. They also found that dimples of

spherical shape and long drop shape were superior as compared to short drop shape and that the orientation of these dimples with respect to the sliding direction was also significant. The area density of the long drop shape dimples had a large influence on the anti-seizure ability with optimum values being less than 20%.

2.3.5 Benefits in dry sliding condition

Surface texturing has been shown to provide tribological improvements not just in the presence of some form of lubrication, but also in dry sliding conditions. Borghi et al. [40] compared the performance of textured 30NiCrMo12 nitriding steel against untextured specimen in the absence of any lubricant. In comparison to the untextured specimen, the textured specimen showed a lower and more stable value. Comparison of the SEM images (Figure 2.10) of the wear tracks of the textured and untextured specimen provided a clear understanding for the difference in behavior.

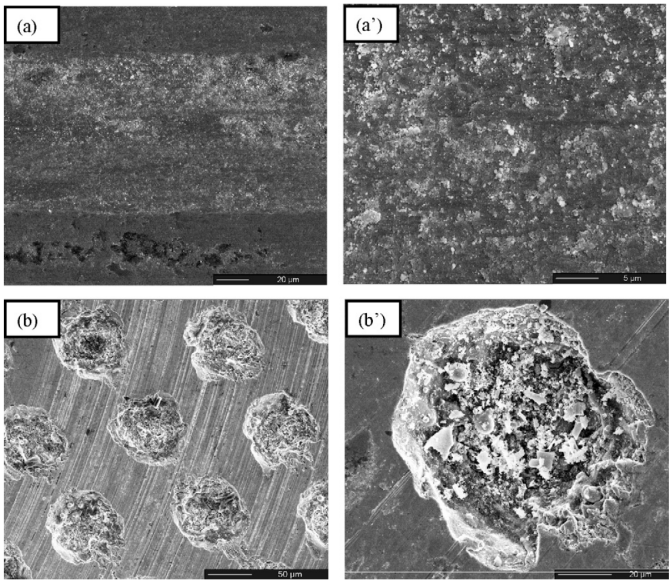

Figure 2.10: SEM images of the untextured (a and its enlarged detail a') and textured (b and its enlarged detail b') surfaces after the dry tests [40]

From Figure 2.10, the wear track can be seen for both the textured and untextured surfaces. For the textured surface, however, a spread of wear debris is clearly visible (Figure 2.10 (a')) while no wear debris is seen on the surface between the dimples for the textured case. A high magnification image of one of the dimples however shows some wear particles trapped inside it (Figure 2.10(b')). This clearly indicates that the loose wear particles were able to move into the dimples during the testing, which led to the improved behavior of the textured surfaces. This is however true only if the wear debris is abrasive in nature.

Similar benefits have also been reported in [45] and [46]. Results [45] showed that the escape of wear debris into the micro-dimples resulted in 84% reduction of electrical contact resistance of the textured fretting surfaces compared to untextured surfaces. The effect of texturing on the fretting fatigue life was shown [46] when the removal of wear debris from the interface by the micro-dimples resulted in an improvement in the fretting fatigue resistance and almost doubled the fretting fatigue life.

2.4 Specimen materials and surface texturing used in this work

In this work, tribological experiments were conducted in a pin-on-disk configuration using an Ultra High Pressure Tribometer (UHPT). The nominally flat stationary pin was held in a self-aligning holder in contact with an upper rotating disk. The pin and disks were made from gray cast iron, which is a common compressor material. The diameter of the pin was 6.3 mm and that of the disk was 76 mm. Figure 2.11 shows the picture of the disk and untextured pin.

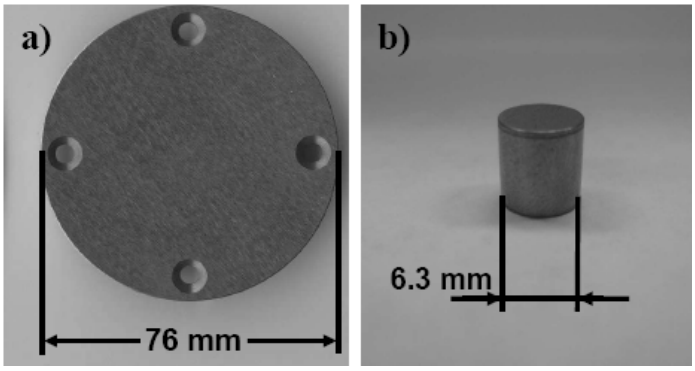

Figure 2.11: Gray cast iron samples used for testing; (a) disk and (b) pin (untextured)

For the textured pin specimens, micro-dimples were created by laser surface texturing. The texturing was performed by MLPC Inc. Three types of texture patterns were created and two types of area densities were achieved on the surface of the pins, the details of which are shown in Table 2.1.

Table 2.1: Details of the texture patterns used in the study

Pattern	Diameter, d (μm)	Depth, h (μm)	Diameter to depth ratio (d/h)	Area density (%)
A1	40	10	4	5
B1	60	7.5	8	5
C1	60	4	15	5
A2	40	10	4	20
B2	60	7.5	8	20
C2	60	4	15	20

The textured pins obtained from MLPC Inc. were characterized by optical images, high magnification SEM images and surface profile measurements. Figure 2.12 shows

optical images and Figures 2.13 and 2.14 show high magnification SEM images of the texture patterns.

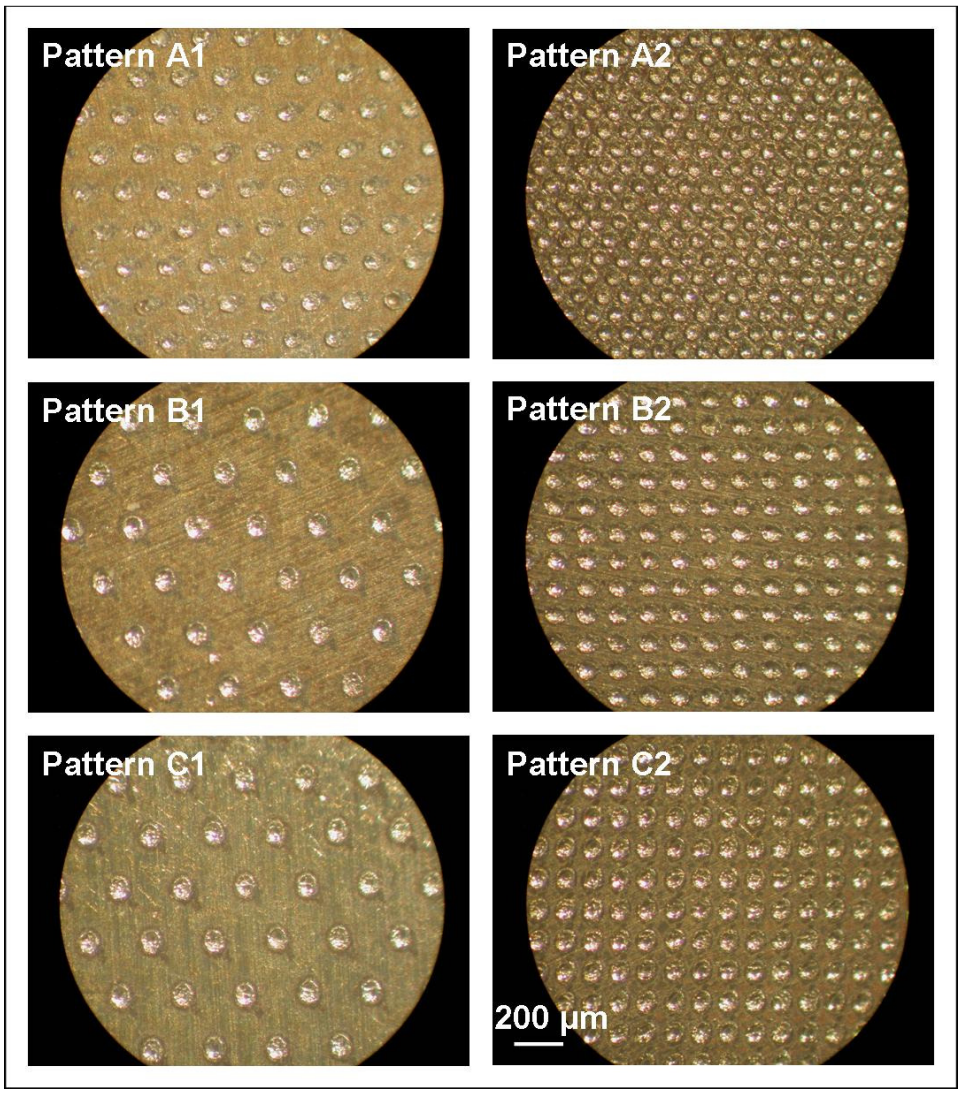

Figure 2.12: Optical images of all the as-recieved texture patterns

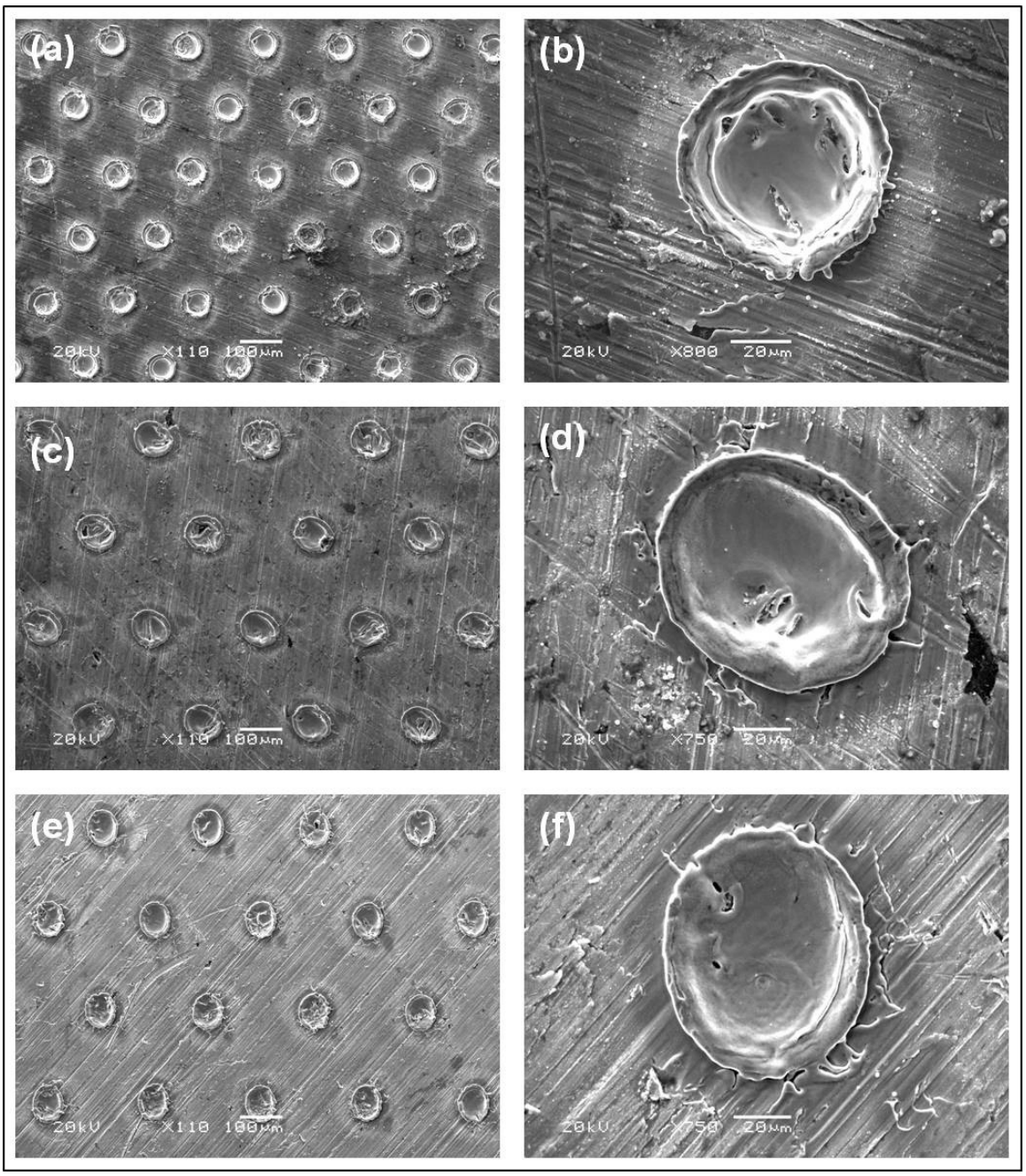

Figure 2.13: SEM images of the as-received texture patterns (a) A1 and (b) its high magnification, (c) B1 and (d) its high magnification and (e) C1 and (f) its high magnification

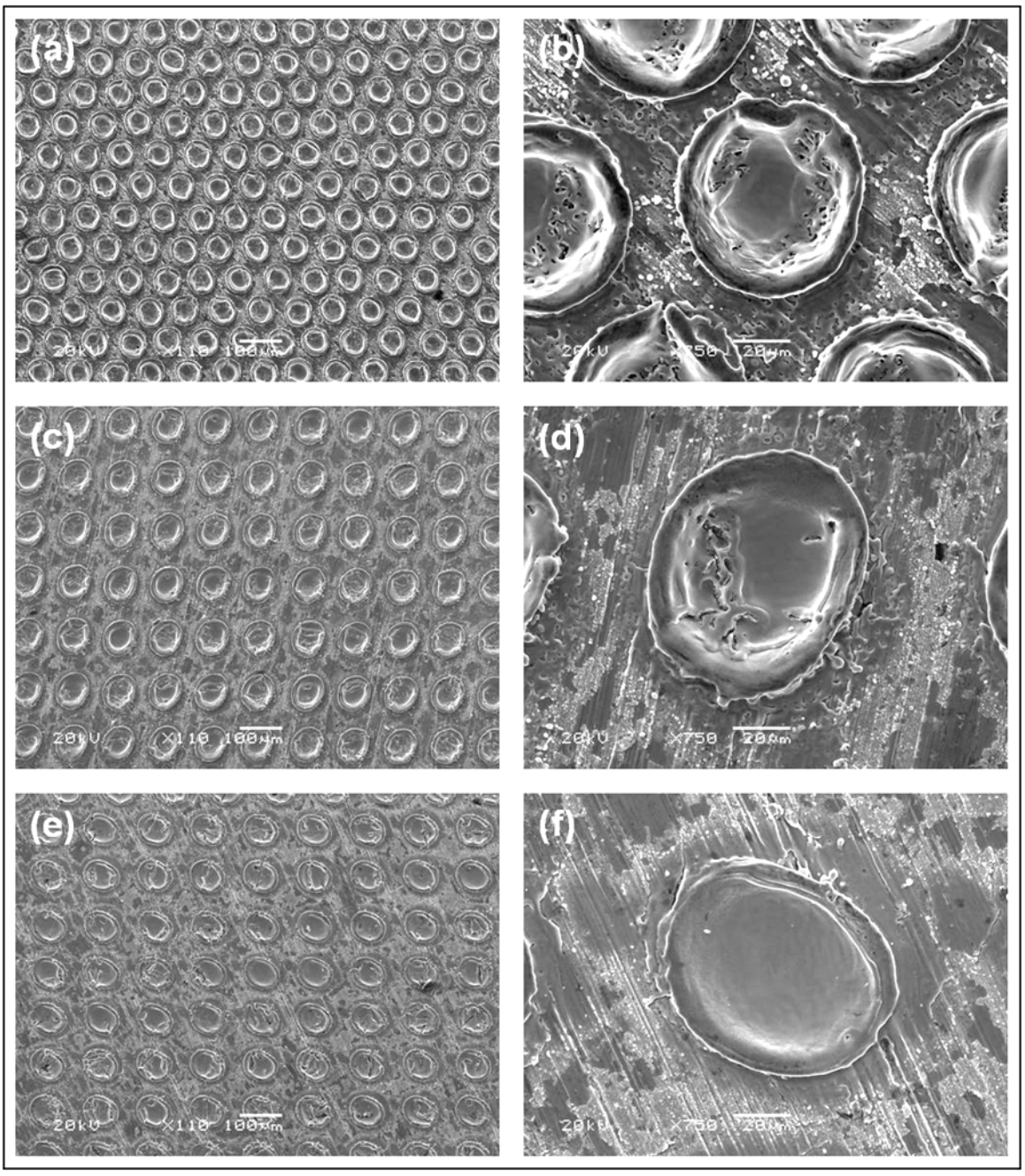

Figure 2.14: SEM images of the as-received texture patterns (a) A2 and (b) its high magnification, (c) B2 and (d) its high magnification and (e) C2 and (f) its high magnification

From the high magnification SEM images of the texture patterns (Figure 2.13 and 2.14), it can be seen that the laser surface texturing process resulted in material pile-ups around the micro-dimples. This was expected as laser texturing process is usually accompanied by appearance of melt material in the form of ridges or pile-ups around the dimples [21]. To quantify the texture geometries such as micro-dimple diameter and depth, and to quantify the extent of material pile-ups around the micro-dimples, surface profile measurements were performed on the surfaces of the textured pins. Figure 2.15 shows the 1-D line scans 800 μm long, done on the texture patterns A1, B1 and C1. For better visualization, a 2-D areal scan of texture pattern A2 is also shown in Figure 2.16.

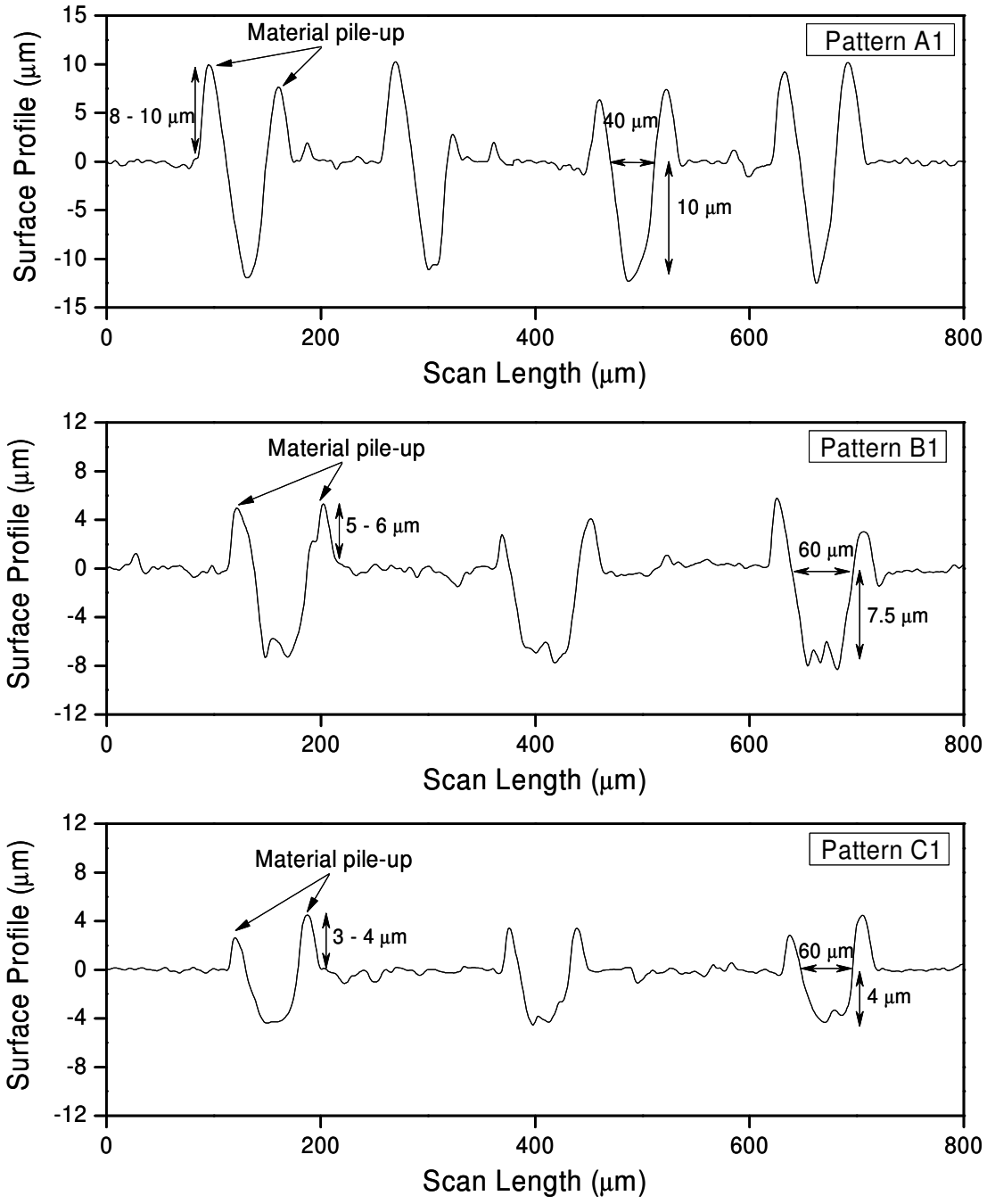

Figure 2.15: Surface profiles of the as-received texture patterns A1, B1, C1

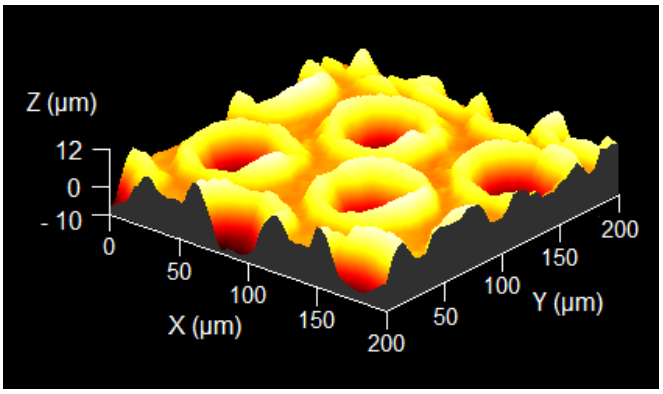

Figure 2.16: 2-D areal scan of an as received texture pattern A2

As can be seen in Figures 2.15 and 2.16, the material pile-ups around the micro-dimples were quite significant. The height of the pile-ups was of the order of the dimple depths in all the cases. However, it should be noted that although in Figure 2.15, the material pile-ups appear as sharp needle like structures, in reality they are not. This is because the surface profile measurements shown are not in 1:1 ratio in the X and Y axes. Figure 2.17 shows the surface profile measurement of one micro-dimple on texture pattern A1with the X and Y axes in 1:1 ratio.

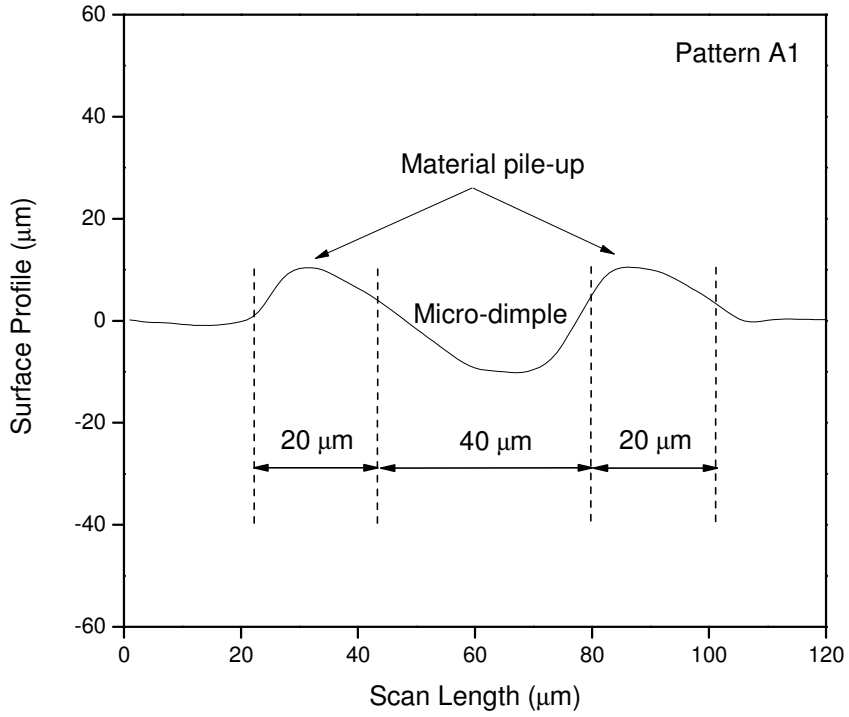

Figure 2.17: Surface profile of one micro-dimple from texture pattern A1 presented in a 1:1 ratio of the X and Y axes

The tribological experiments in this work are done in a pin-on-disk configuration. When the disk is brought in contact with the pin, the initial contact would occur at the top of these material pile-ups or bulges. The 1-D surface profile of these material pile-ups or bulges on either side of the micro-dimple can be represented geometrically simply by a truncated semi-circle, as shown in Figure 2.18. The initial contact patch on the top of the micro-dimples has been shown schematically in a top view of one micro-dimple in Figure 2.19.

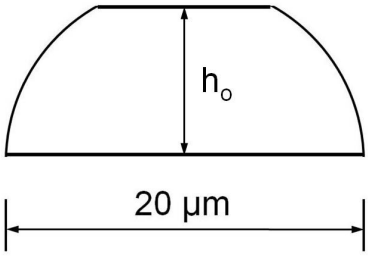

Figure 2.18: Simple geometrical representation of the 1-D surface profile of a material pile-up on either side of the micro-dimple

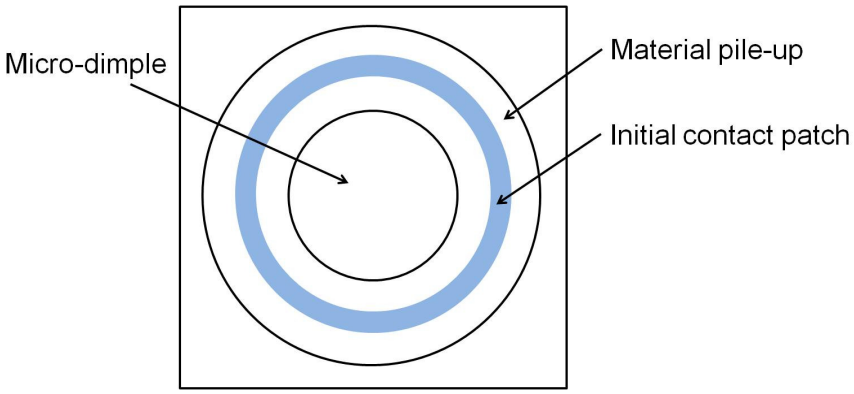

Figure 2.19: Schematic of the top-view of one micro-dimple showing the initial contact patch

From Figure 2.15 it can be seen that the height of the material pile-ups of bulges, represented as h_o in the simple geometrical schematic of Figure 2.18, are of the order of the depth of the micro-dimples for the different texture patterns. Table 2.2 shows the height parameters h_o for the different texture patterns.

Table 2.2: Height parameter h_o for the different texture patterns

Pattern	h_o
A1	9
B1	6
C1	4

Using the information in Table 2.2 and the simple geometrical representation in Figure 2.18, the initial contact patch area can be easily calculated. Thus, the actual area of contact and hence the contact pressure can be calculated. In this work, typically all experiments are performed at a normal load of 178 N. Table 2.3 presents the initial contact area and pressure for the different texture patterns. These simplistic calculations are useful in giving an idea about the order of contact pressures, especially immediately after the initial contact occurs.

It should be noted that the contact pressure calculations are based on assumption that all material pile-ups are similar with same heights which is clearly not the case as can be seen in Figure 2.15. For comparison, maximum contact pressures based on hertzian calculations (assuming $E_{\text{cast iron}}$ = 140 GPa and $\upsilon_{\text{cast iron}}$ = 0.25) and are also performed. Note that for hertzian calculations, the 1-D geometrical representation of the material pile-up as a truncated semi-circle is no longer valid. Instead, the material pile-up can be approximated as a toroid around the micro-dimple making a line contact with the disk. The nominal contact pressure of the untextured surface, for a normal load of 178 N, can be easily calculated and is found to be 5.7 MPa. The calculated contact pressures based on the simplistic geometrical representation of the material pile-ups as well as hertzian calculations are presented in Table 2.3 as a ratio over the nominal contact pressure for the untextured surface.

Table 2.3: Calculated initial contact area and contact pressures for different texture patterns based on simple geometrical representation of micro-dimples and hertzian calculations expressed as a ratio over the nominal contact pressure for untextured surface

Pattern	No. of micro-dimples	Total contact area (mm^2)	Contact Pressure (MPa)	Contact Pressure/Nominal Pressure	Hertzian Contact Pressure/Nominal Pressure
A1	1241	2.04	87.25	15.3	235.79
B1	552	1.66	107.23	18.81	332.11
C1	552	1.91	93.19	16.35	293.51
A2	4962	8.15	21.84	3.83	117.54
B2	2205	6.65	26.77	4.69	166.14
C2	2205	7.62	23.36	4.09	146.84

Usually in the literature, researchers deal with the issue of material pile-ups or bulges around the micro-dimples by polishing the surface after the texturing has been carried out. But, that includes an additional process step and adds to the cost when the technology is scaled up to be used on a component level. Moreover, the process has to be controllable. For example, if some textures have shallow micro-dimples then they could be partially or fully removed by polishing if it is not well controlled. So, for all the experiments done in this study no attempt was made to polish the surfaces and remove the material pile-ups or bulges. All textured pins were used as-received from MLPC Inc. This would also highlight the importance of the material pile-ups and their effect on the tribological behavior.

CHAPTER 3: WEAR EXPERIMENTS IN THE PRESENCE OF REFRIGERANT ENVIRONMENT

3.1 Objective

To evaluate the tribological behavior of sliding interfaces, wear experiments are commonly conducted with a constant load and a specific sliding speed for a set duration. The critical outcomes of such experiments are friction coefficient and wear rate. For compressor realistic testing conditions, such experiments are routinely used for testing refrigerants, lubricants and advanced material systems like surface coatings. Direct comparison between different types of coatings, lubricants, refrigerants can be done by comparing the friction coefficient and wear rate under identical conditions of testing.

The objective of constant load wear experiments for surface textured pins is to understand the tribological behavior of such pins in compressor realistic conditions. Such experiments would also facilitate comparison with other surface engineering solutions such as hard and soft polymeric coatings that are also under investigation to be used to improve the tribological performance of critical tribo-contacts in compressors.

3.2 Experimental Procedure

Tribological tests were conducted in a pin-on-disk configuration using an Ultra High Pressure Tribometer (UHPT), shown in Figure 3.1. The UHPT is a custom-designed tribometer capable of handling high chamber pressures, which is essential for tribological testing in the presence of refrigerant R-744. It can be pressurized up to 13.8 MPa (2000 psi).

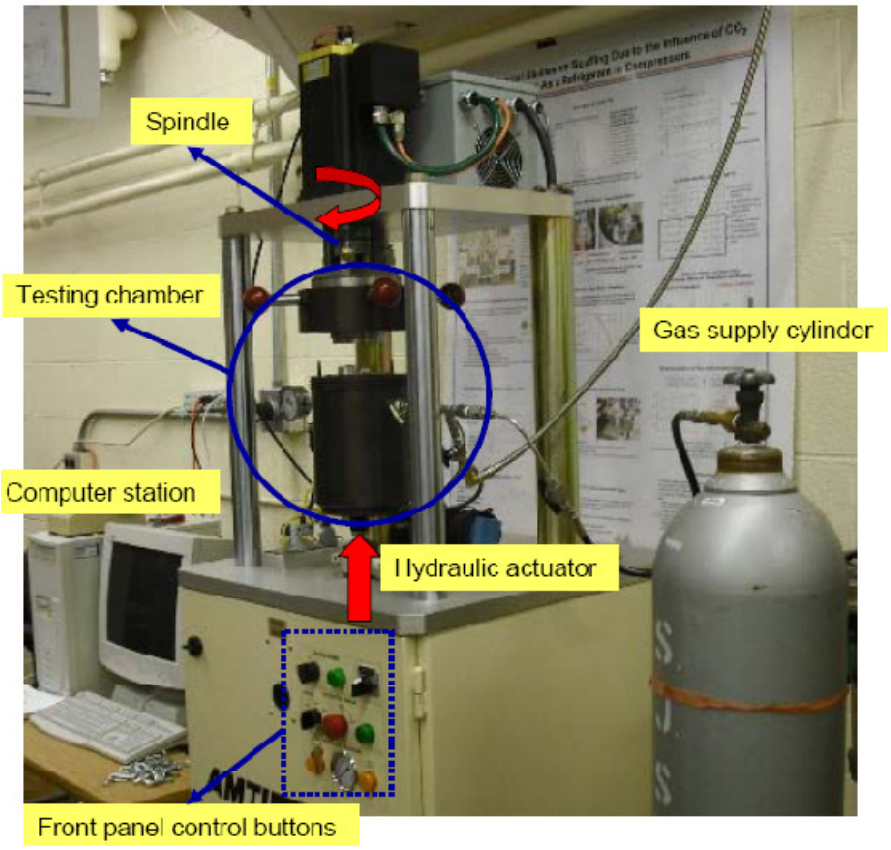

Figure 3.1: The Ultra High Pressure Tribometer (UHPT)

The lower part of the UHPT is hydraulically actuated and controlled in a closed loop fashion. The testing chamber (shown in Figure 3.2) consists of an upper rotating part and lower stationary part. A six-axis strain gauge force transducer (covered by the aluminum plate in Figure 3.2) in-situ measures the normal (Fz) and tangential forces (Fx and Fy). By choosing the appropriate transducer, normal loads as high as 4450 N can be applied. Rotational speeds up to 2000 rpm can be applied by the AC servo control motor.

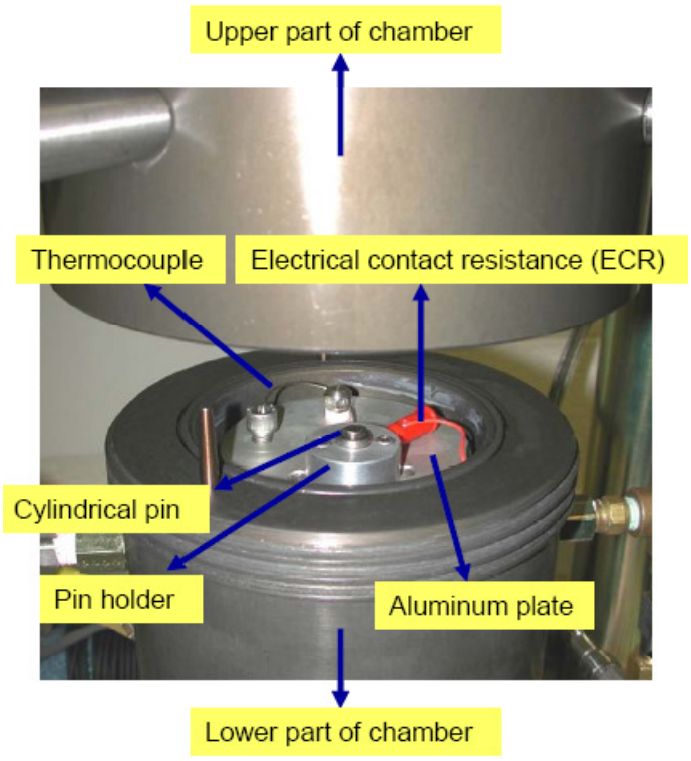

Figure 3.2: Testing chamber of the UHPT

There is an arrangement to measure the near contact temperature by means of a thermocouple inserted into a miniature hole drilled up to 2 mm below the surface at the bottom of the pin. In addition, the temperature inside the chamber can be controlled from 0 °C to 120 °C by re-circulating a heat transfer fluid.

The UHPT has been used earlier for the tribological testing of gray cast iron materials in the presence of R-744 (CO_2) refrigerant [47, 48]. Nunez et al. [5] conducted studies at different phases (such as gas, liquid, trans-critical) of R-744 using the UHPT with cast iron pins and disks at 89N load and 2.4 m/s sliding speed under unlubricated condition to investigate the lubricity effect of R-744. For tests conducted at room temperature, they reported that the average friction coefficient values ranged from 0.11 to 0.17 for R-744 at chamber pressures of 2.75, 4.13 and 5.51 MPa. However, as the

chamber pressure was increased to 6.89 MPa, the friction coefficient decreased to approximately 0.07 exhibiting a positive lubricity or "superlubricity" effect. However, they noted that at the lower range of tested chamber pressures, the friction performance was poor. They also concluded that the chamber pressure was more significant than the actual amount of R-744 unless it was below 10 grams. Thus, as a starting point in this study, preliminary tests were conducted under unlubricated conditions with the textured and untextured pins at 89N load and 2.4 m/s sliding speed in presence of refrigerant R-744 at a lower chamber pressure of 1.93 MPa. Figure 3.3 shows the friction coefficient and near contact temperature for a test done with an untextured surface to establish baseline performance.

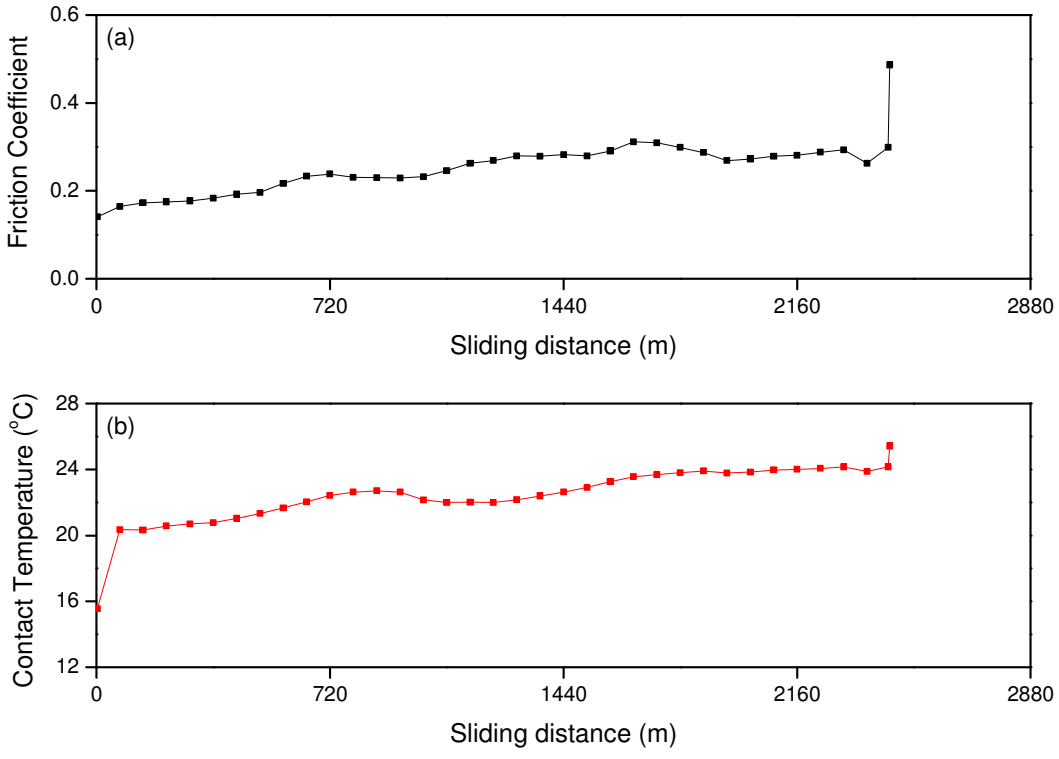

Figure 3.3: (a) Friction coefficient and (b) Near contact temperature of untextured pin tested in unlubricated condition at 89 N normal load and 2.4 m/s sliding speed in the presence of R-744 at a chamber pressure of 1.93 MPa

Even at a low normal load of 89 N, the interface was unable to survive the entire duration of testing and scuffed at approximately 2500 meters. Scuffing is characterized by the instantaneous and simultaneous increase in friction coefficient and near contact temperature, as shown in Figure 3.3. Such a performance was expected, since bare materials cannot operate for long duration of time under unlubricated condition. It is also in line with the findings of Nunez et al. [5] that the presence of R-744 doesn't induce any positive lubricity unless at high chamber pressures.

Texture pattern A1 was used for the comparison and tested under identical conditions in unlubricated condition. However, the textured pin scuffed instantly as the test was initiated. Figure 3.4 shows the optical images of the scuffed surfaces of the untextured pin and texture pattern A1.

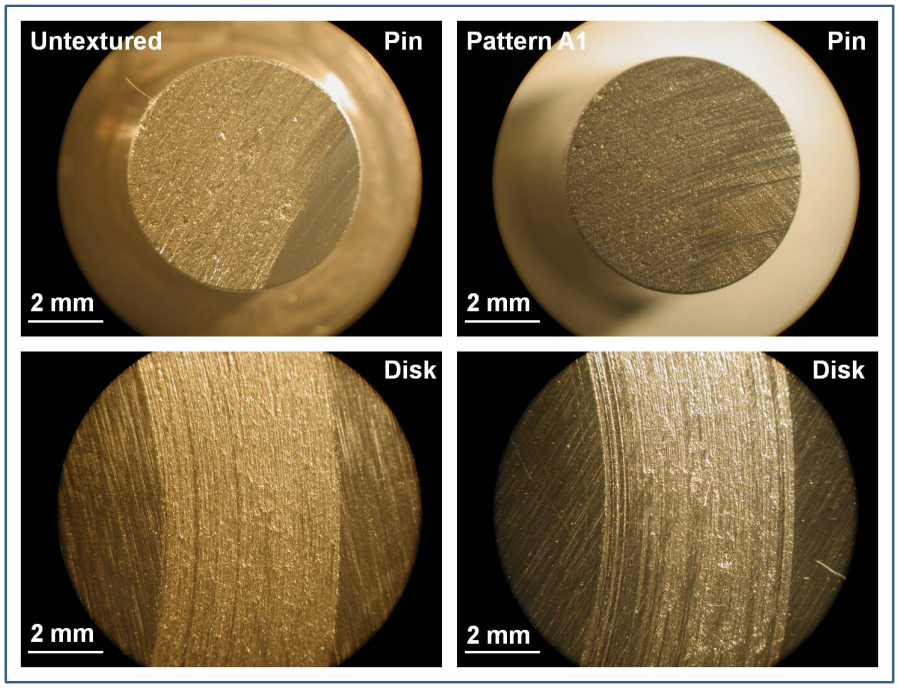

Figure 3.4: Optical images showing the scuffed surfaces on the pins and wear tracks on the disks

The instant failure of the texture pattern A1 can be attributed to the material pile-ups or bulges around the micro-dimples. The initial contact between the pin and the disk occurs at the top of the material pile-ups or bulges, which means that the contact pressure is much more than that experienced by the untextured pin. In the absence of lubrication, as the test is initiated, the pile-ups get worn instantly and generate loose wear debris that gets trapped between the sliding interfaces causing aggressive three-body abrasion resulting in instant scuffing of the textured pin. Thus it is clear that under unlubricated sliding condition texturing deteriorates the tribological performance, if the material pile-ups or bulges around the dimples are still present. It is, however, not known if removing the material pile-ups by polishing could have any beneficial effect under unlubricated condition and needs to be investigated in the future. One way to get around this problem is to use lubrication, which is the main goal of this work.

The critical components of the compressors are known to be operating primarily in the boundary/mixed type of lubrication regime [11,12]. Thus, constant load boundary/mixed type of lubrication tests were planned. Boundary/mixed lubrication regime was achieved by directly applying one drop of oil, quantified by the mass of the oil, at the contact interface. Figure 3.5 shows 23 mg of PAG lubricant (one drop) added on top of the pin surface before testing. Clearly, the volume of the lubricant is more than the volume of the micro-dimples, which means enough lubricant is available to completely fill the micro-dimples when contact occurs.

Figure 3.5: One drop of PAG applied on to the pin surface before test

Two normal loads were used such as 89N and 178N to compare between untextured pins and the texture patterns. The contact pressures for such loading depends on the texture pattern as the initial contact occurs at the top of the material pile-ups of bulges around the micro-dimples and were discussed in Chapter 2. Testing was done at a sliding speed of 2.4 m/s, ambient laboratory conditions of 16-20 °C and 40-50% RH, and 1.93 MPa of R-744. Prior to testing, the samples were immersed in a pool of acetone and cleaned ultrasonically, followed by rinsing with propanol and blow drying with warm air.

Two types of experiments were performed to understand the tribological performance of surface textured specimens under compressor realistic operating conditions: *Wear experiments* and *Durability experiments*.

3.3 Wear experiments

Wear experiments were designed as one hour long boundary/mixed lubricated constant load tests. It should be emphasized that under realistic compressor conditions, usually test duration of 20 mins (which at 2.4 m/s sliding speed corresponds to a sliding distance of 2880 meters, as in Figure 3.3) is sufficient to extract the key performance

parameters such as friction coefficient and wear rate. However, one hour long tests were planned so as to take care of any aggravated running-in due to the material pile-ups around the micro-dimples resulting from surface texturing. Such tests were also designed to help compare the untextured pins with the texture patterns and also between the different texture patterns, refrigerants and lubricants combinations.

Comparison between the untextured pin and texture patterns was done at 89N normal load at a sliding speed of 2.4 m/s in the presence of R-744 at a chamber pressure of 1.93 MPa. All the texture patterns were tested at 178N normal load. Boundary/mixed/starved lubrication was achieved by directly applying one drop of PAG lubricant at the interface. The amount of lubricant was measured and found to be 23 mg.

Figure 3.6 shows the friction coefficient and near contact temperature as a function of the sliding distance for untextured pin and texture pattern A1. The untextured pin survived the duration of the testing under a normal load of 89 N. However, it can be noted that the friction coefficient begins to rise after ~ 4,000 m of sliding distance. This is indicative of the loss of lubricant from the interface as the test progressed, causing greater metal-to-metal contact leading to higher friction

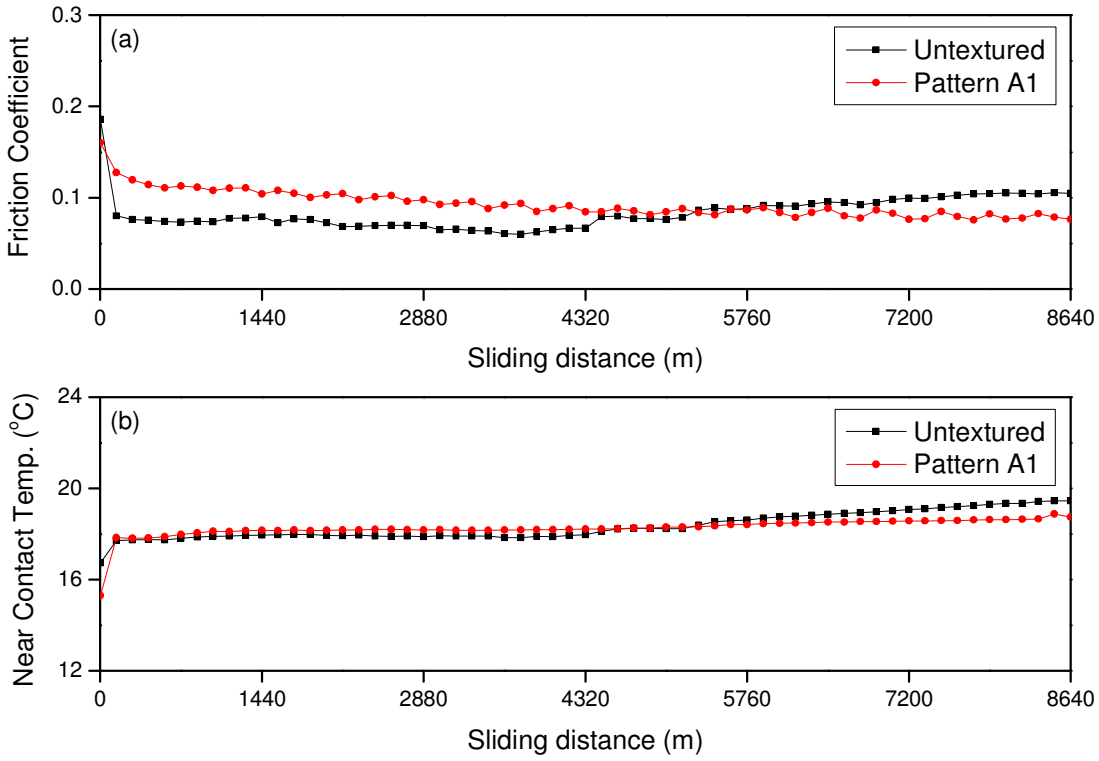

Figure 3.6: Comparison of (a) Friction coefficient and (b) Near contact temperature of texture pattern A1 against an untextured surface at 89 N normal load and 2.4 m/s sliding speed in the presence of R-744 at a chamber pressure of 1.93 MPa with 23 mg of PAG lubricant directly applied at the interface

On the other hand, the friction coefficient of pattern A1 decreases from an initial high value to about 0.08 during the later part of the test duration. During the initial part of the test, the friction coefficient of the textured pin is higher than the untextured pin. This is because the surface of the textured pin is irregular due to the material pile-up around the micro-dimples, thus it takes more time to reach steady state than the nominally flat untextured pin. However, as the test progresses the micro-dimples on the surface of the textured pin serve as lubricant reservoirs and supply lubricant to the pin-disk interface leading to improved friction performance compared to the untextured pin. The near contact temperatures in both cases were fairly similar and followed the same trend as the friction coefficient.

Although the friction performance of the untextured pin was not as good as the textured pin, it survived the entire duration of the test. To make the testing conditions more aggressive, as the next step, experiments were conducted at double the initial normal load i.e., 178 N. To establish baseline performance, an untextured surface was tested first. As the load was increased to 178 N, the friction coefficient of the untextured surface increased sharply, shortly after the test was initiated. To verify that it is indeed the case, experiments with the untextured pin was repeated three times and similar performance was observed, as shown in Figure 3.7.

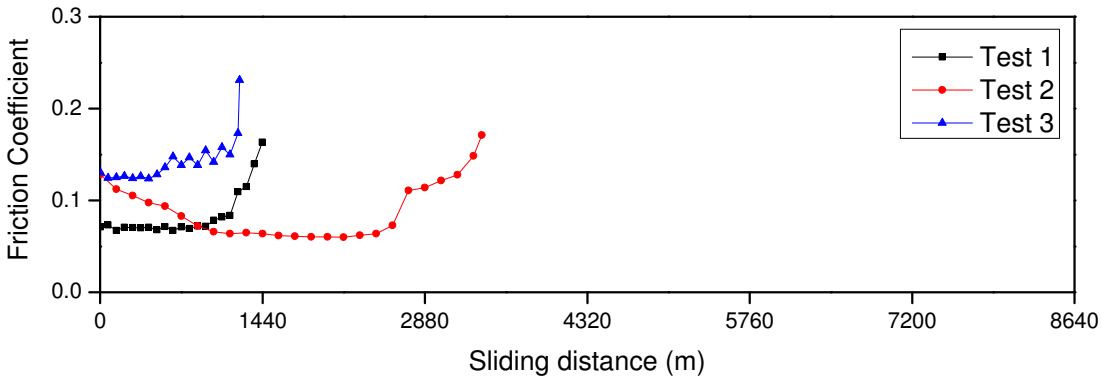

Figure 3.7: Friction performance of an untextured surface tested three times at 178 N normal load and 2.4 m/s sliding speed in the presence of R-744 at a chamber pressure of 1.93 MPa with 23 mg of PAG lubricant directly applied at the interface

In all instances, a sharp increase in the friction coefficient was observed and was simultaneously accompanied by large vibrations at the pin-disk interface shortly after initiating the test. The UHPT was stopped immediately to avoid any damage to the sensitive force transducer. The difference in the survival duration and the friction coefficient between the three tests could be attributed to the differences in the surface conditions of the particular untextured pin used for the study as well as the slight variation in the amount of lubricant applied. However, clearly untextured surfaces fail to

operate successfully at a load of 178 N which points to the inability of a nominally flat surface to hold lubricant at the interface.

Figure 3.8 shows the friction coefficient and near contact temperature of the texture patterns A1, B1, C1 compared against the untextured surface tested under identical conditions.

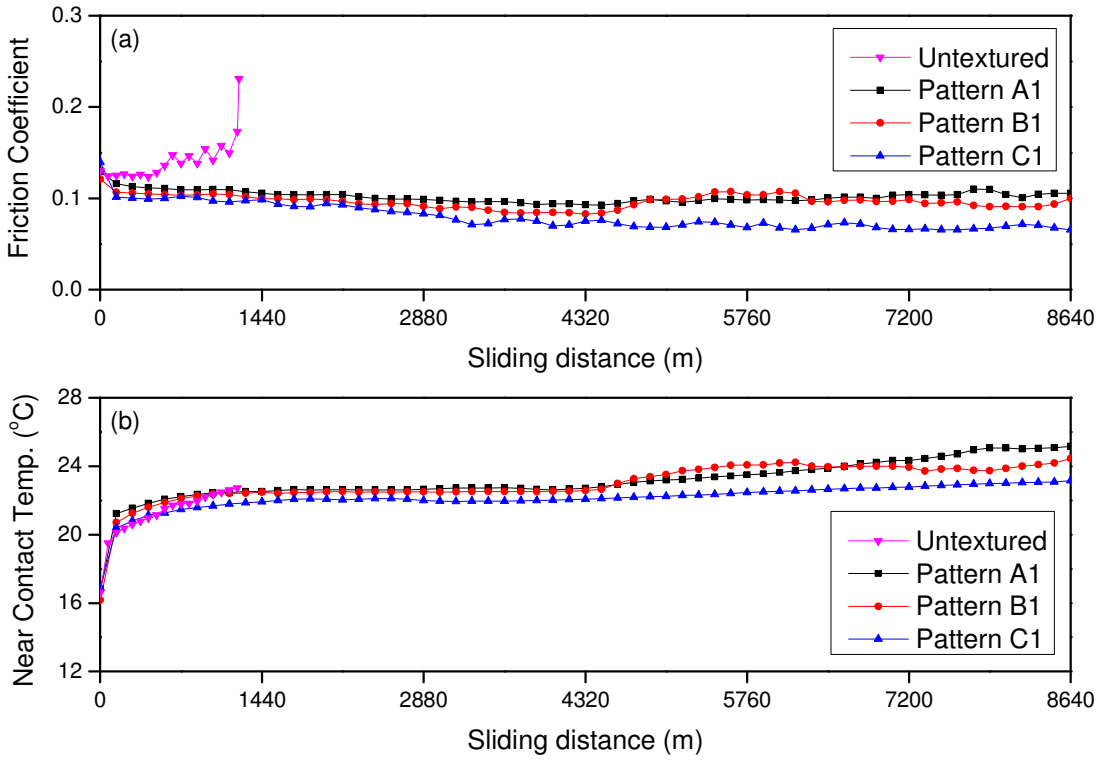

Figure 3.8: (a) Friction coefficient and (b) Near contact temperature of texture patterns A1, B1 and C1 compared against an untextured surface at 178 N normal load and 2.4 m/s sliding speed in the presence of R-744 at a chamber pressure of 1.93 MPa with 23 mg of PAG lubricant directly applied at the interface

All the three texture patterns A1, B1 and C1 were able to survive the entire duration of testing. The initial running-in period of all the texture patterns are identical, beyond which there was a difference between the friction performance of the texture patterns. To calculate the average friction coefficient values, data from 5,760 meters to

8,640 meters was used, which corresponds to the last 20 mins of the test duration. The average friction coefficient values for patterns A1 and B1 were similar at 0.09-0.1 while that of pattern C1 was the lowest with a value of approximately 0.06. Thus, it was found that the texture patterns with larger diameter and smaller depth of micro-dimples behaved better under the tested conditions. The near contact temperatures were fairly similar and followed the same pattern as the friction coefficient, as can be seen in Figure 3.8.

To understand the role of the micro-dimples area density on the friction performance, similar feasbility tests were conducted with patterns A2, B2 and C2. These patterns have the same geometry (dimple diameter and depth) but have an area density of 20% compared to 5% in case of A1, B1 and C1. Figure 3.9 shows the friction coefficient and near contact temperature of the texture patterns A2, B2, C2 tested under identical conditions. Compared to texture patterns A1, B1 and C1, the friction behavior of these patterns was more erratic, especially for pattern A2 and C2.

In general, increasing the area density of the micro-dimples from 5% to 20% made matters worse. The average friction coefficient values of patterns A2, B2 and C2 are higher when compared to the earlier patterns. Pattern A2 showed the highest variation, first increasing then decreasing and finally increasing slightly again towards the end of the test. The initial running-in behavior of pattern A2 and the higher friction for these patterns may be explained by the fact that they had greater number of micro-dimples on the surface, as the area density was larger. So, during sliding, a lot of wear debris is generated leading to such a behavior. This is corroborated by the fact that the near contact temperatures for patterns A2, B2 and C2 are relatively higher than patterns A1, B1 and C1. Wakuda et al. [39] conducted boundary lubricated experiments with

different texture geometries and reported that the friction coefficient increased when the area density was increased. However, they attributed it to the increased contact pressure due to reduced contact area as the micro-dimples area density increased. Kovalchenko et al. [42] also reported an increase in the friction coefficient values as the area density of the dimples was increased.

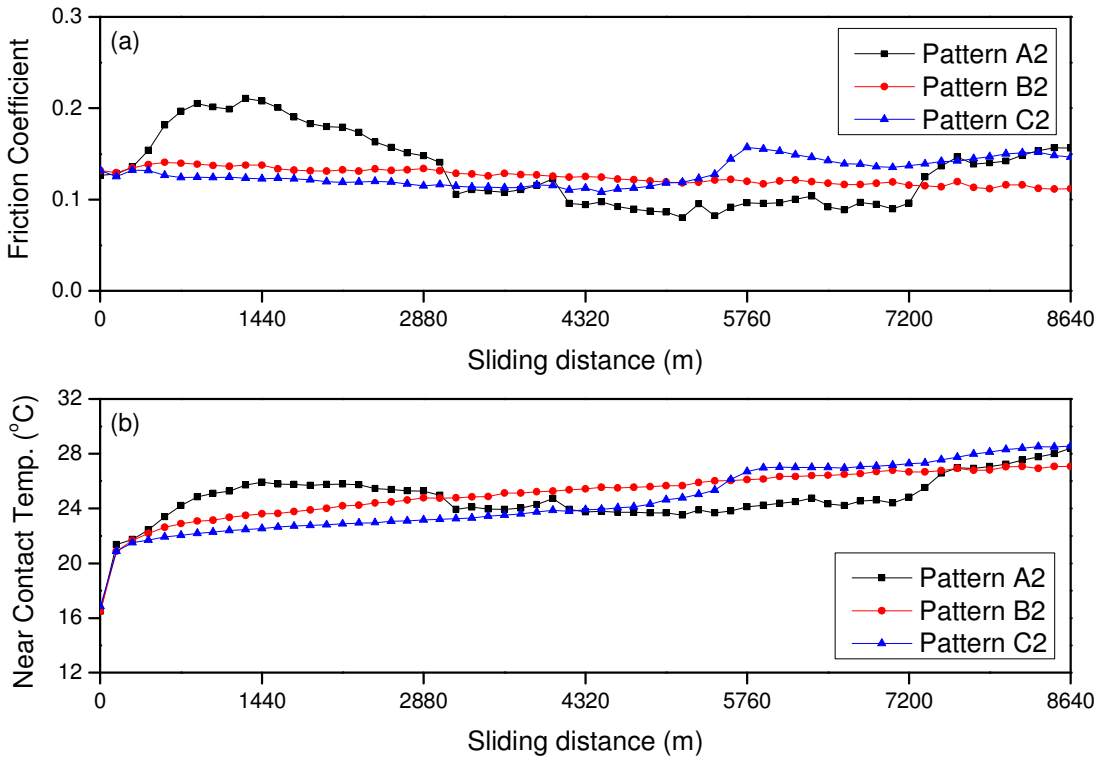

Figure 3.9: (a) Friction coefficient and (b) Near contact temperature of texture patterns A2, B2 and C2 at 178 N normal load and 2.4 m/s sliding speed in the presence of R-744 at a chamber pressure of 1.93 MPa with 23 mg of PAG lubricant directly applied at the interface

Figure 3.10 summarizes the friction coefficient and contact temperature of all the patterns tested and Figures 3.11 - 3.14 show the optical images of the disks and pins after the wear experiments.

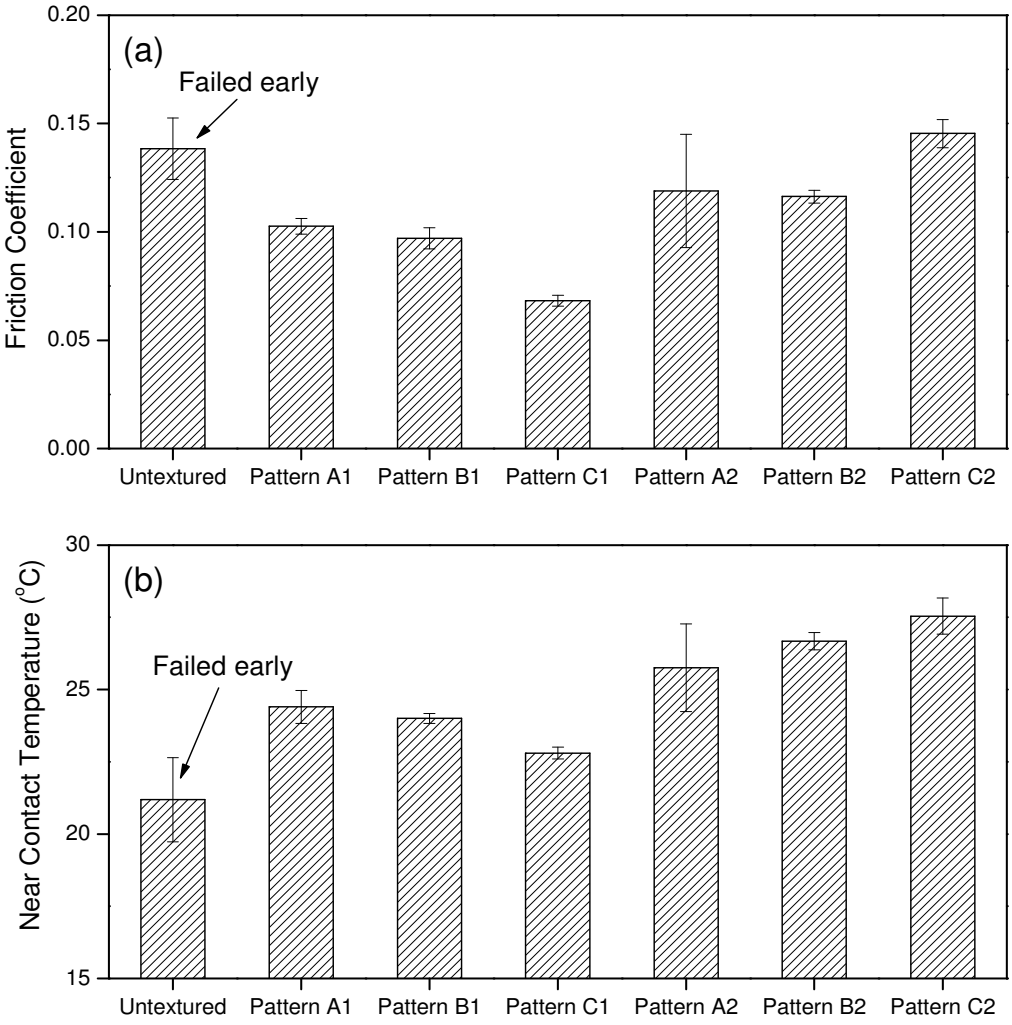

Figure 3.10: Comparison of (a) Friction coefficient and (b) Near contact temperature for all the untextured and texture patterns tested under identical conditions

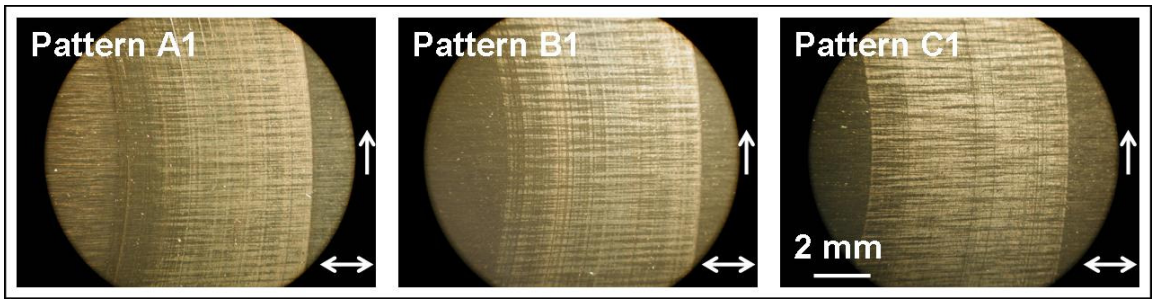

Figure 3.11: Optical images of the disks after the wear experiments tested against texture patterns A1, B1 and C1 at a load of 178 N and sliding speed of 2.4 m/s in the presence of R-744 at a chamber pressure of 1.93 MPa with 23 mg of PAG lubricant applied at the interface (Horizontal double arrows indicate direction of machining marks and vertical arrows indicate direction of sliding)

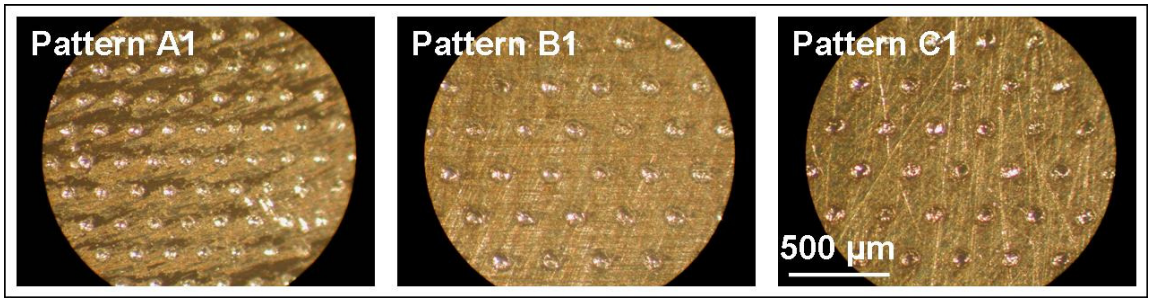

Figure 3.12: Optical images of the texture patterns A1, B1 and C1 after the wear experiments at a load of 178 N and sliding speed of 2.4 m/s in the presence of R-744 at a chamber pressure of 1.93 MPa with 23 mg of PAG lubricant applied at the interface

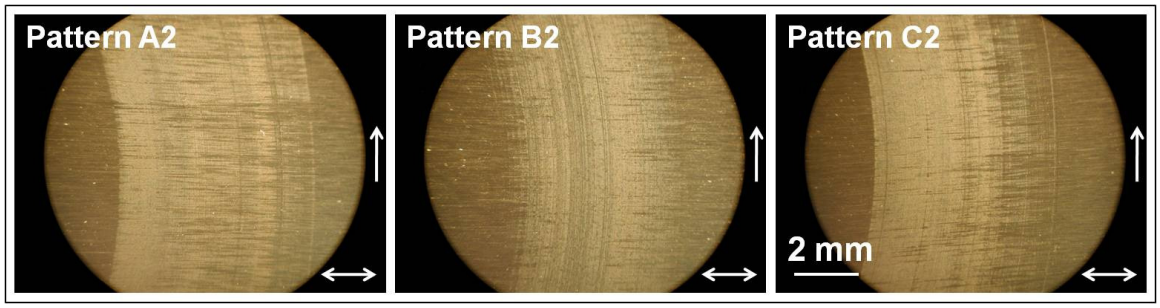

Figure 3.13: Optical images of the disks after the wear experiments tested against texture patterns A2, B2 and C2 at a load of 178 N and sliding speed of 2.4 m/s in the presence of R-744 at a chamber pressure of 1.93 MPa with 23 mg of PAG lubricant applied at the interface (Horizontal double arrows indicate direction of machining marks and vertical arrows indicate direction of sliding)

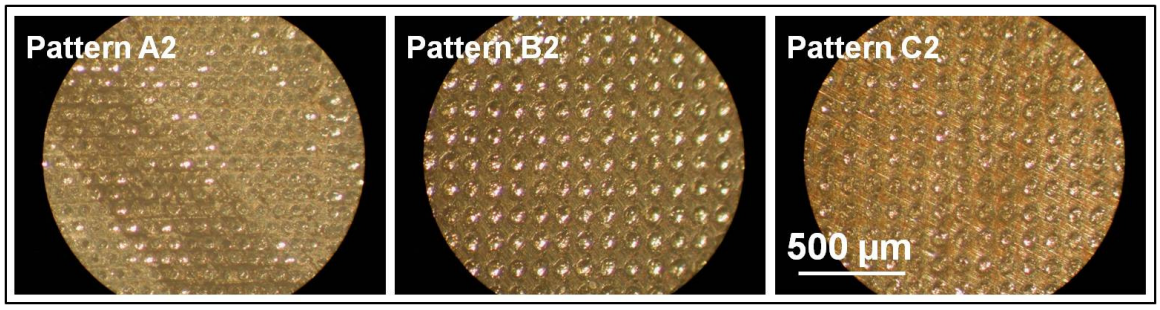

Figure 3.14: Optical images of the texture patterns A2, B2 and C2 after the wear experiments at a load of 178 N and sliding speed of 2.4 m/s in the presence of R-744 at a chamber pressure of 1.93 MPa with 23 mg of PAG lubricant applied at the interface

From Figure 3.10, it is clear that all the texture patterns perform better than the untextured surface which failed early during the testing. Texture patterns A2, B2 and C2

had higher friction coefficient compared to patterns A1, B1 and C1. The texture geometries namely diameter and depth of the micro-dimples are the same for these two sets of patterns, the difference being the area density of the micro-dimples. As the area density increases, the number of micro-dimples increases which means that the wear debris generated will be more when sliding occurs. This is further confirmed from the optical images of the texture patterns in Figures 3.12 and 3.14. The texture patterns A2, B2 and C2 appear to have worn out more than the patterns A1, B1 and C1. This could be possible if there were more wear debris acting as third body abrasives. Later, in Section 3.5, the small wear is quantified through surface profile measurements of the pins before and after testing and the wear rate is calculated.

Among the two sets of texture patterns, the trend in friction coefficient behavior appears to be the opposite. The friction performance of pattern C1 is the best among A1, B1 and C1 while pattern C2 is the worst among A2, B2 and C2. In both cases, however, patterns A1, B1 and A2, B2 exhibit similar performance. Although the lubricant storage ability of pattern C1 is the least among A1, B1 and C1, as it has the shallowest micro-dimples, the wear debris at the interface would also be the least, as it has the smallest material pile-ups of bulges. Thus, the friction performance in such constant load experiments may be attributed to the trade-off between the lubricant storage ability of the micro-dimples and the wear debris generated during the sliding experiments, which in turn depend on the area density of the micro-dimples.

It appears that below some critical area density, the friction performance is dominated by the material pile-ups or bulges around the micro-dimples while for higher area density, the lubricant storage ability is the dominant factor. Additional experiments

should be performed in the future with an aim to identify such critical area density and to optimize the texture geometries for best performance under compressor realistic conditions. Kovalchenko et al. [42] conducted some studies with LST samples with and without post-texturing lapping to remove the material pile-ups or bulges around the micro-dimples. They found that samples without the lapping displayed higher friction coefficient and recommended removing the pile-ups before optimizing the texture geometries for best performance. Thus, the effect of removing the material pile-ups or bulges before the tests on the tribological performance under compressor realistic conditions should be explored in the future through further experimental studies and analysis.

3.3.1 Effect of sliding speed

The critical sliding interfaces in some compressors operate at really high sliding speeds. This puts an extra stress on the interface making it more prone to failure, especially when there is limited lubrication. Sliding speed also has an effect on the maximum load the interface can withstand. Scuffing resistance of a sliding interface typically follows the relationship PV = constant. This means that as the sliding speed increases, the scuffing resistance or the maximum load carrying capacity of the interface decreases.

The objective of this study was to evaluate the performance of surface texturing at different sliding speeds. Tests were conducted at three different speeds, namely 0.96 m/s, 2.4 m/s and 3.84 m/s to investigate the effect of sliding speed. Representative tests were conducted with some of the textured patterns (B1, B2 and C2) and compared against an

untextured pin. B1 and B2 were identical in the micro-dimple geometry, the difference being in the area density of the micro-dimples on the pin surface. So, they were selected so as to understand the effect of area density. B2 and C2 were selected to understand the role of micro-dimple geometry such as dimple depth. They had the same diameter (60 µm) and area density (20 %) but differed in the dimple depth. Pattern B2 had a depth of 7.5 µm while C2 had a depth of 4 µm.

All the tests were conducted at a normal load of 178 N and ambient laboratory conditions of 16-20 °C and 40-50% RH in the presence of 1.93 MPa of R-744. 23 mg of PAG was added directly at the interface before initiating the test.

Figure 3.15 shows the friction coefficient and near contact temperature for the untextured and textured pins tested at a sliding speed of 0.96 m/s. At this lower speed, the untextured pin is able to survive the entire duration of the test without failure. However, there is a lot of variation and the friction behavior of the untextured pin is somewhat erratic, especially towards the end of the experiment. This is probably because as the test proceeds, the interface slowly runs out of lubricant. The behavior of all the textured pins is identical with all the textured pins exhibiting similar friction coefficient values. The near contact temperatures of all the pins are fairly similar too, indicating similar behavior at low speed.

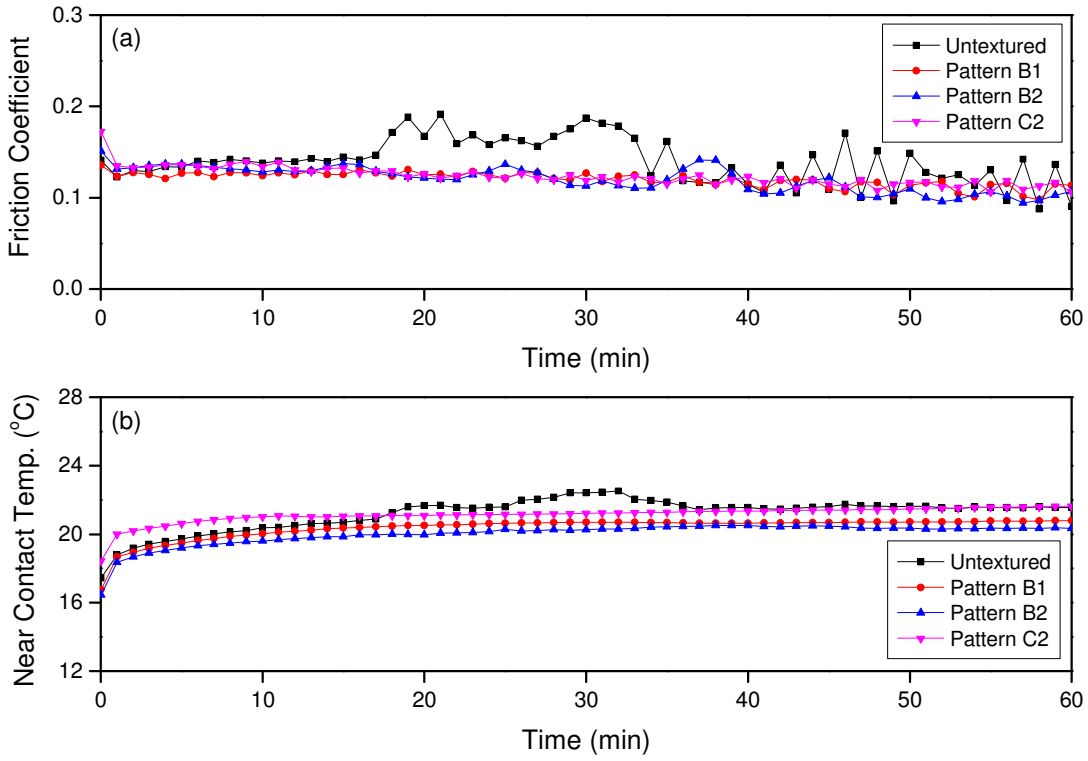

Figure 3.15: Comparison of (a) Friction coefficient and (b) Near contact temperature of different texture patterns against an untextured surface when tested at 178 N normal load and 0.96 m/s sliding speed in the presence of R-744 at a chamber pressure of 1.93 MPa with 23 mg of PAG lubricant directly applied at the interface

At a sliding speed of 0.96 m/s, negligible wear occurred on the disk tested against the untextured pin compared to the disks tested against the texture patterns, as can be seen in Figure 3.16. This is because the untextured pin has a nominally flat surface, while the texture patterns have a lot of material pile-ups which causes the initial burnishing of the disk. Figure 3.17 shows the optical images of the untextured surface and texture patterns B1, B2 and C2 after the test. The untextured surface shows only mild burnishing while none of the texture patterns show any sign of significant wear. Only the material pile-ups or bulges around the micro-dimples appear to have been polished.

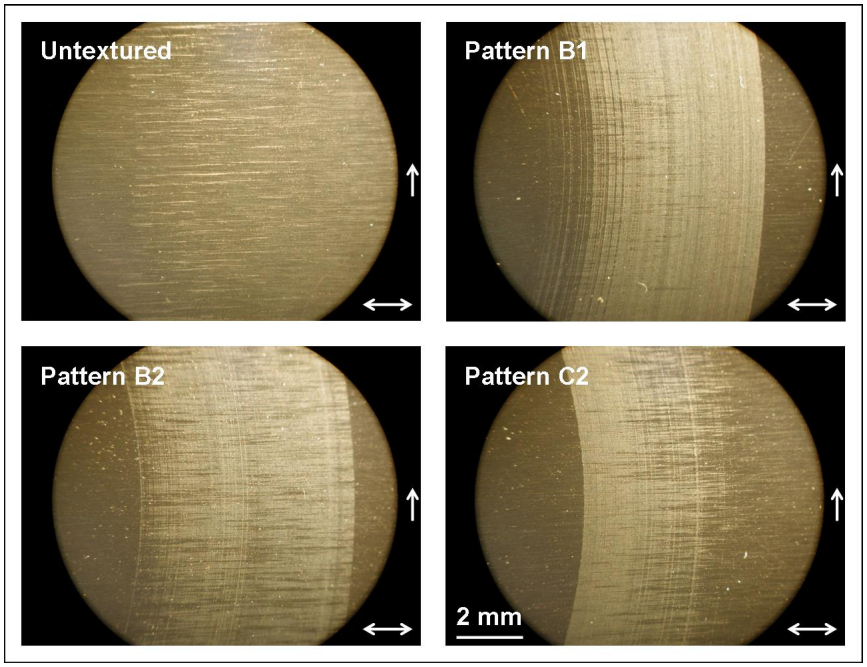

Figure 3.16: Optical images of the disks tested against untextured pin and texture patterns B1, B2 and C2 at a load of 178 N and sliding speed of 0.96 m/s in the presence of R-744 at a chamber pressure of 1.93 MPa with 23 mg of PAG lubricant applied at the interface (Horizontal double arrows indicate direction of machining marks and vertical arrows indicate direction of sliding)

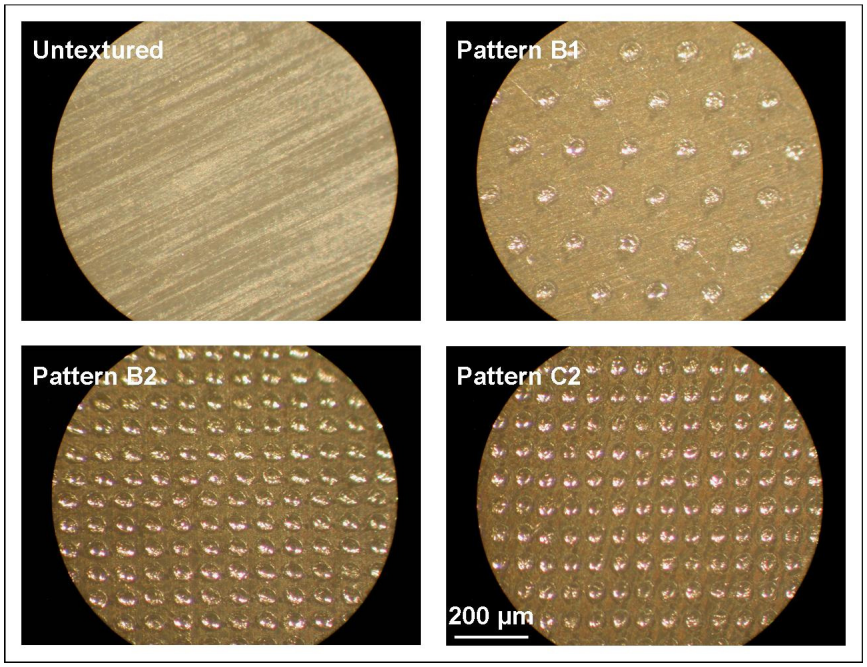

Figure 3.17: Optical images of untextured pin and texture patterns B1, B2 and C2 tested at a load of 178 N and sliding speed of 0.96 m/s in the presence of R-744 at a chamber pressure of 1.93 MPa with 23 mg of PAG lubricant applied at the interface

As the sliding speed is increased to 2.4 m/s, the behavior of the different pins is more distinct, as shown in Figure 3.18. The untextured pin is unable to survive the entire duration of testing and fails prematurely, while all the textured pins tested are able to operate successfully under identical conditions, indicating the positive effect of texturing. Among all the textured pins, clearly pattern B1 is the best performing both in terms of friction coefficient and near contact temperature. Pattern B2 results in a higher friction coefficient than pattern B1, indicating that larger area density of the micro-dimples is detrimental to the friction behavior.

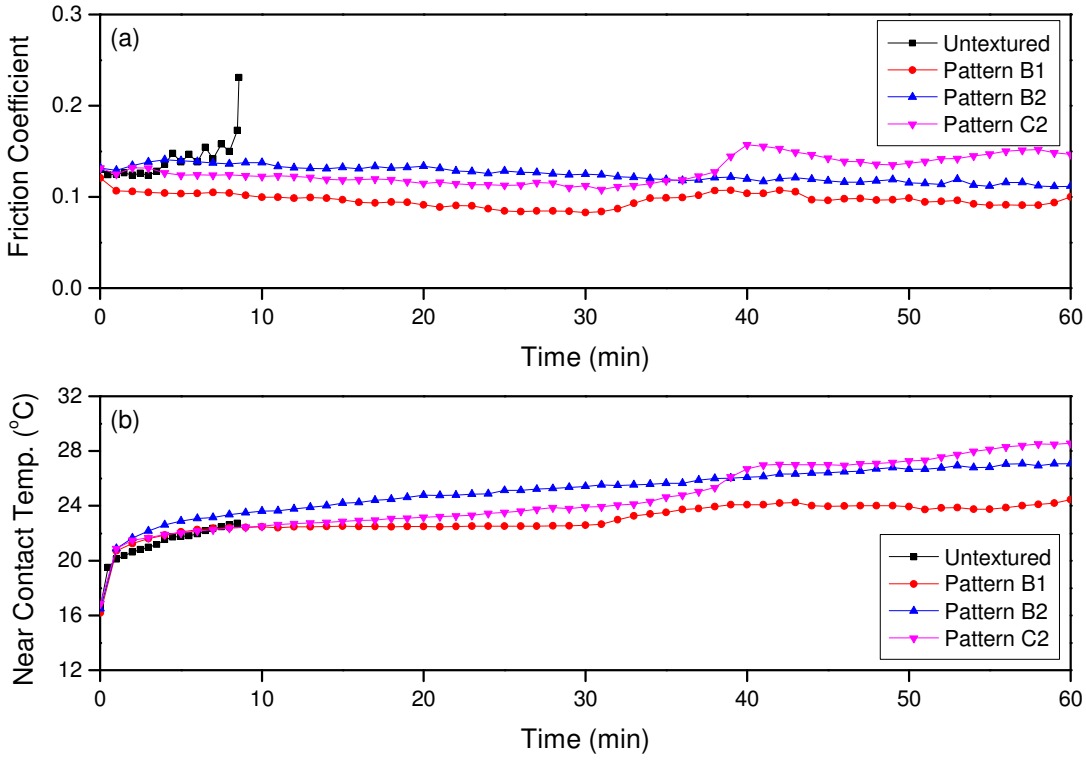

Figure 3.18: Comparison of (a) Friction coefficient and (b) Near contact temperature of different texture patterns against an untextured surface when tested at 178 N normal load and 2.4 m/s sliding speed in the presence of R-744 at a chamber pressure of 1.93 MPa with 23 mg of PAG lubricant directly applied at the interface

It should be noted that although the untextured pin failed prematurely, the wear on the pin and disk was negligible as seen in Figure 3.19 and 3.20. This is because the untextured pin has a nominally flat surface while the texture patterns have material pile-ups which cause the initial burnishing of the counter disk surface. Also, for the untextured pin the test was stopped when the friction coefficient increased sharply and significant vibration was noticed at the interface, to prevent damage to the UHPT.

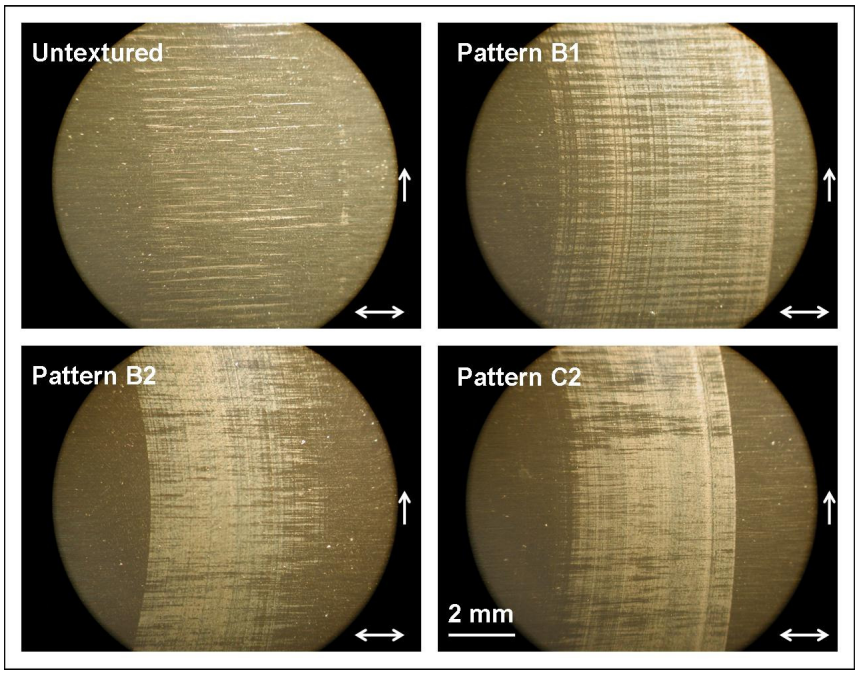

Figure 3.19: Optical images of the disks tested against untextured pin and texture patterns B1, B2 and C2 at a load of 178 N and sliding speed of 2.4 m/s in the presence of R-744 at a chamber pressure of 1.93 MPa with 23 mg of PAG lubricant applied at the interface (Horizontal double arrows indicate direction of machining marks and vertical arrows indicate direction of sliding)

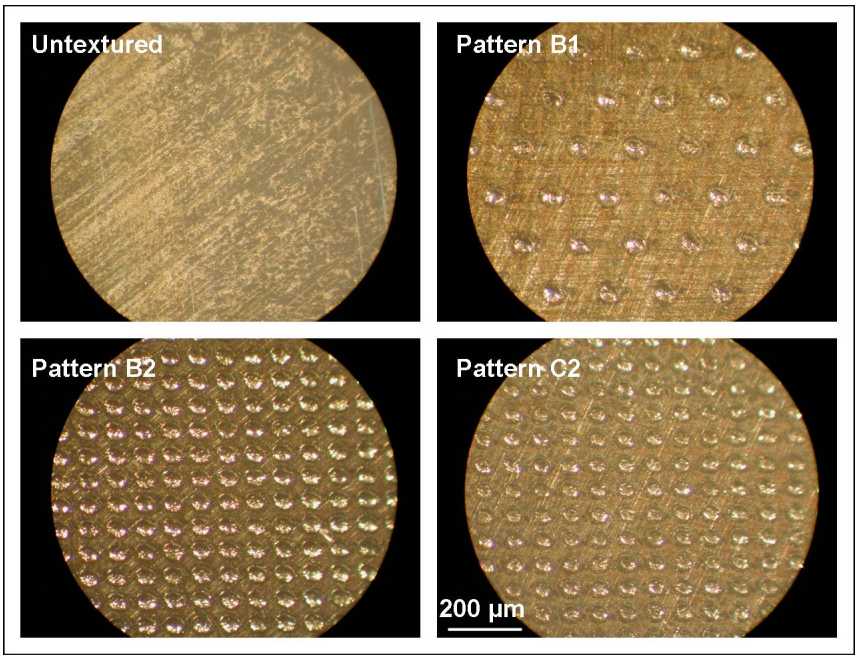

Figure 3.20: Optical images of untextured pin and texture patterns B1, B2 and C2 tested at a load of 178 N and sliding speed of 2.4 m/s in the presence of R-744 at a chamber pressure of 1.93 MPa with 23 mg of PAG lubricant applied at the interface

Pattern C2 has a similar friction behavior as pattern B2 until approximately 40 minutes, after which it increases and is more than that of pattern B2. The trend for pattern C2 is repeated when testing was done at 3.84 m/s, as shown in Figure 3.21. Pattern B2 exhibits an erratic running-in at higher sliding speed, eventually showing lower friction coefficient than pattern C2. Again, pattern B1 shows the best performance at the higher sliding speed of 3.84 m/s. Since the untextured pin was unable to operate at a sliding speed of 2.4 m/s, it was not tested at the higher speed.

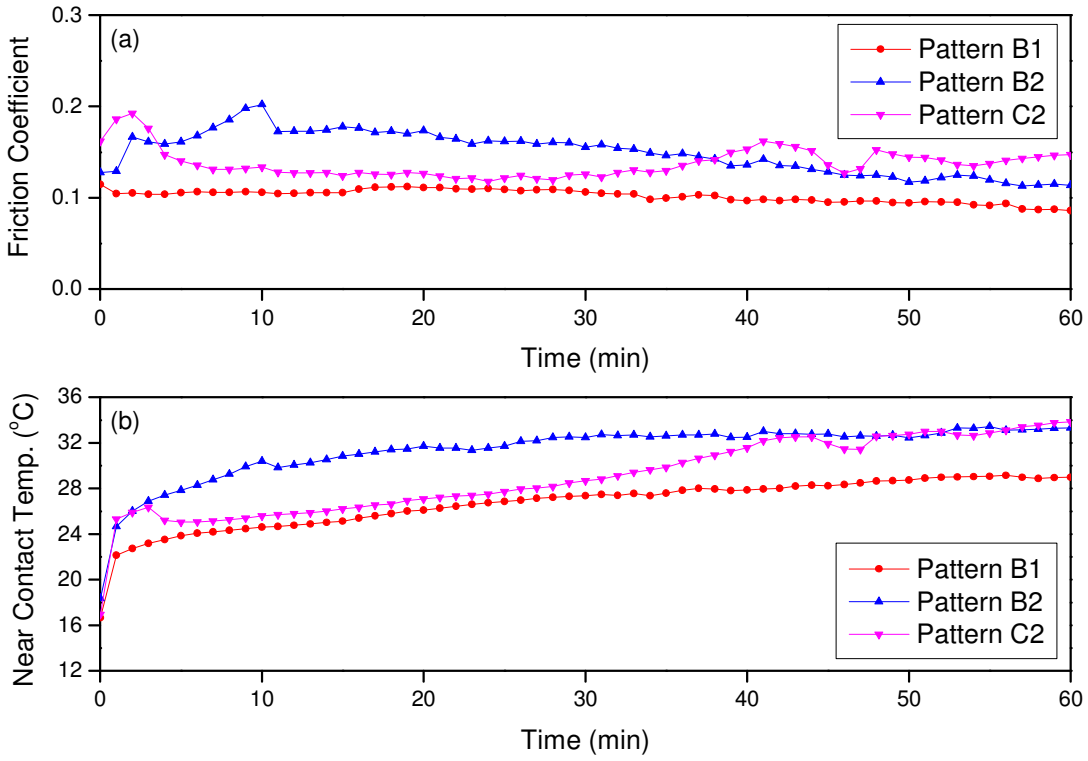

Figure 3.21: Comparison of (a) Friction coefficient and (b) Near contact temperature of different texture patterns when tested at 178 N normal load and 3.84 m/s sliding speed in the presence of R-744 at a chamber pressure of 1.93 MPa with 23 mg of PAG lubricant directly applied at the interface

Even as the sliding speed was increased to 3.84 m/s, the overall wear was insignificant as seen in Figure 3.22 and 3.23. In case of texture pattern C2, however, some polished regions are seen on the pin surface indicating some mechanical contact between the pin and disk. Same is noted in case of the corresponding disk, which appears to have been burnished more that the others.

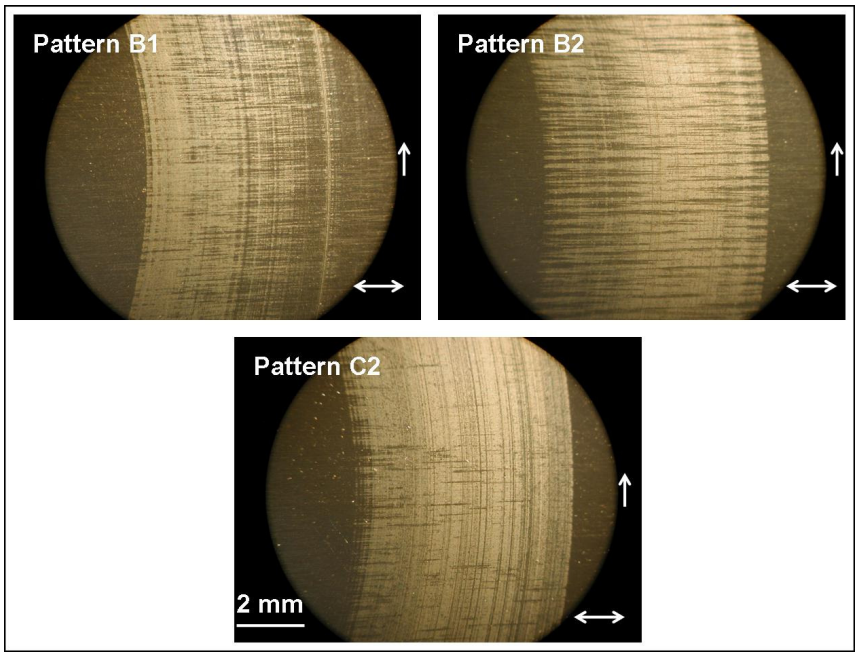

Figure 3.22: Optical images of the disks tested against texture patterns B1, B2 and C2 at a load of 178 N and sliding speed of 3.84 m/s in the presence of R-744 at a chamber pressure of 1.93 MPa with 23 mg of PAG lubricant applied at the interface (Horizontal double arrows indicate direction of machining marks and Vertical arrows indicate direction of sliding)

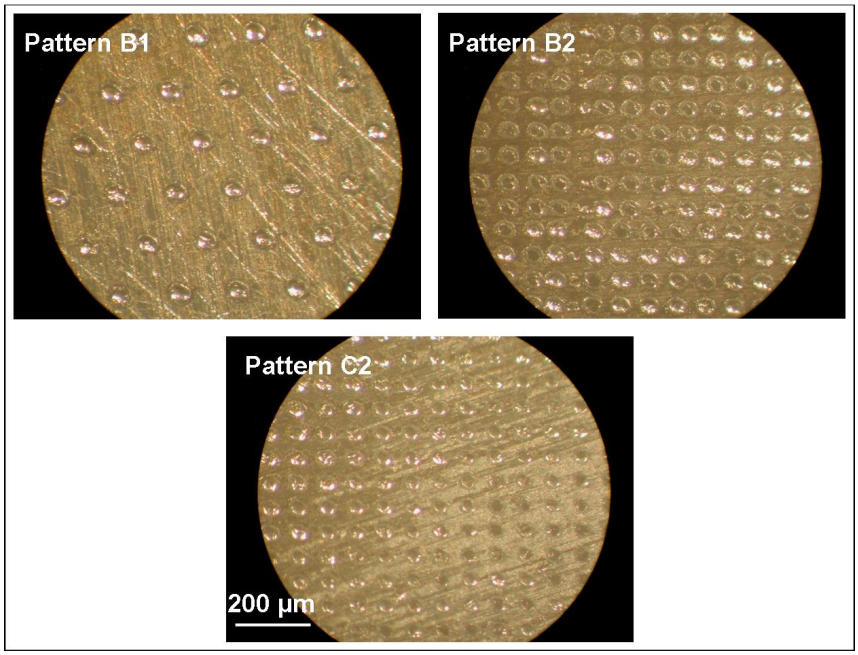

Figure 3.23: Optical images of the texture patterns B1, B2 and C2 tested at a load of 178 N and sliding speed of 3.84 m/s in the presence of R-744 at a chamber pressure of 1.93 MPa with 23 mg of PAG lubricant applied at the interface

The friction performance of the untextured surface and textured patterns is summarized in Figure 3.24, which shows the friction coefficient as a function of the sliding speed for the different surfaces used in the study. The untextured surface failed when tested at 2.4 m/s. So, the friction coefficient value used in Figure 3.24 for untextured pin at 2.4 m/s is the average value till failure occurred. Also, since the untextured surface failed when tested at a sliding speed of 2.4 m/s, it was not tested at a sliding speed of 3.84 m/s.

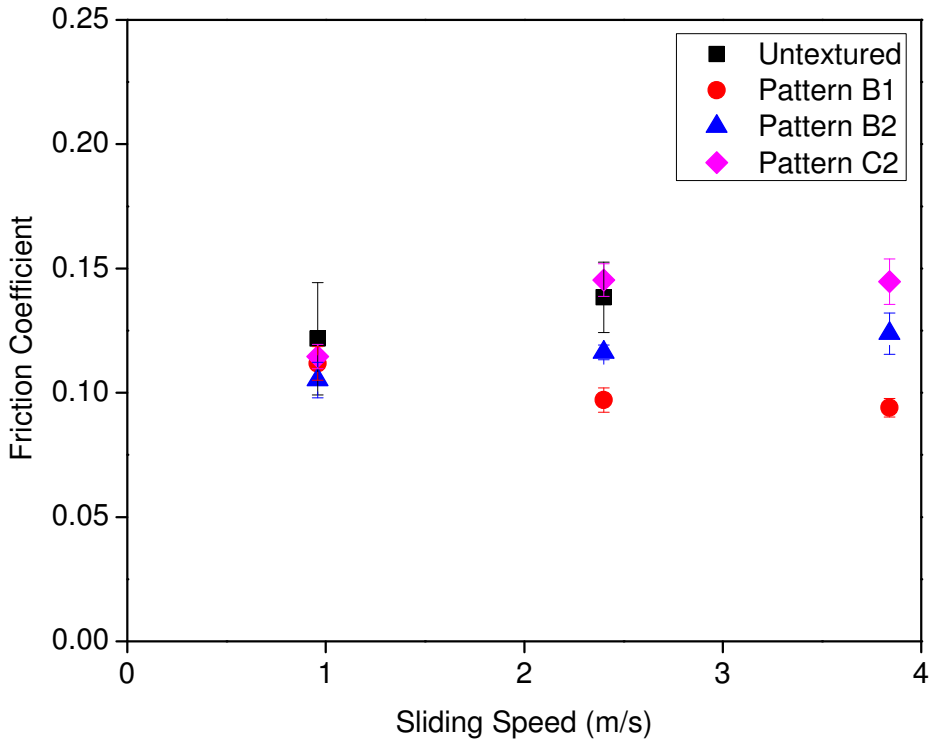

Figure 3.24: Variation of average friction coefficient with sliding speed

At lower sliding speed, although the texture patterns displayed slightly lower friction coefficient values than the untextured surface, the difference was not significant. Also the friction coefficient values of the textured patterns were fairly similar, indicating

that the effect of the texture geometry was not significant at lower sliding speeds either. More importantly, the untextured surface was able to survive the entire duration of testing. So, benefits from texturing at lower sliding speeds are not remarkable. However, as the speed is increased, the operating conditions become aggressive and the effect of texturing becomes clearly visible. Compared to the untextured surface, which is unable to operate under such aggressive conditions, the texture patterns perform distinguishably well. Also, the friction coefficient of the textured patterns are different from each other at 2.4m/s and 3.84 m/s, which points to the strong influence of the texture geometry on the performance at aggressive operating conditions. The wear performance also appeared to be good, with no significant wear, as observed from the optical images. Later, in Section 3.5, an attempt will be made to quantify the small wear through surface profile measurements and calculate the wear rate.

3.3.2 Effect of lubricant type

Lubrication is a key issue for mechanical systems, especially for ones with critical sliding interfaces. For air-conditioning and refrigeration systems in particular, the choice of proper lubricant is of great significance as there is interaction between the lubricant and the refrigerant. Polyalkylene glycol (PAG) and polyolester (POE) are two commonly used synthetic lubricants that work well with alternative refrigerants such as R-744 [11]. In some compressors, readily available mineral oils are also used, especially to keep the cost down.

The objective of this part of the study was to identify if the tribological benefit observed earlier is due to surface texturing alone, or if the type of lubricant and lubricant-

refrigerant interaction plays a significant role. Three different lubricants were chosen for this purpose: PAG, POE and Mineral oil. Details about the lubricants are given in Table 3.1. Only texture pattern C1 was used for the study, as it was the best performing texture pattern in the wear tests in the presence of R-744, presented earlier.

Table 3.1: Different lubricants used in the study

Lubricant Type	**Manufacturer**	**Viscosity**	**Mass of 1 drop**
PAG	Emkarate RL	300 SUS	21-23 mg
POE	Emkarate RL	300 SUS	24-26 mg
Mineral oil (C-4s)	Calumet Lubricants	300 SUS	25-27 mg

All the tests were conducted in the presence of R-744 at a chamber pressure of 1.93 MPa under a normal load of 178 N, sliding speed of 2.4 m/s and ambient laboratory conditions of 16 - 20 °C and 40-50% RH. One drop of lubricant was added at the interface before initiating the test.

Figure 3.25 shows the friction coefficient and near contact temperature for texture pattern C1 tested with the three different lubricants. Clearly, the best performance with respect to friction coefficient and contact temperature is achieved in the presence of PAG. The friction coefficient in case of POE closely follows PAG for almost half the test duration, beyond which it increases and more variation in observed. For the mineral oil, the friction coefficient remains fairly stable and lies in between that of PAG and POE. The near contact temperatures also follow similar trend.

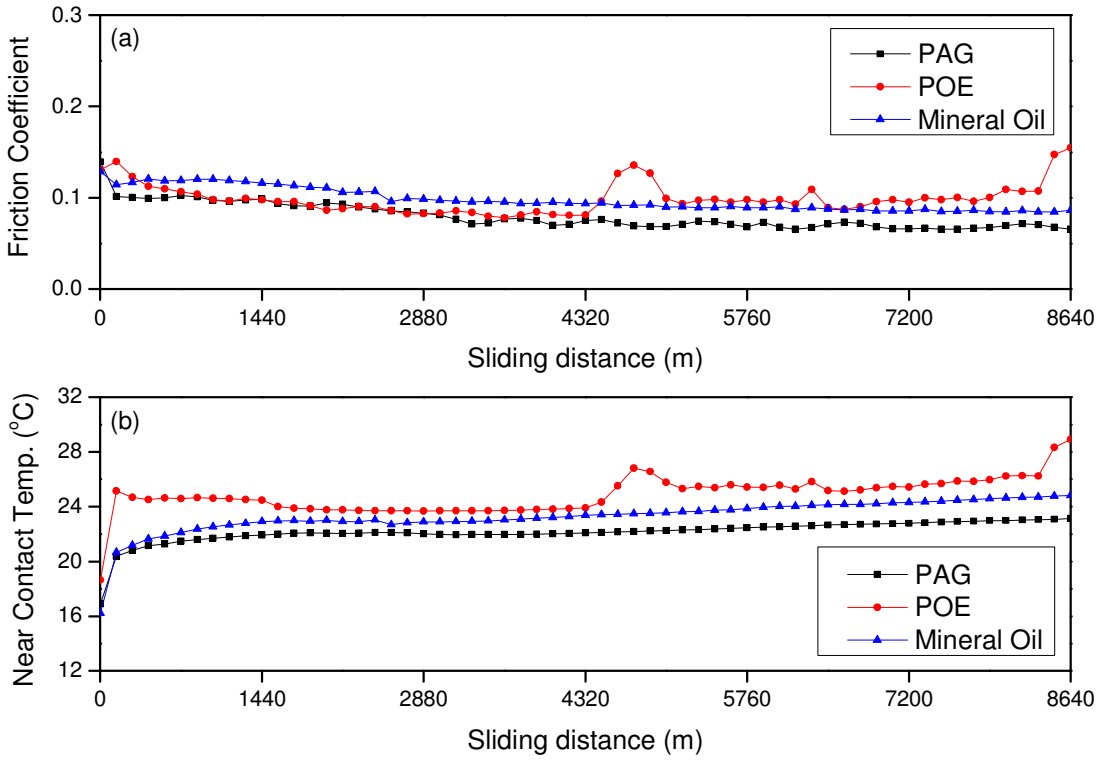

Figure 3.25: Comparison of (a) Friction coefficient and (b) Near contact temperature of texture pattern C1 when tested at 178 N normal load and 2.4 m/s sliding speed in the presence of R-744 at a chamber pressure of 1.93 MPa with a drop of different lubricant applied directly at the interface

It should be noted that the difference in friction performance between all three oils is not too large although for the test done in presence of POE, the friction coefficient increases at the end. Figures 3.26 and 3.27 show the optical images of the disks and texture pattern C1 tested with different lubricants such as PAG, POE and Mineral oil. Although none of the lubricants behaved very differently in terms of wear, it is clear from visual inspection that PAG exhibited the best performance. The disk and pins tested in the presence of PAG showed minimum damage to their surfaces. The disk tested with POE showed a lot of burnishing followed by the disk tested in mineral oil. The corresponding texture patterns followed similar trends. While the texture pattern C1 tested with PAG showed only few minor scratches on the surface, those tested with POE

and mineral oil showed smooth polished regions indicating mechanical contact between pin surface and disk during testing. Nunez et al. [11] conducted starved lubrication experiments and compared the performance of PAG and POE in the presence of R-744 refrigerant environment on Al390-T6/SAE 52100 steel material pairs. They reported that the disks lubricated with PAG suffered less burnishing than those lubricated by POE, which is similar to what is observed here.

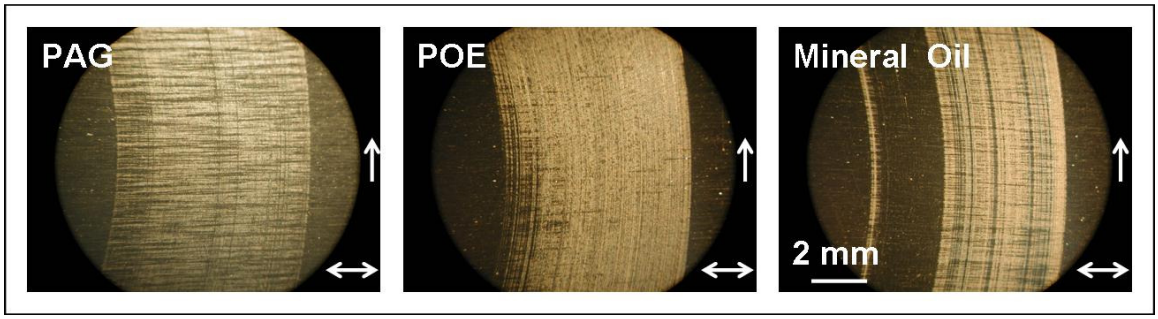

Figure 3.26: Optical images of the disks tested against texture pattern C1 at a load of 178 N and sliding speed of 2.4 m/s with different lubricants in the presence of R-744 at a chamber pressure of 1.93 MPa (Horizontal double arrows indicate direction of machining marks and vertical arrows indicate direction of sliding)

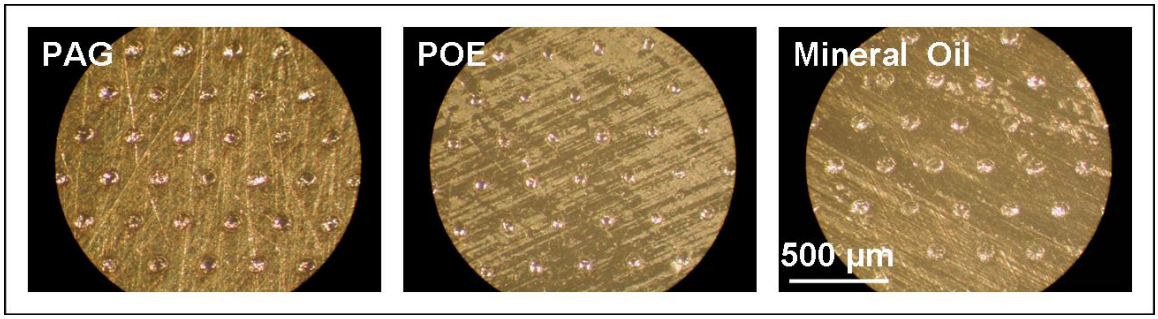

Figure 3.27: Optical images of the texture pattern C1 tested at a load of 178 N and sliding speed of 2.4 m/s with different lubricants in the presence of R-744 at a chamber pressure of 1.93 MPa

Thus, under the tested conditions the tribological performance can be attributed largely to the effect of surface texturing. Comparable performance is observed for the

inexpensive mineral oil as compared to expensive advanced synthetic compressor lubricants such as PAG or POE, which highlights the positive effect of surface texturing.

3.3.3 Effect of different refrigerants

To make the study more general, additional tests were conducted in the presence of other refrigerant/lubricant combinations. R-134a is a HFC based refrigerant which is widely used but suffers from the disadvantage of high global warming potential (GWP). The use of HFC based refrigerants has been regulated by the Kyoto Agreement of 1997[1] and thus there is a thrust on environmentally friendly refrigerants. A new refrigerant R-1234yf has been recently introduced jointly by Honeywell and DuPont [1]. It has negligible GWP and is being touted as a direct replacement to R-134a because the working pressures for R-1234yf are similar to that of R-134a. This implies that no significant re-engineering of the existing systems would be necessary. However, changing the refrigerant might have an effect on the tribological behavior of sliding interfaces. Also, the compatibility of any new refrigerant with the lubricant needs investigation. Extensive work on the tribological performance of critical tribo-contacts in compressors in the presence of R-134a has been done already. However, research in tribology is limited for R-1234yf in the open literature and the Tribology Laboratory at UIUC is actively working in this area.

Wear studies (one hour duration) were conducted at a load of 178 N and 2.4 m/s sliding speed at ambient laboratory conditions of 16 - 20 °C and 40-50% RH. CO_2 (R-744) compressors are high pressure systems compared to R-134a and R-1234yf. So, while R-744 tests were conducted at 1.93 MPa (280 psi) of chamber pressure, tribological

studies in the presence of R-134a and R-1234yf were conducted at 0.69 MPa (100 psi) of chamber pressure. Boundary/mixed lubrication regime was achieved by directly applying a small amount of lubricant (approximately one drop) at the interface. Two of the texture patterns (C1 and C2) were used for this study and compared against an untextured surface.

Figure 3.28 shows the friction coefficient as a function of sliding distance for untextured and textured pins tested in the presence of refrigerant R-134a and PAG. Only texture patterns C1 and C2 were tested. This is because C1 was the best performing texture pattern in both the wear and durability tests carried out in the presence of R-744 and C2 was chosen to understand the effect of the area density of micro-dimples.

At a normal load of 178 N, it is interesting to observe that the untextured pin survived the entire duration of testing. This is in contrast to the results obtained when testing was done under identical conditions in the presence of refrigerant R-744. Untextured pins were unable to operate under such conditions and failed, marked by a sharp increase in friction coefficient and a visually unstable interface exhibiting a lot of vibration. This is an indication of a positive interaction between the lubricant PAG and refrigerant R-134a during sliding.

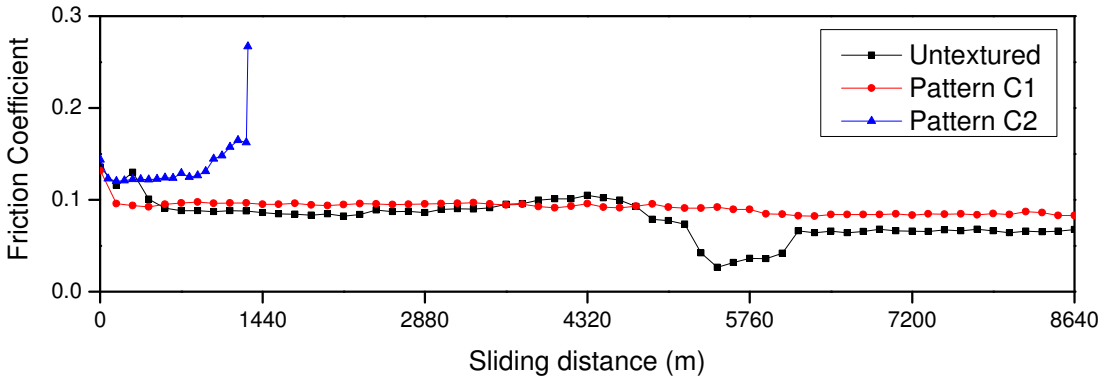

Figure 3.28: Friction coefficient of an untextured surface and texture patterns C1 and C2 at 178 N normal load and 2.4 m/s sliding speed in the presence of R-134a at a chamber pressure of 0.69 MPa with small amount of PAG applied at the interface

It can also be seen from Figure 3.28 that the average friction coefficient of the untextured interface is slightly lower when compared to that of the texture pattern C1. Also, the texture pattern C2 was unable to survive the entire duration of testing and failed prematurely at a sliding distance of approximately 1,400 meters. This is an important finding because it points to the importance of the effect of the material pile-ups around the micro-dimples with respect to any beneficial tribo-layers formed at the interface during sliding especially during boundary/mixed lubrication. The results with pattern C2 is in contrast to those obtained during the wear studies with R-744, in which case pattern C2 was able to operate successfully and survive the entire duration of testing without failure. However, the similarity in both cases (R-744 and R-134a) is that the friction performance of pattern C1 is better than that of pattern C2. This might be attributed to the fact that pattern C2 has a higher area density of micro-dimples which leads to a larger number of material pile-ups around the micro-dimples. During sliding these pile-ups wear out generating wear debris. Thus, the amount of wear debris generated will be more for pattern C2 than pattern C1, causing an increase in friction.

Figure 3.29 shows the results from the tests conducted in the presence of refrigerant R-1234yf. As in the case with R-134a, tests were conducted with texture patterns C1 and C2 and compared against an untextured surface. Since R-1234yf is a newly introduced refrigerant, the compatibility with the existing commonly used lubricants such as PAG and POE is not known in the open literature. So, tests were conducted in the presence of both PAG and POE.

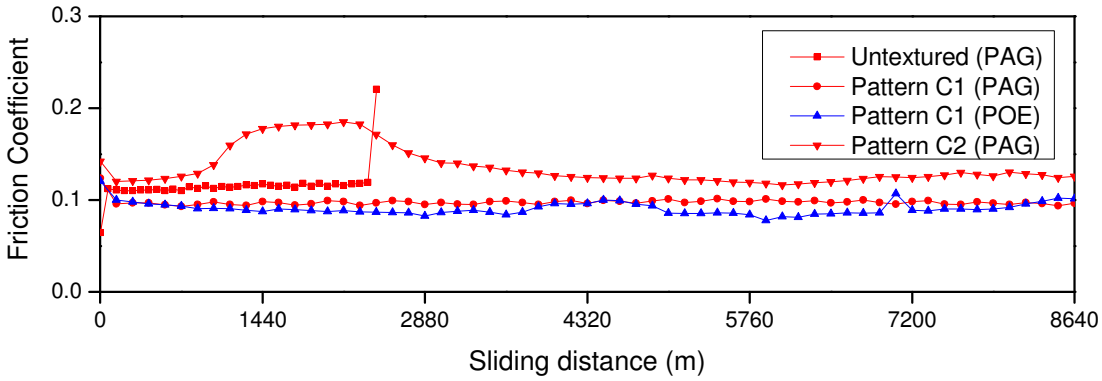

Figure 3.29: Friction coefficient of an untextured surface and texture patterns C1 and C2 at 178 N normal load and 2.4 m/s sliding speed in the presence of R-1234yf at a chamber pressure of 0.69 MPa with small amount of PAG/POE applied at the interface

The untextured pin failed to survive the entire duration of testing and failed at a sliding distance of approximately 2,500 meters. On the other hand, the textured pins survived the entire duration of testing, pointing to the benefits derived from the lubricant storage ability of the micro-dimples on the pin surface. Pattern C1 shows similar friction behavior when tested with PAG and POE. However, the trend is opposite to what was seen in the presence of R-744 (Figure 3.25) which underlines the importance of the refrigerant-lubricant relationship on the tribological performance for compressor systems. Pattern C2 again showed a higher friction when compared to pattern C1, when tested in

PAG. This again proves the hypothesis of large amount of wear debris in pattern C2 causing an increase in friction.

The presence of the refrigerant environment has a critical effect on the tribological performance. To highlight this, few experiments were done in the absence of any refrigerant environment i.e., in ambient air. Figure 3.30 shows the friction coefficient obtained when an untextured surface and texture patterns B1 and C1 were tested at a normal load of 178 N, sliding speed of 2.4 m/s in ambient air with 23 mg of PAG lubricant applied directly at the interface.

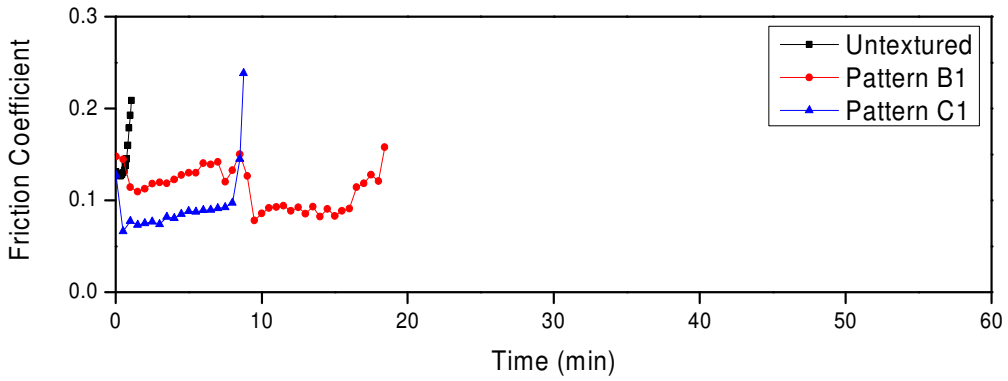

Figure 3.30: Friction coefficient of untextured pin and texture patterns B1 and C1 tested at 178 N normal load and 2.4 m/s sliding speed in ambient air with 23 mg of PAG lubricant applied at the interface

The untextured surface failed within a minute of initiating the test. In comparison, the textured patterns ran successfully for 10 and 20 minutes before failure. Failure was characterized by a sudden increase of the friction coefficient and an unstable interface visually marked by significant vibration. This highlights the importance of the refrigerant environment while conducting tests in a compressor realistic condition. Furthermore, though the textured patterns did fail eventually, they survived the test longer than the untextured surface under identical testing conditions pointing to the benefit of surface

texturing. Pattern B1 has micro-dimples with the same diameter as pattern C1 but are deeper. This means that the lubricant storage ability of pattern B1 is better than that of pattern C1, which is why pattern B1 lasted longer than pattern C1.

Figures 3.31 and 3.32 show the optical images of the disks and pins tested in the presence of different refrigerant environments of R-744, R-134a and R-1234yf. All tests were done in the presence of 23 mg of PAG lubricant at the interface. It should be noted that for R-744 and R-1234yf, the untextured surface failed prematurely while for R-134a, texture pattern C2 failed within minutes of testing. This again points to the importance of the lubricant-refrigerant relationship.

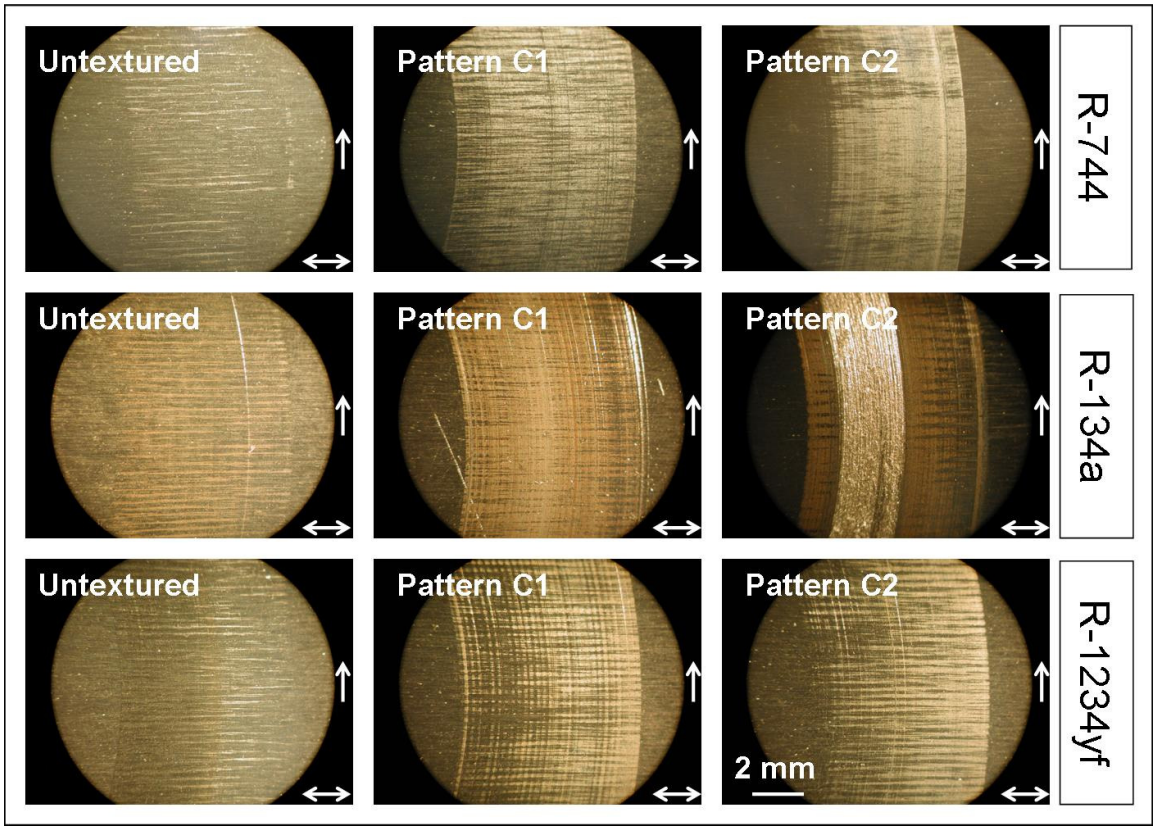

Figure 3.31: Optical images of the disks tested against an untextured surface and texture patterns C1 and C2 at a load of 178 N and sliding speed of 2.4 m/s in the presence of different refrigerants with 23 mg of PAG lubricant applied directly at the interface (Horizontal double arrows indicate direction of machining marks and vertical arrows indicate direction of sliding)

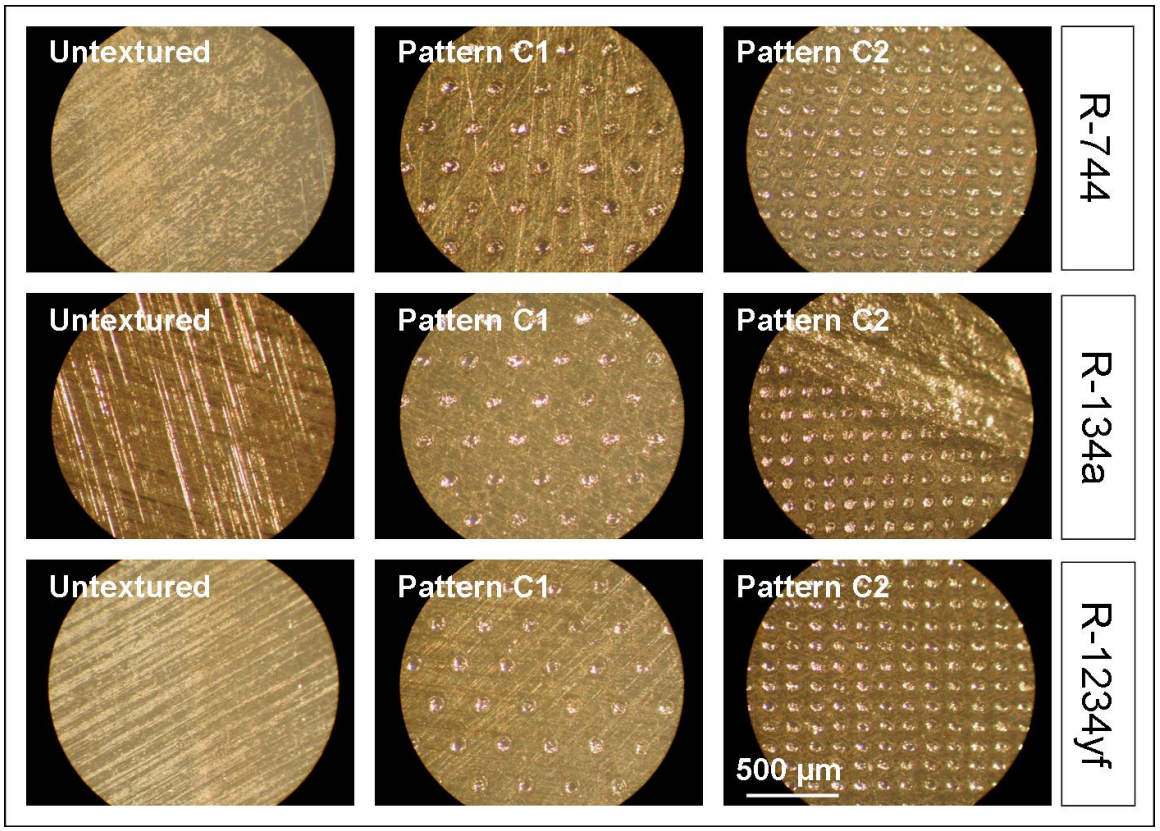

Figure 3.32: Optical images of an untextured surface and texture patterns C1 and C2 tested at a load of 178 N and sliding speed of 2.4 m/s in the presence of different refrigerants with 23 mg of PAG lubricant applied directly at the interface

Figure 3.33 summarizes the friction performance of the untextured surface and texture patterns C1 and C2 in different refrigerant environments and ambient air in the presence of PAG lubricant at the interface. In cases, where any surface failed during the testing, friction coefficient and near contact temperature values till failure were used to calculate the average. For the remaining tests, friction coefficient and contact temperature were averaged over the last 20 minutes of the test duration.

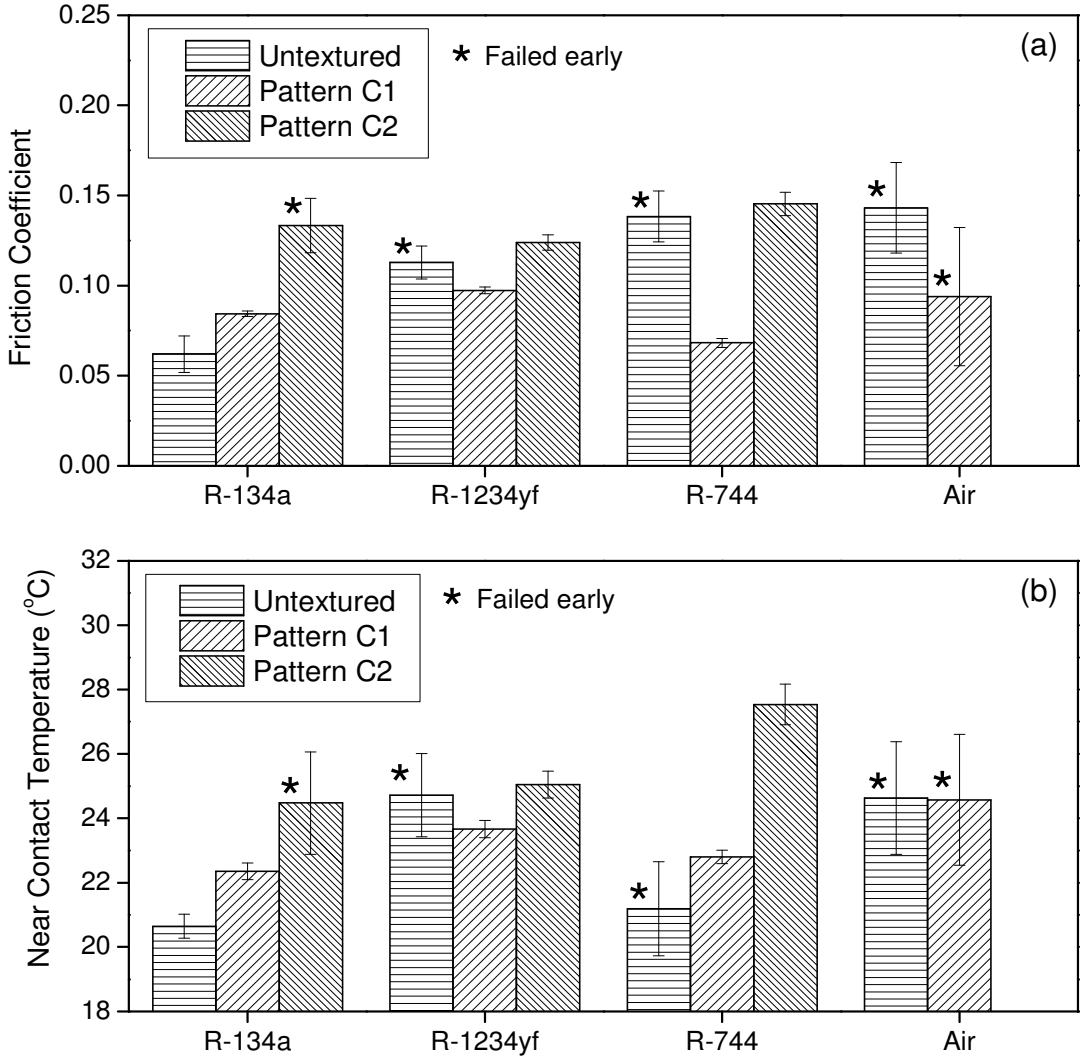

Figure 3.33: Comparison of (a) Friction coefficient and (b) Near contact temperature for texture patterns C1 and C2 with an untextured surface in the presence of different refrigerants and ambient air when tested at a load of 178 N, sliding speed of 2.4 m/s with 23 mg of PAG lubricant applied directly at the interface

In general, the refrigerant environment had a strong influence on the untextured surface. The untextured surface performed the best with the lowest friction coefficient in the presence of R-134a and survived the entire duration of testing. In comparison, it failed in the presence of other refrigerants such as R-1234yf and R-744. The average friction coefficient values calculated till failure were higher than that in R-134a. In case

of texture patterns, the refrigerant did not have a very significant influence with the texture pattern behaving similarly in the presence of any refrigerant. However, the texture geometry had a strong influence on the performance. As the area density increased, the friction performance became worse. The near contact temperature values followed a similar trend, except for R-744 when the untextured surfaces displayed the lowest near contact temperature despite a relatively higher friction coefficient. Both the untextured surface and texture pattern C1 failed early when tested in ambient air indicating the strong influence of refrigerant on the performance and the need for realistic tribo-testing.

3.4 Durability (or Life) experiments

Durability experiments were designed to evaluate the ability of the textured specimens to withstand extended periods of operation under starved lubrication conditions. These tests were conducted for a duration of three hours. At a sliding speed of 2.4 m/s it amounted to a significantly large sliding distance of 25,920 meters. Such tests would clearly identify the benefits of using surface texturing to improve the durability of the compressor components. Only texture patterns A1, B1 and C1 were used for this study. All the tests were done at a load of 178 N, sliding speed of 2.4 m/s in the presence of R-744 at a chamber pressure of 1.93 MPa at ambient laboratory conditions of 16 - 20 °C and 40-50% RH. Figure 3.34 shows the friction results from the durability experiments and Figures 3.35-3.36 shows the optical images of the disks and pins after the tests.

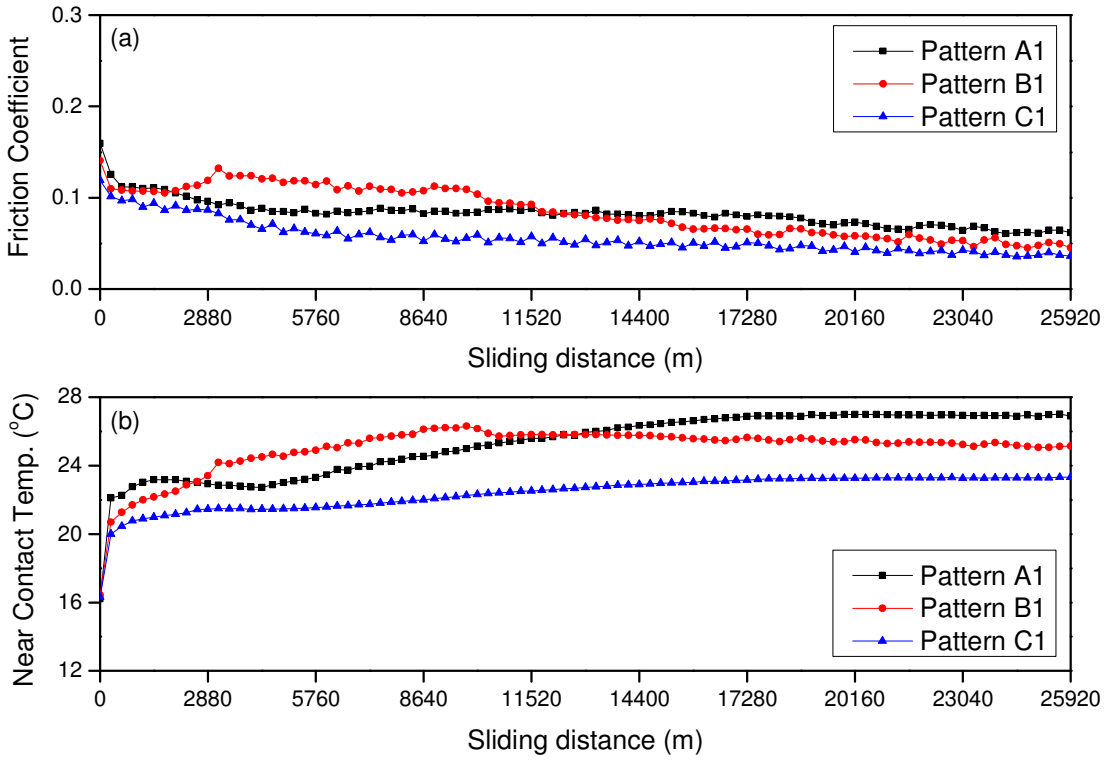

Figure 3.34: (a) Friction coefficient and (b) Near contact temperature of texture patterns A1, B1 and C1 during durability testing at 178 N normal load and 2.4 m/s sliding speed in the presence of R-744 at a chamber pressure of 1.93 MPa with 23 mg of PAG lubricant directly applied at the interface

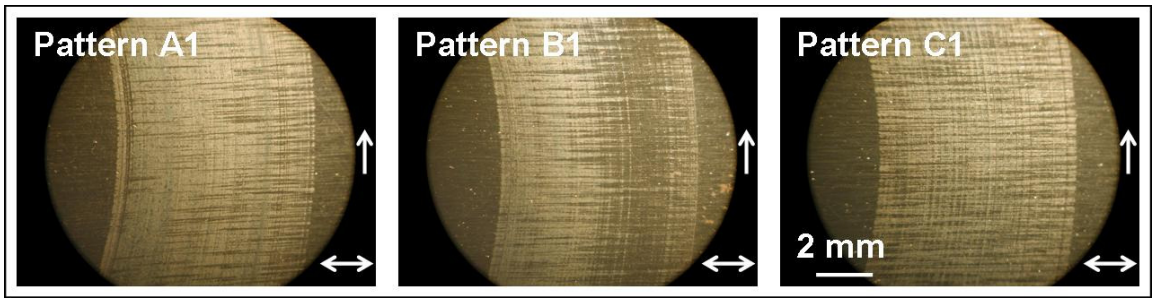

Figure 3.35: Optical images of the disks after the durability experiments tested against texture patterns A1, B1 and C1 at a load of 178 N and sliding speed of 2.4 m/s in the presence of R-744 at a chamber pressure of 1.93 MPa with 23 mg of PAG lubricant applied at the interface (Horizontal double arrows indicate direction of machining marks and vertical arrows indicate direction of sliding)

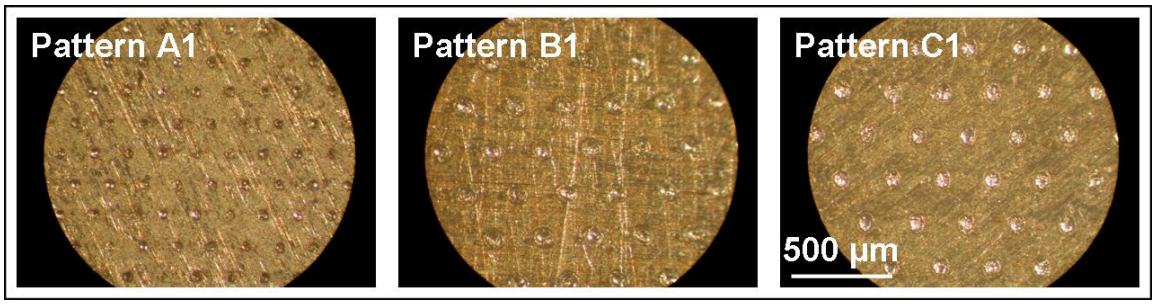

Figure 3.36: Optical images of the texture patterns A1, B1 and C1 after the durability experiments at a load of 178 N and sliding speed of 2.4 m/s in the presence of R-744 at a chamber pressure of 1.93 MPa with 23 mg of PAG lubricant applied at the interface

The results of the durability experiments are very encouraging. It is of particular importance, because compared to the untextured surfaces which failed in approximately 10 minutes during the wear testing, all the texture patterns lasted for the entire test duration of three hours, which is a very significant improvement. The ability of textured surfaces to sustain low friction over long intervals of time was demonstrated by Wakuda et al. [39]. It should be further emphasized that like the wear testing, durability testing were also conducted with only a small amount of 23 mg of PAG (approximately one drop) applied directly at the interface. Borghi et al. [40] showed the long term performance of textured surfaces under "single drop" configuration, similar to what is used in this work. As can be seen in Figure 3.34, the friction coefficient values were low for all the texture patterns with pattern C1 performing the best. Similar results were obtained for the wear experiments although the friction coefficient values were slightly higher. From the optical images of the disks it appears that no significant wear occurred during the testing. In some of the cases, the wear tracks on the disks were distinct but only mild burnishing was observed. For texture pattern A1, some smooth polished regions were observed after the durability testing, as shown in Figure 3.36, which probably meant that some mechanical rubbing occurred between the pin and the disk. It should be further

emphasized that even under such extended periods of testing the wear of the pins and disks was not large and later, in Section 3.5, the wear rate for the durability experiments through surface profile measurements of the texture patterns before and after the tests is calculated. Figure 3.37 compares the friction coefficient and near contact temperature of texture patterns A1, B1 and C1 for the wear and durability experiments.

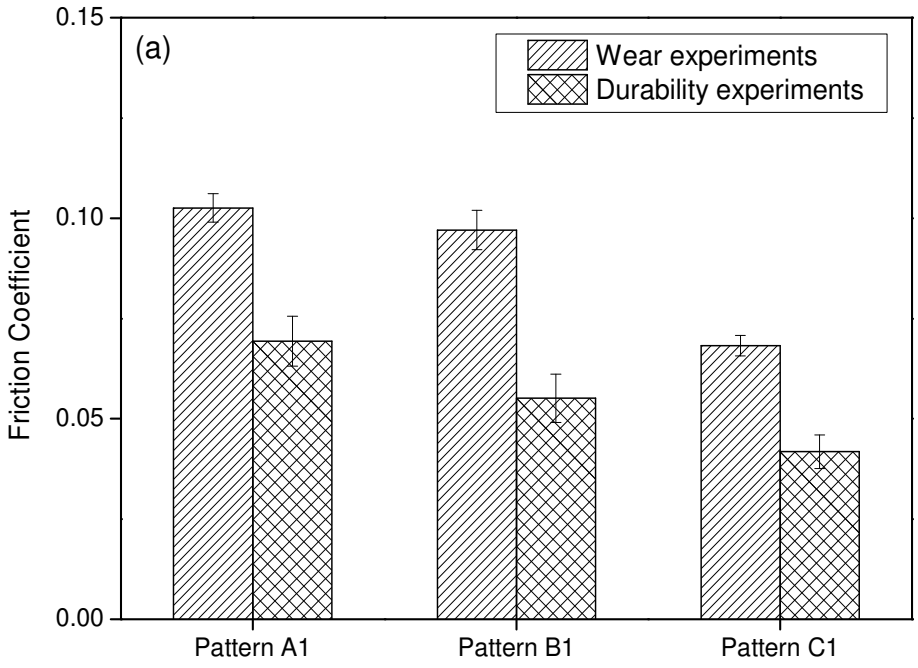

Figure 3.37 (continued on next page)

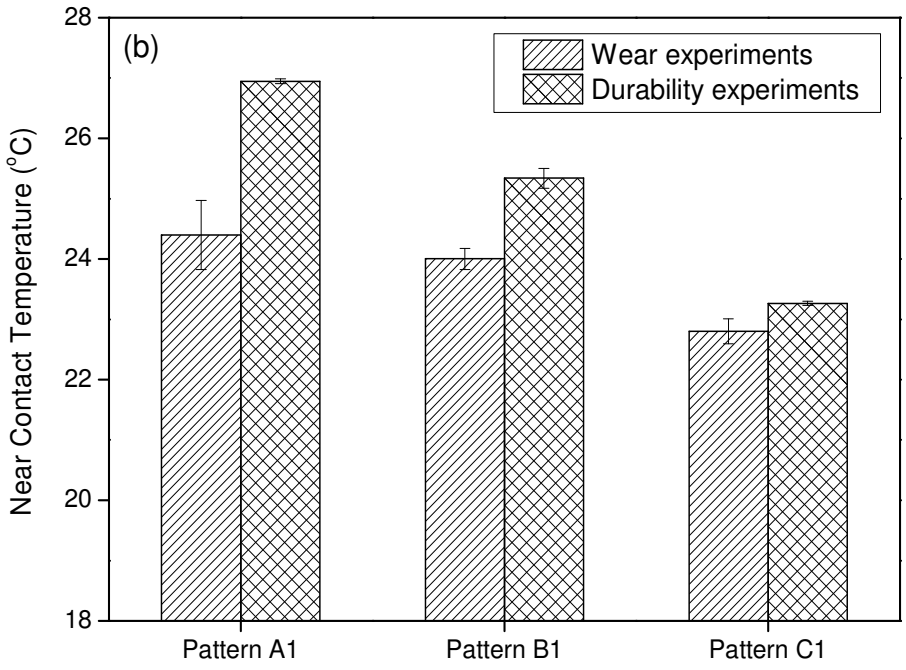

Figure 3.37: Comparison of (a) Friction coefficient and (b) Near contact temperature for the texture patterns A1, B1 and C1 during the wear and durability experiments

From Figure 3.37, it can be realized that the average friction coefficient for the durability experiments were 32 to 43% lower than those for the wear experiments. Since the wear experiments were of 60 minutes duration, this indicates that a stable sliding interface is established after 60 minutes under the tested conditions with starved lubrication. The near contact temperatures followed the reverse trend with higher values for the durability experiments. This is expected because the durability experiments were three times longer in duration than the wear experiments. However, the difference in the near contact temperatures was not significant which points to the benefits of surface texturing even under extended periods of operation.

3.5 Wear analysis

Wear is typically defined as the removal of material when two bodies are sliding against each other. There are different ways to analyze wear. A quick method is visual inspection of the sliding interfaces through an optical microscope. It gives a firsthand impression of the nature of the wear. However, it is only qualitative in nature and cannot be used for the purpose of quantification or comparison. Wear is usually quantified by the loss of mass of the pin or disk used in a pin-on-disk type tribological experiment. Typically, the disks used are much heavier than the pins and so the mass loss of the disks is negligible. Thus, surface profile measurements are commonly used to measure the depth of the wear track formed on the disk to quantify wear, especially for the cases when the wear is minor/small as is the case here.

In the case of the experiments done with the textured patterns, wear was first analyzed in a qualitative manner by the use of an optical microscope and was presented in the preceding sections. In general, all optical images point to the insignificant wear and hence the excellent wear performance of the textured pins. To quantify the wear of the disks and pins, surface profile measurements were carried out. Also, the mass loss of the pins and disks used in this study were negligible even after extended periods of durability testing. Thus to quantify wear, surface profile measurements were done on the disks and pins in an effort to quantify wear.

3.5.1 Profilometric wear scans

Wear on gray cast iron counter disks was quantified by measuring the depth of the wear track formed. After the testing was complete, the disk was removed from the UHPT

and ultrasonically cleaned in a pool of acetone for 10 minutes followed by rinsing with propanol. This was done to ensure the disk is clean and free from any wear debris and/or residual oil to get an accurate measure of the wear depth. Figure 3.38 shows a typical wear track on the tested disk. 1-D line scans of 10 mm scan length were performed across the wear track on the disks with the Tencor® P-15 Contact Profilometer to measure the wear depth after the testing was complete.

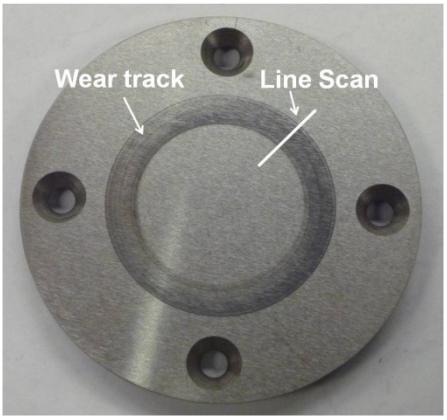

Figure 3.38: Gray cast iron disk showing a typical wear track and the line scan to measure the wear depth

Figure 3.39 shows the wear profiles for the disks on which wear experiments were carried out with texture patterns A1, B1 and C1 in the presence of R-744 with small amount of PAG at the interface at a normal load of 178 N and sliding speed of 2.4 m/s. The wear profile measurements corroborate the qualitative findings from the optical images of the disks. It is clear that no significant wear occurred. All the three disks suffered only mild burnishing with wear depths less than 0.5 µm. The disk tested against pattern C1 appears to have the mildest burnishing.

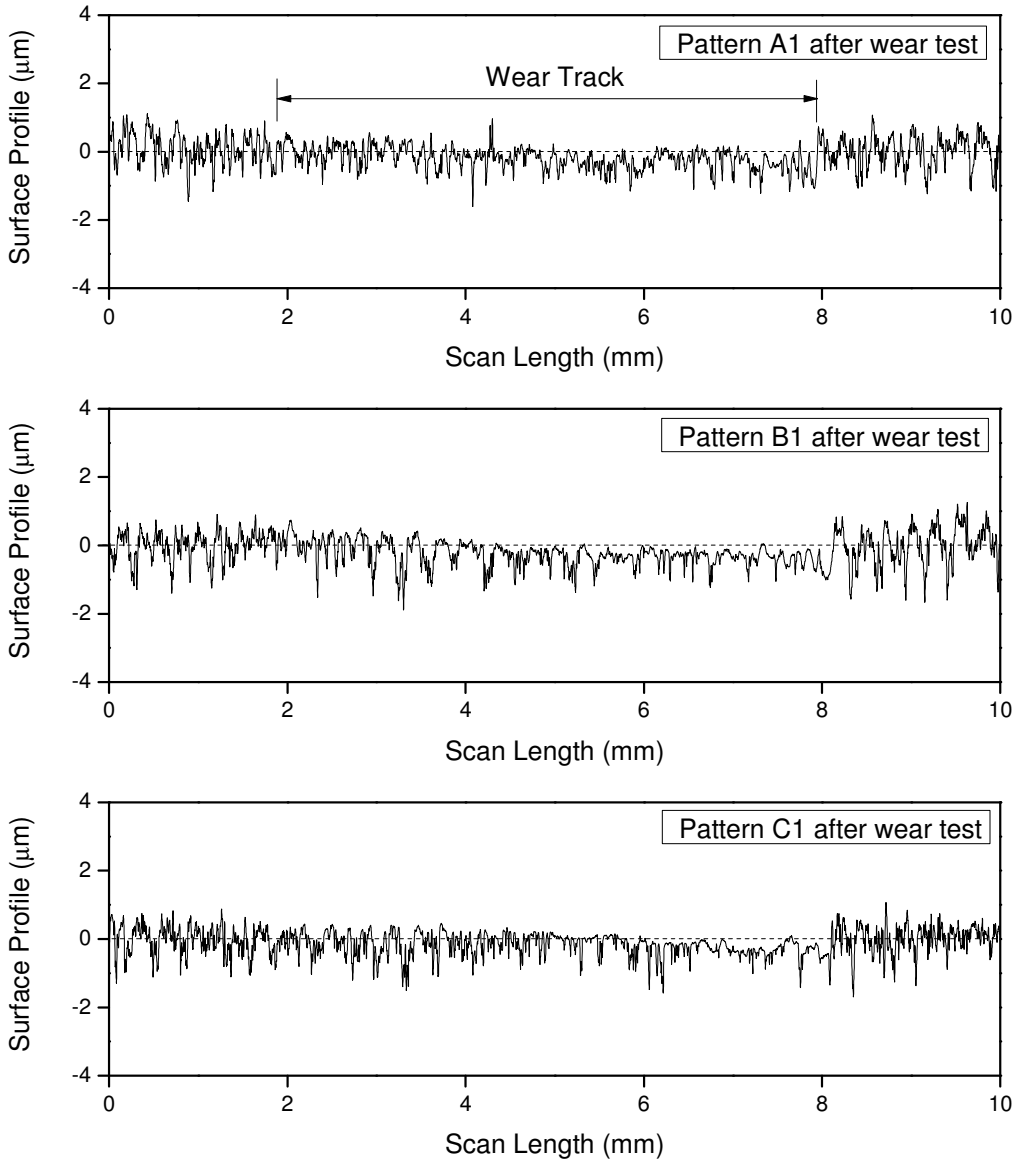

Figure 3.39: Wear profiles of the disks used in wear experiments against texture patterns A1, B1 and C1 tested at a load of 178 N and sliding speed of 2.4 m/s in the presence of R-744 at a chamber pressure of 1.93 MPa with 23 mg of PAG lubricant applied at the interface

Figure 3.40 shows the wear profiles for the disks on which durability experiments were carried out with texture patterns A1, B1 and C1 in the presence of R-744 with 23 mg of PAG lubricant at the interface at a normal load of 178 N and sliding speed of 2.4 m/s. For texture patterns B1 and C1 the wear depths were of the same order as for the wear experiments. For texture pattern A1, however, the wear depths were a little larger at

approximately 1-2 µm. This might be attributed to the fact that the texture pattern A1 had the highest and more number of material pile-ups. During the course of testing, these material pile-ups get worn and act as third-boy abrasives increasing wear. However, it should be noted that even after such long duration testing, the wear was not significant.

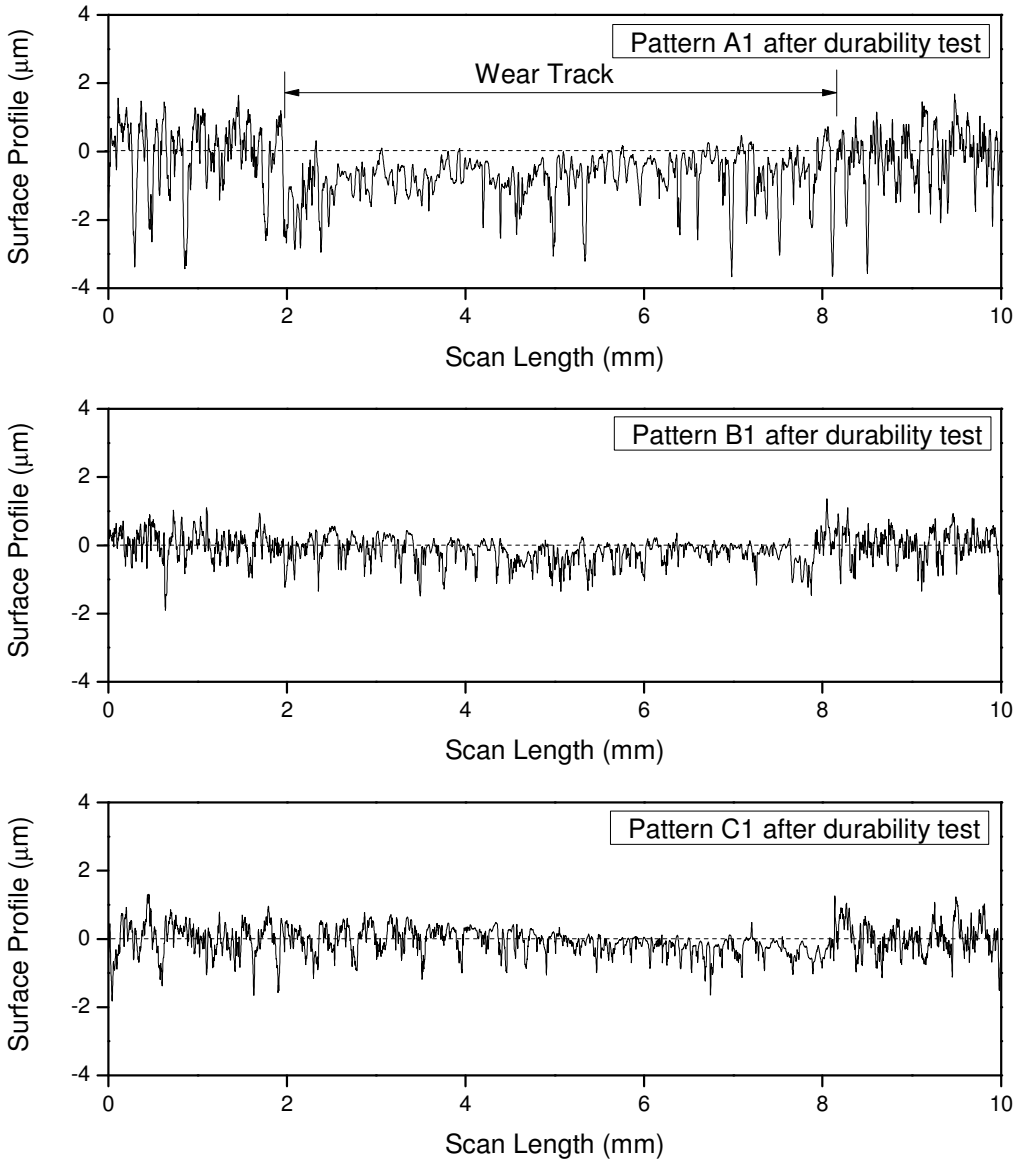

Figure 3.40: Wear profiles of the disks used in durability experiments against texture patterns A1, B1 and C1 tested at a load of 178 N and sliding speed of 2.4 m/s in the presence of R-744 at a chamber pressure of 1.93 MPa with 23 mg of PAG lubricant applied at the interface

3.5.2 Pin wear quantification

From the optical micrographs it was observed that even after extended periods of testing the micro-dimples were intact in most cases. However, the material pile-ups around the micro-dimples were getting polished. To quantify the amount of this polishing or wear, profile measurements were carried out on the surface of the textured pins after the testing.

The pins were removed from the UHPT after the testing and ultrasonically cleaned in a pool of acetone followed by rinsing with propanol. This was done to remove any wear debris and/or residual oil to get an accurate measure of the surface profile of the micro-dimples on the pin surface. 1-D line scans of length 800 μm were carried out using the Tencor® P-15 Contact Profilometer. Figures 3.41-3.43 show the surface profile of texture patterns A1, B1 and C1 after the wear and durability testing.

Before the test the height of the material pile-ups around the micro-dimples are of the order of the dimple depth. As the test progressed, these material pile-ups get polished and worn out gradually. However, after the end of the wear testing, which is of one hour duration, the material pile-ups are not fully removed and are still present in all the texture patterns A1, B1 and C1. The material pile-ups for patterns B1 and C1 were intact even after the durability testing. This is an indication of the excellent wear performance of the textured pins. However, for texture pattern A1, the material pile-ups were fully removed after the durability testing and some contact occurred between the disk and pin surface. This is noted by observing the surface profile of texture pattern A1 after the durability testing in Figure 3.41. The region between two consecutive micro-dimple surface profiles appears smooth, in contrast to the measurements for the other texture patterns, indicating

that the material pile-ups were completely removed and mechanical rubbing occurred between the disk and pin causing the pin surface to get smooth.

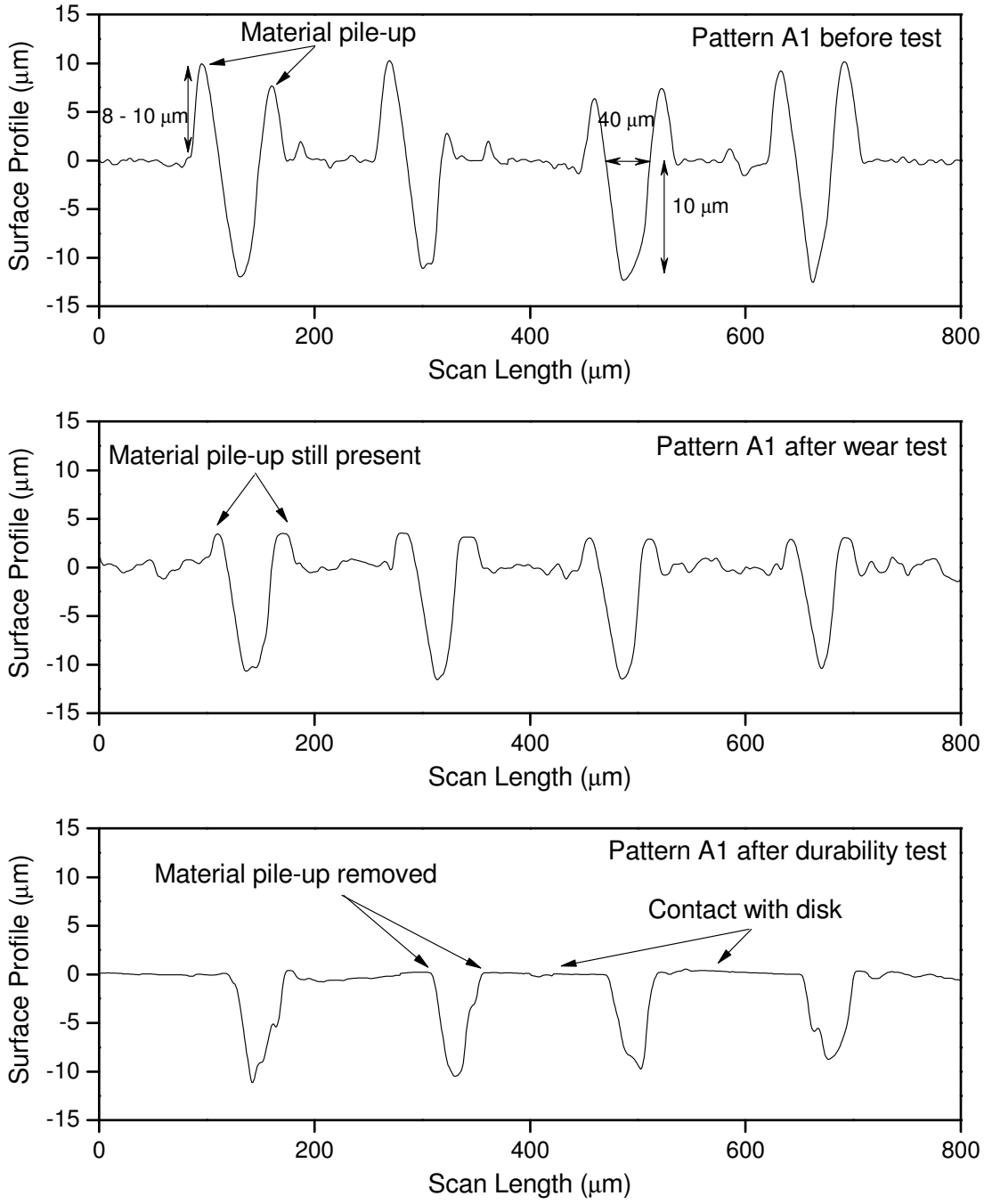

Figure 3.41: Surface profile measurements of texture pattern A1 before and after the wear and durability experiments

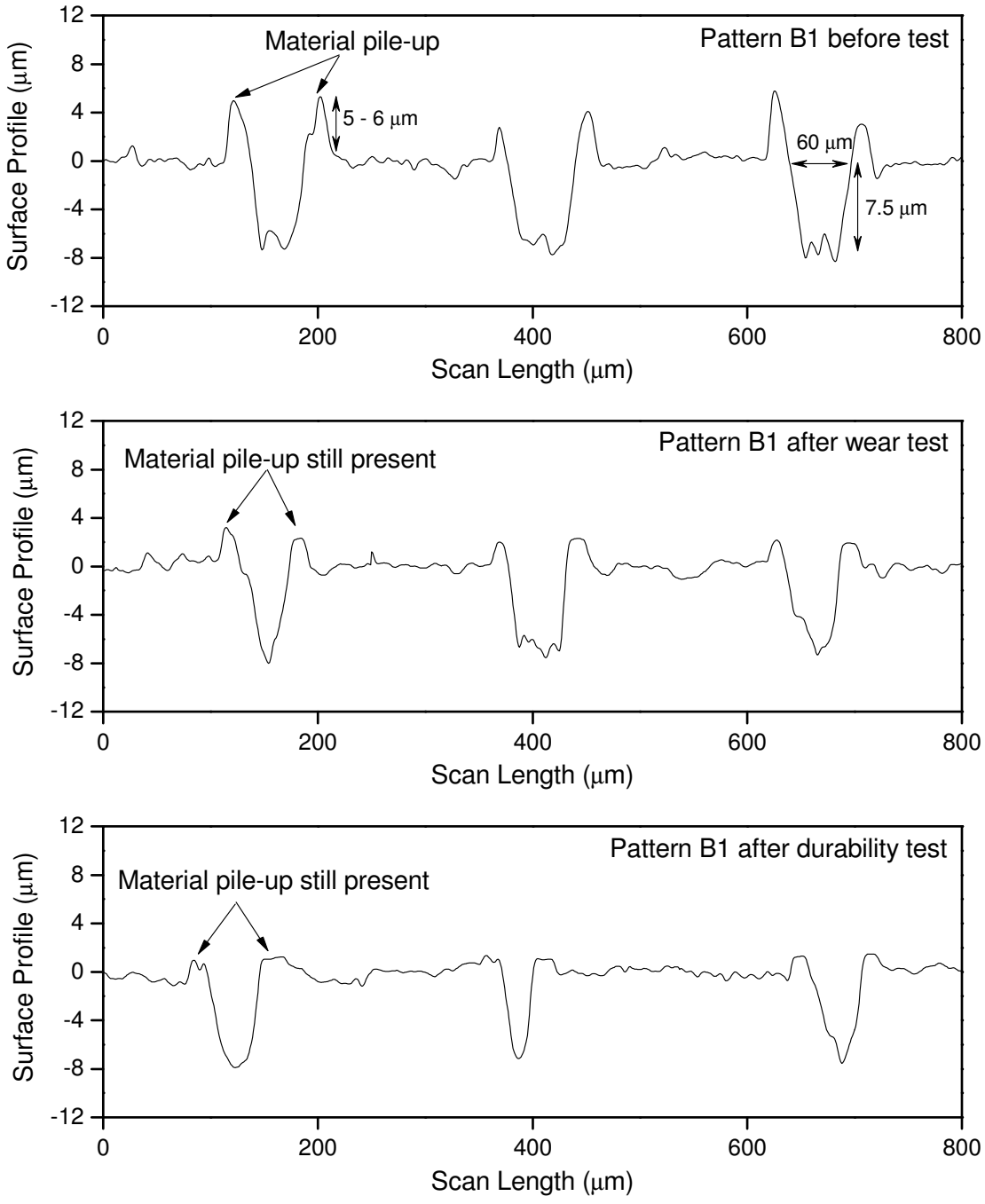

Figure 3.42: Surface profile measurements of texture pattern B1 before and after the wear and durability experiments

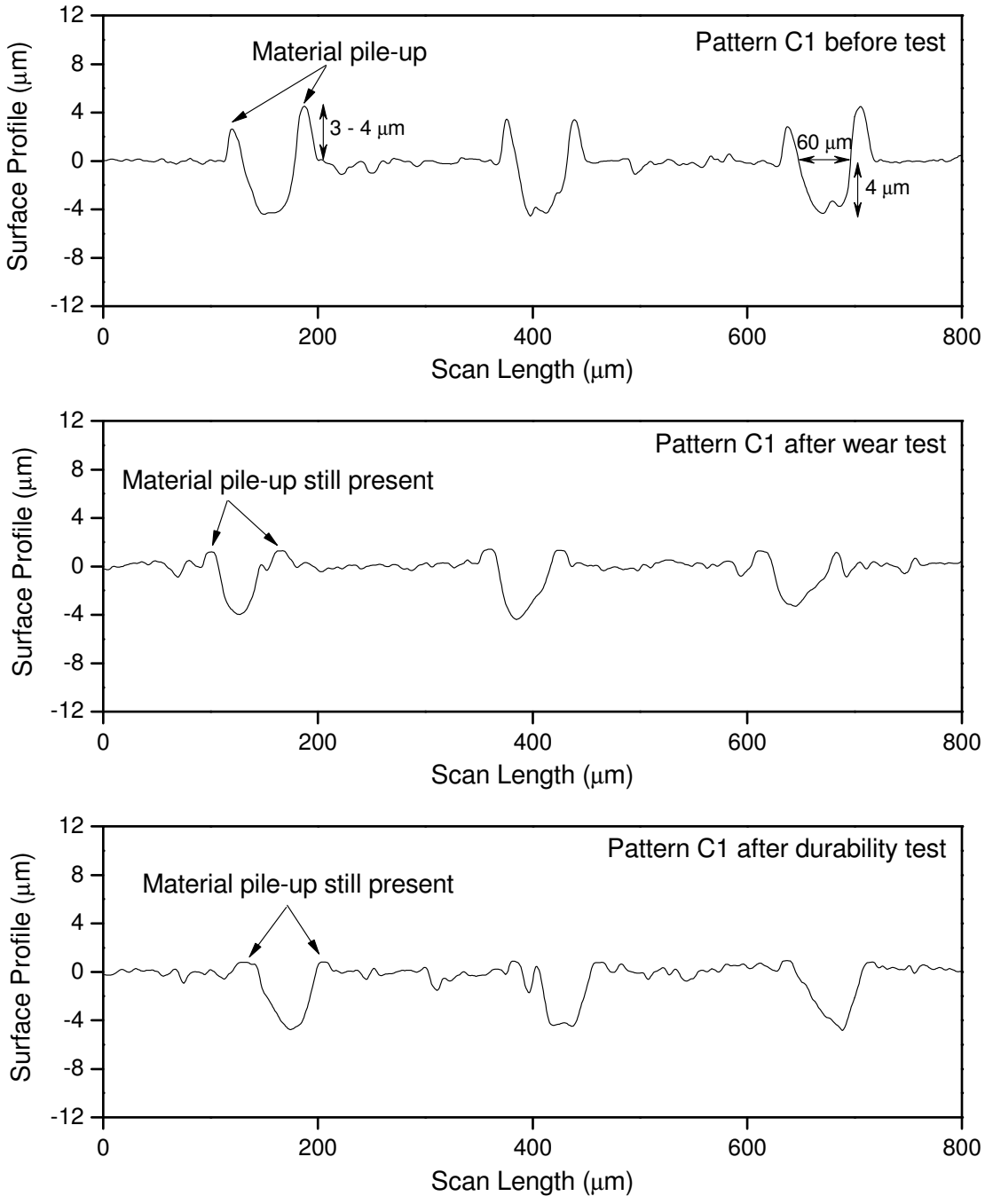

Figure 3.43: Surface profile measurements of texture pattern C1 before and after the wear and durability experiments

Surface profile measurements were also taken for pattern B1 tested at three different sliding speeds and are presented in Figure 3.44.

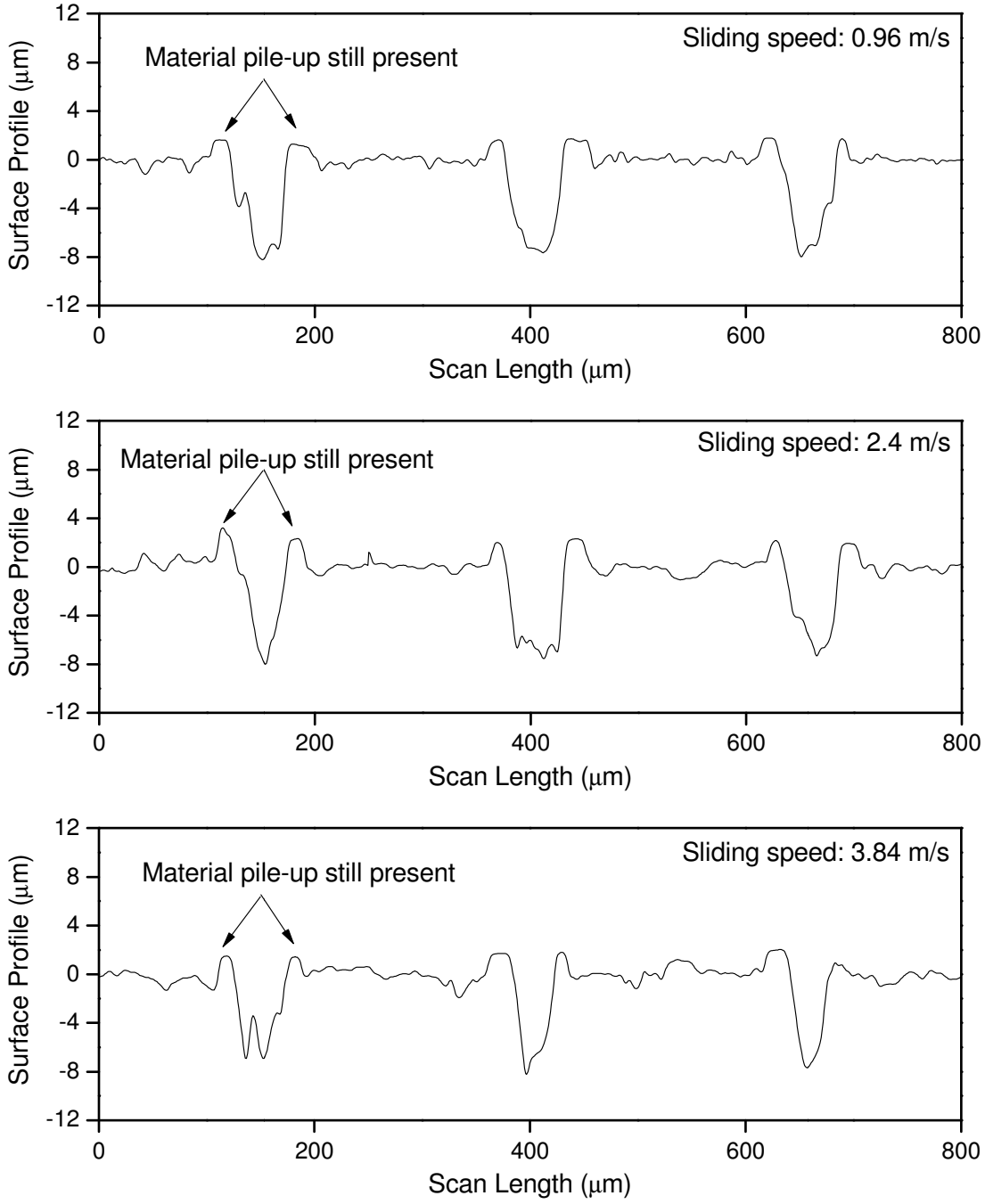

Figure 3.44: Surface profile measurements of texture pattern B1 after testing at three different sliding speeds: 0.96 m/s, 2.4 m/s and 3.84 m/s

As can be seen in Figure 3.44, the height of the material pile-ups or bulges around the micro-dimples is very similar even when tested at three different sliding speeds. This probably means that most of the wear of these pile-ups or bulges occur during the initial contact between the disk and the pin and is not dependent on the sliding speed. The optical images in Section 3.3.1 also showed that the wear of texture pattern B1 was in fact similar irrespective of the sliding speed.

Figure 3.45 shows the surface profiles of texture pattern C1 tested with different lubricants namely PAG, POE and Mineral oil. Texture pattern C1 suffered the maximum burnishing when tested in the presence of POE lubricant. These results corroborate the optical images shown in Section 3.3.2. Although PAG lubricant appeared to be the best performing from the optical images, no significant difference is observed in the surface profiles after the tests with PAG lubricant and Mineral oil. High magnification SEM images will be presented in Section 3.6 to observe more closely the surface of these texture patterns for any morphological changes.

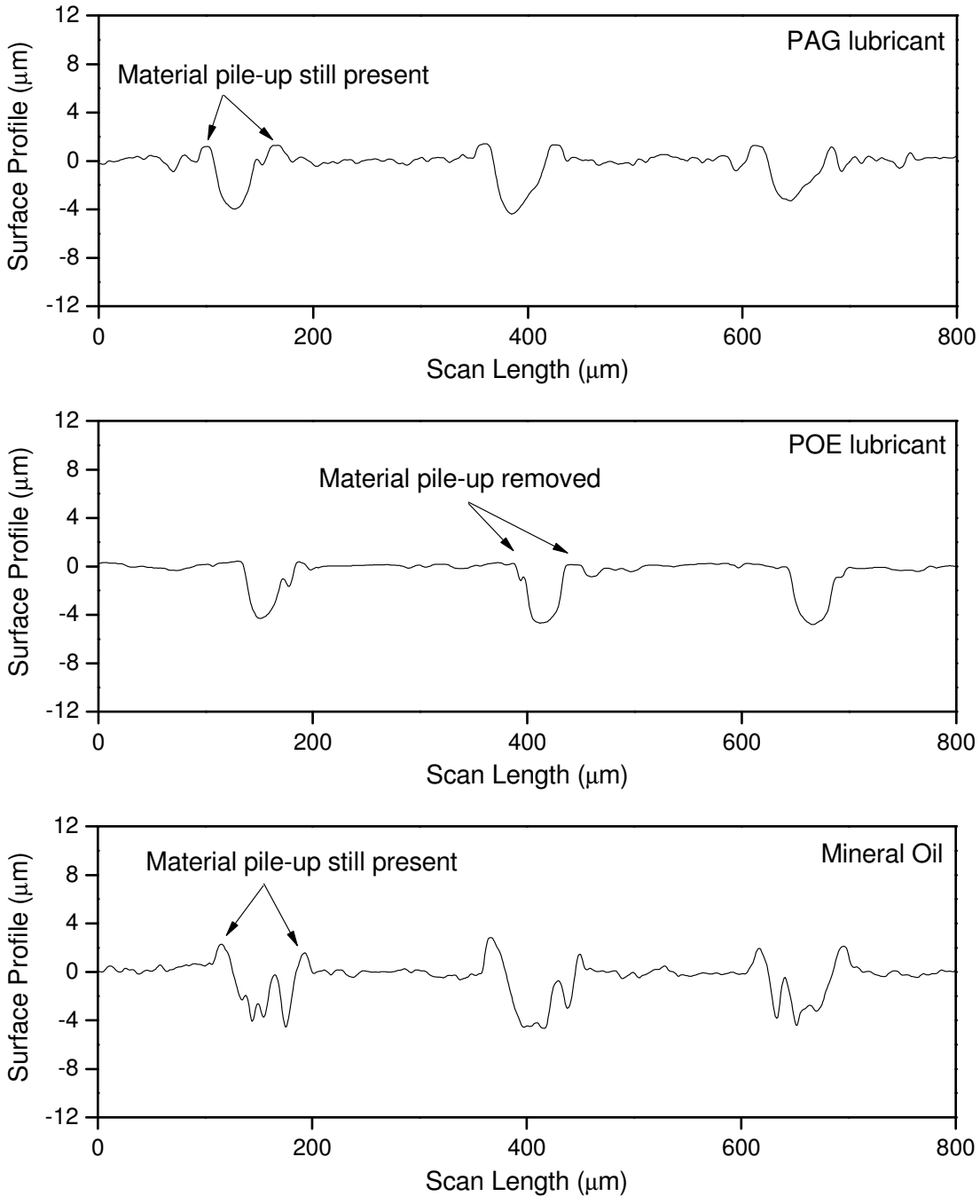

Figure 3.45: Surface profile measurements of texture pattern C1 tested with three different lubricants: PAG, POE and Mineral oil

Figure 3.46 compares the surface profiles of texture pattern C1 after wear testing in the presence of different refrigerants. In all three cases, the wear of the texture pattern

C1 was not significant, as observed through the optical images in Section 3.3.3. However, from the surface profile measurements it appears that the wear performance in the presence of R-744 and R-234yf was similar and better than in the presence of R-134a.

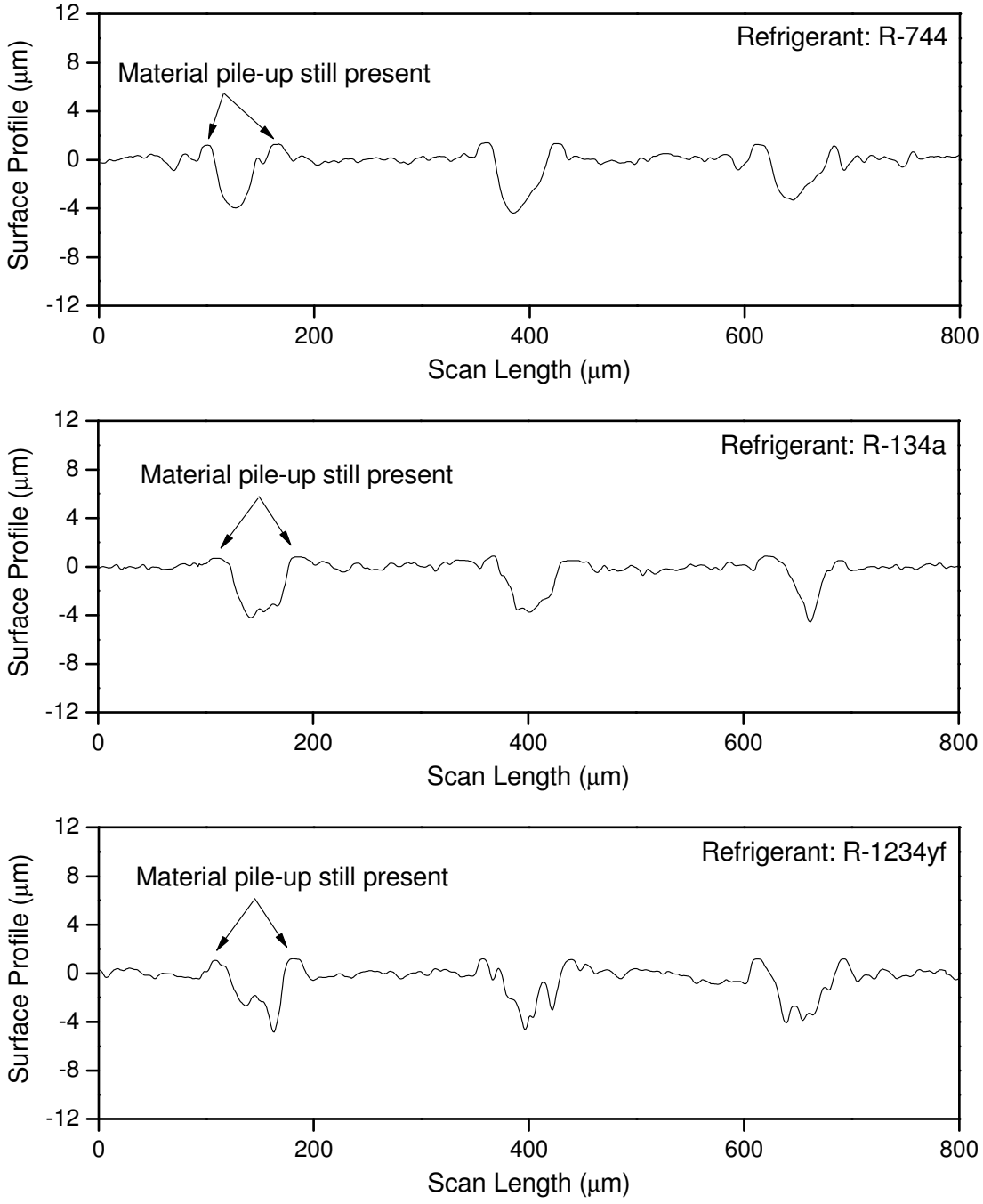

Figure 3.46: Surface profile measurements of texture pattern C1 tested in the presence of three different refrigerants: R-744, R-134a and R-1234yf

3.5.3 Calculation of wear rate

Even after continuous testing for extended periods of time, typical mass loss for the pins, if any, was in the range of 1-2 mg, which is roughly 0.06 – 0.12 % of the pin total mass. Thus, the mass loss of the pins was very small and negligible and could not serve as a good index for wear rate calculation. From the surface profile measurements in Section 3.5.2, it can be seen that textured pins displayed extremely good wear behavior. The material pile-ups around the micro-dimples of all the texture patterns suffered only mild burnishing and got flattened out, except for pattern A1 where they were removed during durability testing. Thus, the wear volume is extremely small. This also indicates that the material pile-ups or bulges are probably harder and more wear resistant. Some preliminary nanoindentation measurements were performed on texture pattern C1. The hardness and reduced elastic modulus of the flat area between the micro-dimples was 9 GPa and 153 GPa respectively. In comparison, measurements were done on the top of the material pile-ups and yielded values of 13 GPa and 175 GPa. Clearly, laser texturing has an effect on the surface nano-mechanical properties, which needs further detailed investigation.

It is difficult to calculate the wear volume from the surface profile measurements, as all the material pile-ups are not identical in shape and it would require measuring each of the material-pileups which would be extremely time-consuming. Even then, the results would not be accurate with the 1-D line scans and full 2-D areal scans would be necessary. Thus, to calculate the wear volume and hence wear rate, the simple geometrical representation of the material pile-ups or bulges, discussed in Chapter 2, can

be used. Figure 3.47 shows a schematic of the proposed geometric model for wear of the material pile-ups.

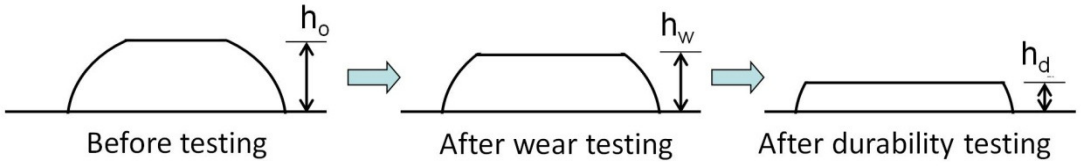

Figure 3.47: Schematic of the proposed wear calculation model for the material pile-ups around the micro-dimples on the textured surfaces (1-D surface profile of the material pile-up on only one side of the micro-dimple is shown)

The following are the assumptions on which the proposed wear calculation model is based:

(a) For all the texture patterns, the truncated spheres have the same diameter; the difference being the height h_o which is obtained from the surface profile measurements

(b) For a particular texture pattern, all the material pile-ups are identical in shape both before and after testing

(c) As the testing progresses, the surface of the truncated sphere wears out evenly only reducing the height of the material pile-ups: h_o is reduced to h_w after wear and h_d after durability testing

Based on the proposed geometric model for wear and the surface profile measurements of the texture patterns after the wear and durability experiments, the heights of the material pile-ups or bulges before the test h_o, after wear test h_w and after durability test h_d for the three texture patterns have been summarized in Table 3.2.

Similarly the heights of the material pile-ups or bulges after testing in different lubricants and refrigerants have been summarized in Table 3.3 and 3.4

Table 3.2: Height of material pile-ups after wear and durability experiments

Texture pattern	h_o (µm)	h_w (µm)	h_d (µm)
A1	9	3	0
B1	6	3	1
C1	4	2	1

Table 3.3: Height of material pile-ups on texture pattern C1 after testing in different lubricants

Lubricant	h_o (µm)	h_w (µm)
PAG	4	2
POE	4	0
Mineral Oil	4	2

Table 3.4: Height of material pile-ups on texture pattern C1 after testing in different refrigerants

Refrigerant	h_o (µm)	h_w (µm)
R-744	4	2
R-134a	4	1
R-1234yf	4	2

Figure 3.48 shows a typical micro-dimple with the material pile-up around it geometrically represented as a truncated semi-circle.

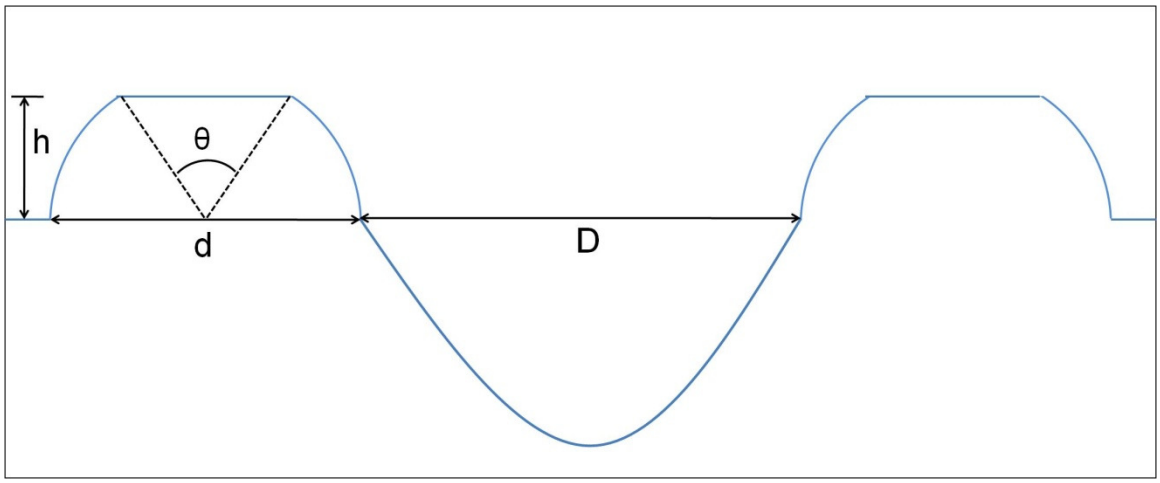

Figure 3.48: Schematic of a typical micro-dimple with the material pile-up geometrical represented as a truncated semi-circle

The area of the material pile-up can be given by

$$A = \frac{d^2}{8}(\pi - \theta + sin\theta)$$

where

$\theta = 2cos^{-1}\left(\frac{2h}{d}\right)$

d = width of the base of the material pile-up, equivalent to the diameter of the semi-circle

h = height of the material pile-up

The volume of the material pile-up can be approximated as follows:

$$V = \pi NA(D + d)$$

where

N = number of micro-dimples on the texture pattern surface

D = diameter of the micro-dimple

Using the information in Tables 3.2-3.4 and the geometrical formula above, the wear volume is calculated. The wear rate is expressed in a normalized manner as a function of the sliding distance and the applied normal load, given by

$$Wear\ rate = \frac{Wear\ volume\ (mm^3)}{Normal\ load\ (N) x\ Sliding\ distance\ (m)}$$

Figure 3.49 shows the comparison of the calculated wear rate for the texture patterns A1, B1 and C1 for the wear and durability experiments. The wear rates for the durability experiments were 45-50% lower than that of the wear experiments. This implies that most of the wear of the material pile-ups or bulges around the micro-dimples occurred during the initial contact and hence wear rate is not uniform.

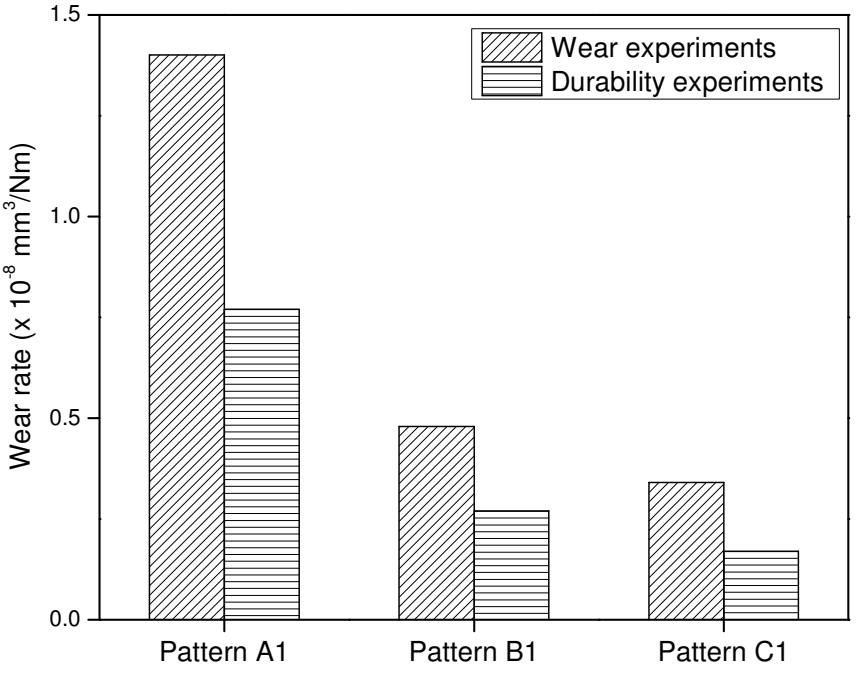

Figure 3.49: Calculated wear rates for the texture patterns A1, B1 and C1 after wear and durability experiments in the presence of R-744 with 23 mg of PAG lubricant applied directly at the interface

Figure 3.50 compares the calculated wear rates for texture pattern C1 tested with different lubricants namely PAG, POE and Mineral oil. It should be noted that the wear rate calculations are based on the surface profile measurements which clearly showed that in the case of tests done with POE lubricant, the material pile-ups or bulges were completely removed. The performance of the PAG lubricant and Mineral oil was comparable, which is reflected in the wear rate values.

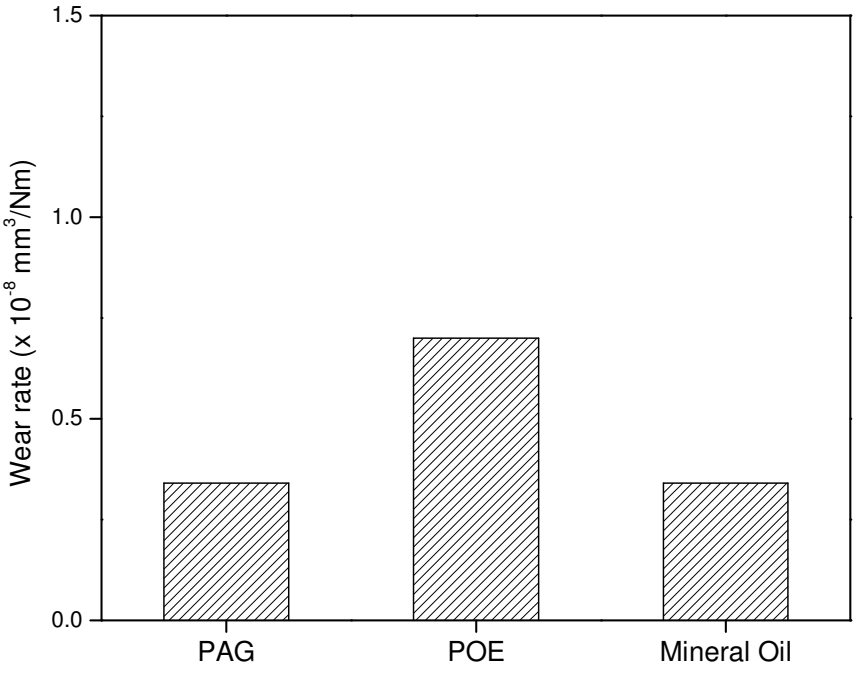

Figure 3.50: Calculated wear rates for texture patterns C1 tested in the presence of R-744 with lubricants PAG, POE and Mineral oil directly applied at the interface

Figure 3.51 shows the wear rate calculated for texture pattern C1 tested in different refrigerant environments namely R-744, R-134a and R-1234yf. R-1234yf is being touted as the direct replacement of R-134a due to environmental concerns and thus, it is encouraging to observe that the wear performance of the texture pattern is better in R-1234yf and comparable to R-744.

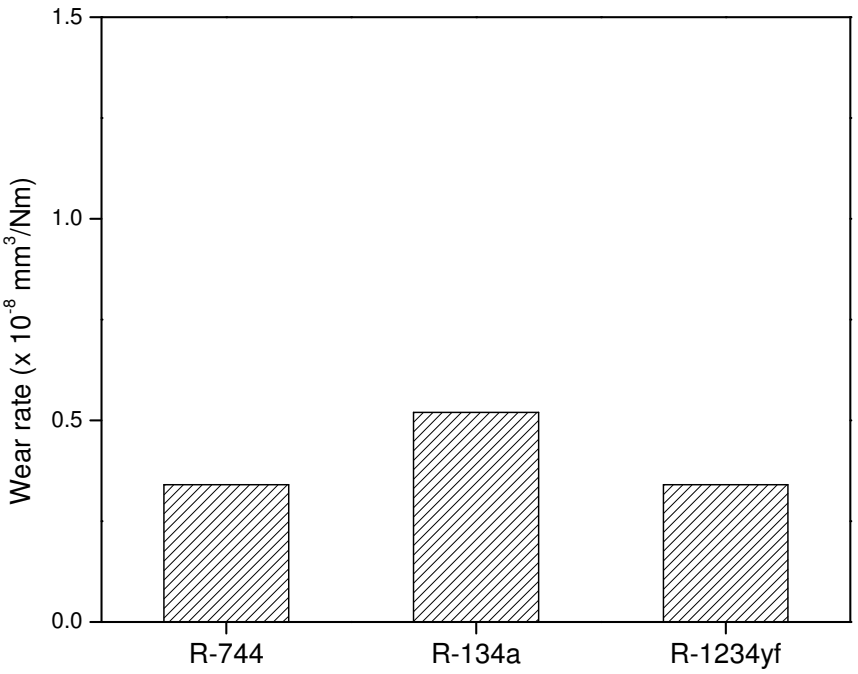

Figure 3.51: Calculated wear rates for texture patterns C1 tested in the presence of different refrigerants R-744, R-134a and R-1234yf with 23 mg of PAG lubricant directly applied at the interface

Overall, the simple geometric representation of the material pile-ups or bulges around the micro-dimples enabled the determination of wear rates for the experiments done under different conditions in this work. Despite small differences, the overall wear rate of the texture patterns at < 10^{-8} mm^3/Nm under starved lubrication conditions is really encouraging and comparable to different protective surface coatings. Nunez et al. [14] tested different PEEK based soft polymeric coatings under starved lubrication conditions in the presence of R-744 and reported the wear rates to be ~ 10^{-6} mm^3/Nm. Wear rate of ATSP/PTFE blends tested in unlubricated conditions have been reported to be ~ 10^{-5} mm^3/Nm [49] while those for WC/C + DLC hard coating in unlubricated conditions in the presence of different refrigerant environments has been reported to be ~ 10^{-9} mm^3/Nm [2].

3.6 SEM/EDS studies

Morphological changes on the pin surfaces after testing were analyzed using a Scanning Electron Microscope. In few cases, EDS was also used to analyze the spectrum at different locations on the pin surface after testing, to further understand any chemical changes that might have occurred on the surface. A JEOL 6060LV SEM working at 20 kV coupled with an EDS detector which measures the relative abundance of emitted X-rays versus their energy, was used for this purpose.

Figure 3.52 shows the SEM images of the surfaces of the texture patterns A1, B1 and C1 after wear testing at a normal load of 178 N, sliding speed of 2.4 m/s in the presence of R-744 at a chamber pressure of 1.93 MPa with 23 mg of PAG lubricant at the interface. Also, are shown are high magnification images of single micro-dimples. From the figure, it is clear that the material pile-ups around the micro-dimples are not fully removed. During the course of testing, these material pile-ups get flattened out and form a stable tribo-contact with the rotating counter disk.

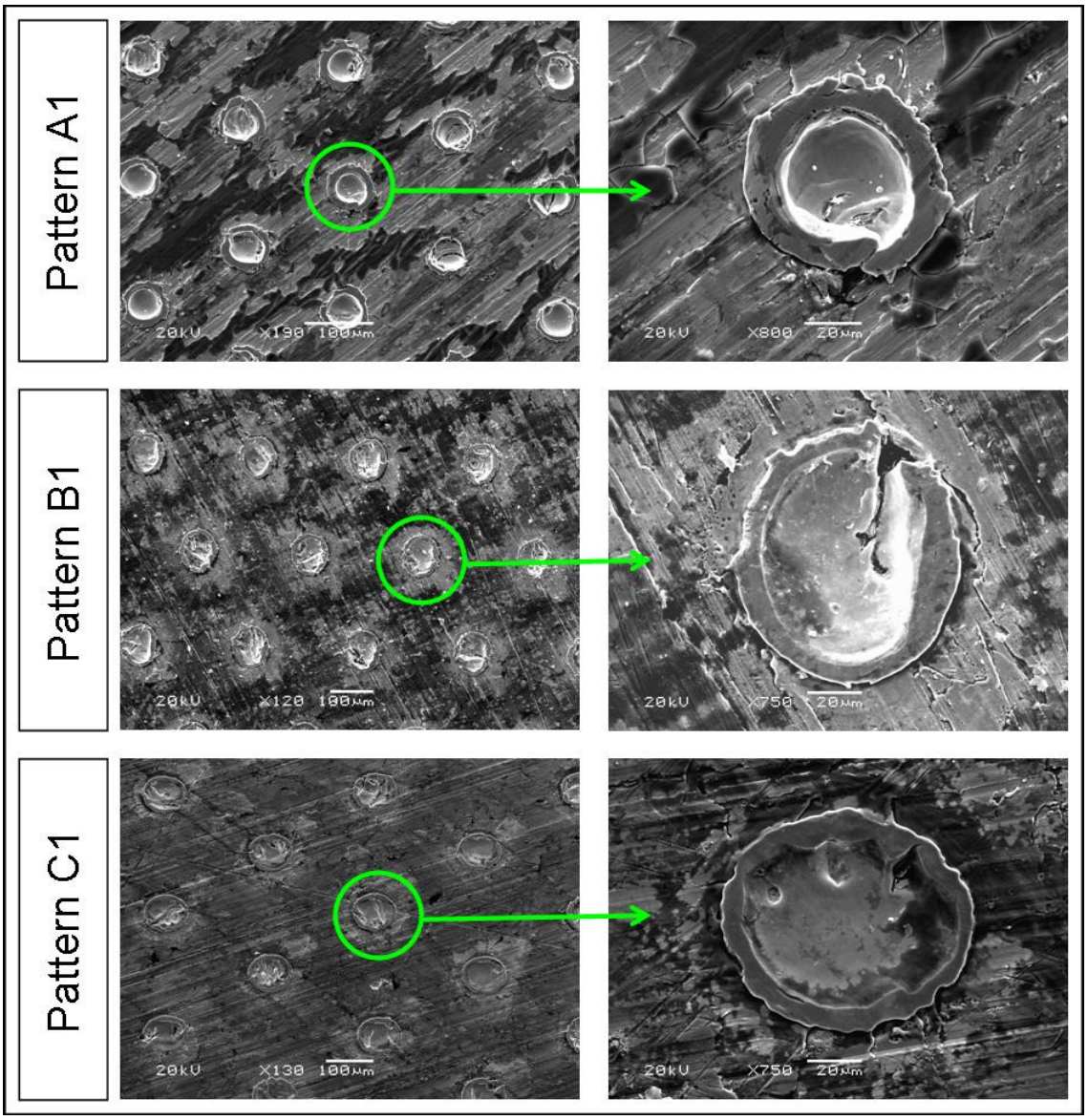

Figure 3.52: SEM images of the texture patterns A1, B1 and C1 after the wear experiments at 178 N normal load, 2.4 m/s sliding speed in the presence of 1.93 MPa R-744 with 23 mg of PAG lubricant applied directly at the interface

Figure 3.53 shows the SEM images of the surfaces of the texture patterns A1, B1 and C1 after durability testing at a normal load of 178 N, sliding speed of 2.4 m/s in the presence of R-744 at a chamber pressure of 1.93 MPa with small amount of PAG at the interface. From the optical images and wear profile measurements, it was suspected that for texture pattern A1 some contact between the pin surface and disk occurs. From the

SEM images, it is confirmed to be the case. Compared to texture patterns B1 and C1, there appear to be lot of polished or smooth regions on the surface of the texture pattern A1. This is possible when there is significant mechanical rubbing between the two surfaces such that the pile-ups are completely removed.

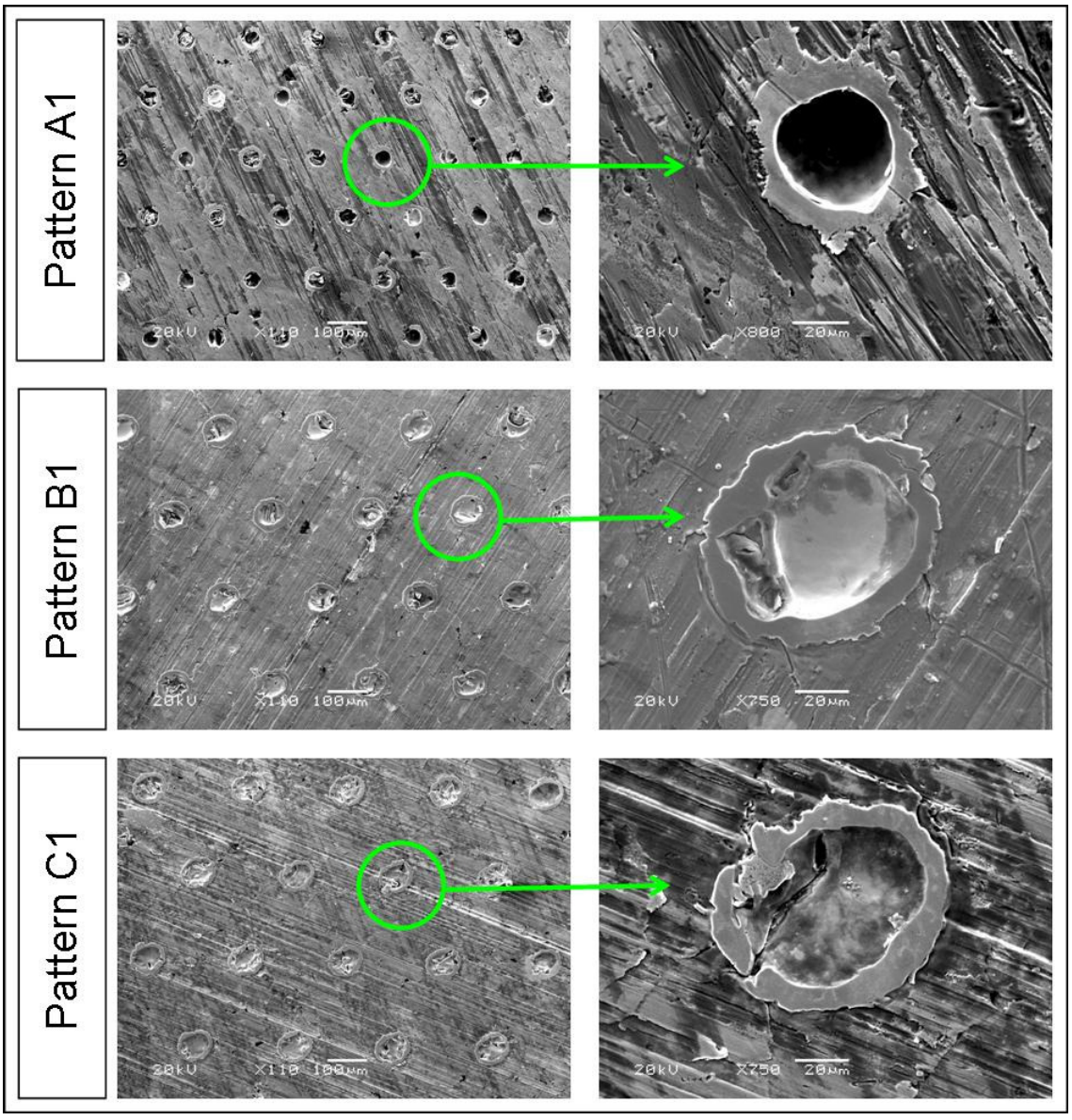

Figure 3.53: SEM images of the texture patterns A1, B1 and C1 after the durability studies at 178 N normal load, 2.4 m/s sliding speed in the presence of 1.93 MPa R-744 with 23 mg of PAG lubricant applied directly at the interface

For the experiments done with the different lubricants, although it was clear that the texture pattern C1 tested with POE lubricant was burnished the most, the surface of the texture pattern tested in Mineral oil also showed some damage in the optical images. Figure 3.54 shows the SEM images of surfaces of the texture pattern C1 tested with POE lubricant and Mineral oil. Clearly, surface damage in the form of a soft flaky film is noticeable when tested with Mineral oil and further investigations such as EDS studies are required to understand if any chemical changes are involved.

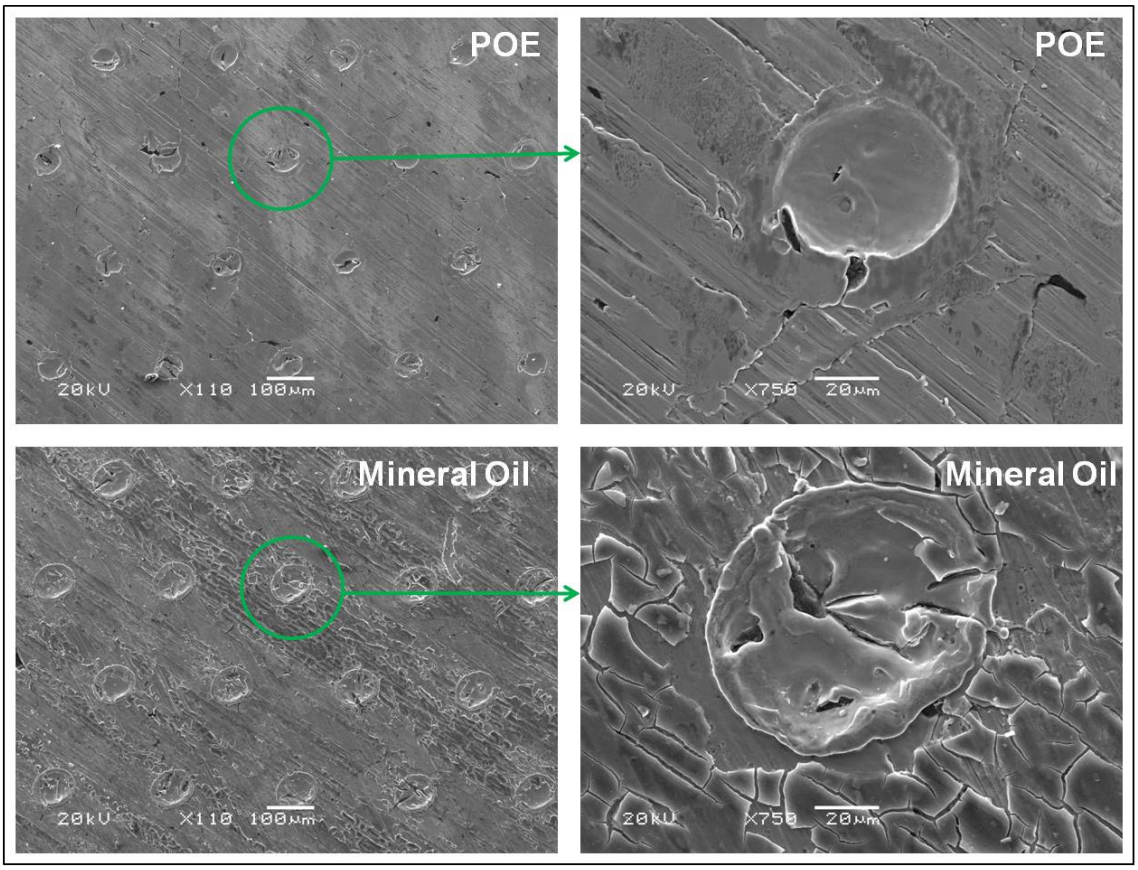

Figure 3.54: SEM images of the texture pattern C1 tested at 178 N normal load, 2.4 m/s sliding speed in the presence of 1.93 MPa R-744 with POE lubricant and Mineral oil applied directly at the interface

To verify that the observed surface morphological changes in some of the texture patterns after testing are due to mechanical rubbing only and not due to any chemical

changes, EDS studies were conducted next. EDS spectra from untextured surface and untested pattern A2 are presented as a baseline in Figures 3.55 and 3.56. This was done to capture any elemental changes due to the laser texturing process. EDS spectra were taken at different regions on each pin sample. In addition to the elements such as Fe, Si, F and C detected in the untextured surface (Figure 3.55), some traces of O were detected in the texture pattern A2 (Figure 3.56). This indicates the formation of some oxides during the laser texturing process. This is expected as laser texturing is a high temperature process, causing melting of the surface material.

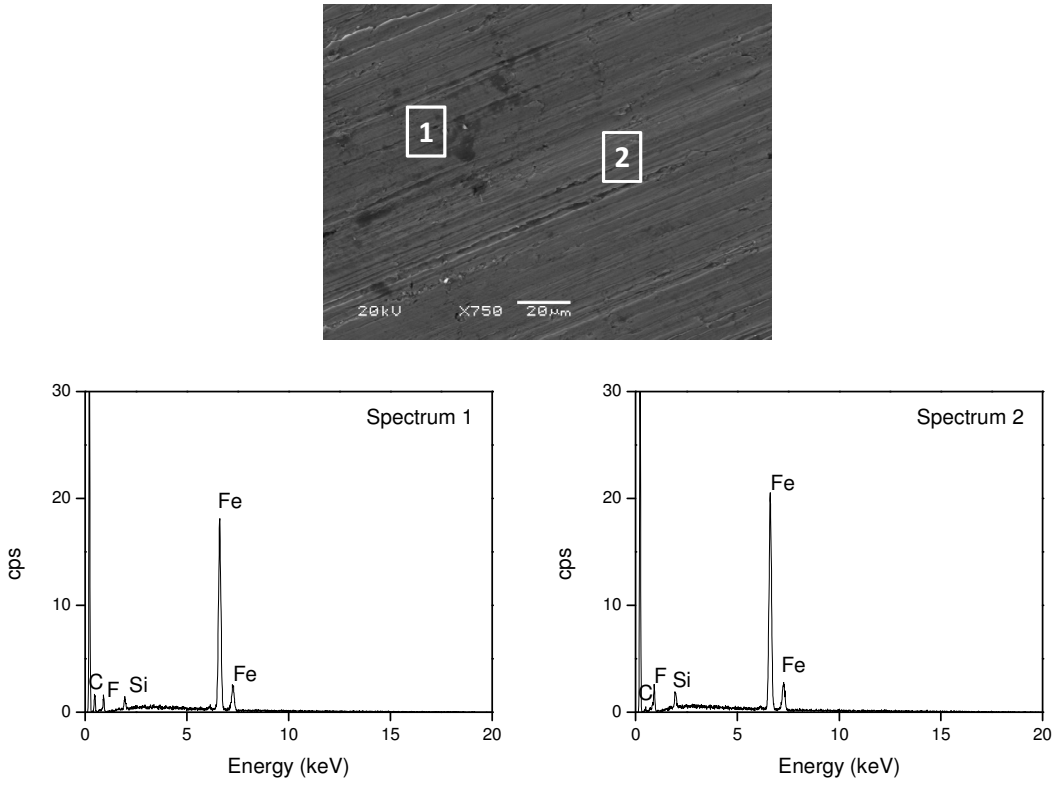

Figure 3.55: EDS spectra at different locations on untextured pin surface before testing

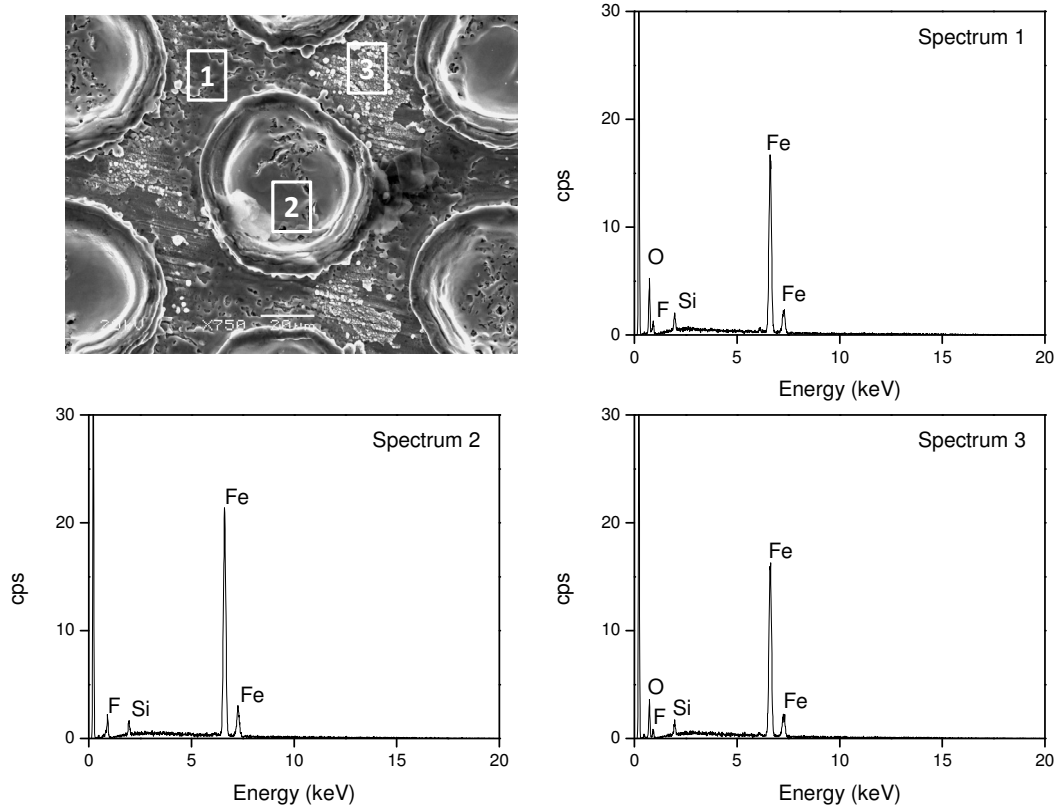

Figure 3.56: EDS spectra at different locations on texture pattern A2 before testing

From the high magnification SEM images in Figure 3.52 and 3.53, it appeared that there were some surface changes for texture pattern A1 after the wear and durability experiments. To investigate if there were any chemical changes, EDS studies were done. Figure 3.57 shows an SEM image of texture pattern A1 after wear experiment along with EDS spectra from two different locations on the surface. The same elements were detected as in the EDS spectra for texture pattern A2. This meant that no chemical changes occurred and the surface changes are due to mechanical rubbing action only.

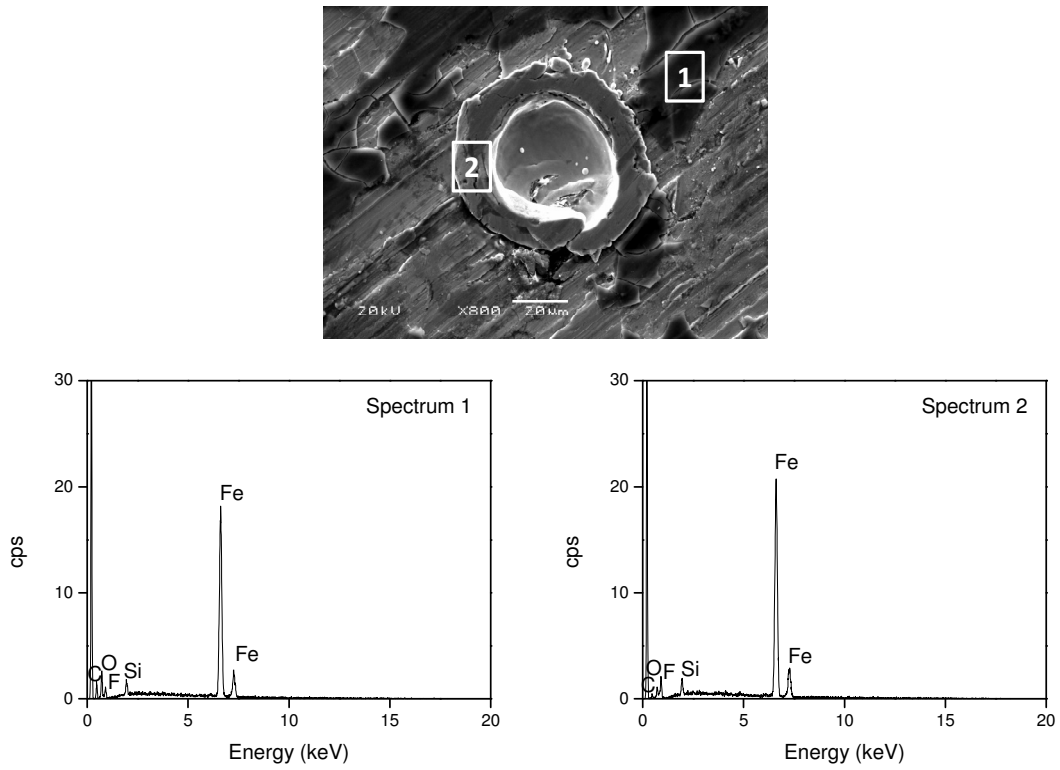

Figure 3.57: EDS spectra at different locations on texture pattern A1 after wear testing

Figure 3.58 shows an SEM image of texture pattern A1 after durability experiment along with EDS spectra from three different locations on the surface. From the SEM image it can be observed that the micro-dimple is filled with wear debris. This is because as the material pile-ups get worn out, the micro-dimples provide an easy escape route to the wear debris by trapping them. This is one of the mechanisms behind the improved wear performance of the textured specimens. From the EDS spectra, the chemical composition seems to be similar at all the three locations. However, traces of O which were seen in the EDS spectra for the texture pattern A2 were not detected, which probably meant that the oxides were completely removed due to the mechanical rubbing action.

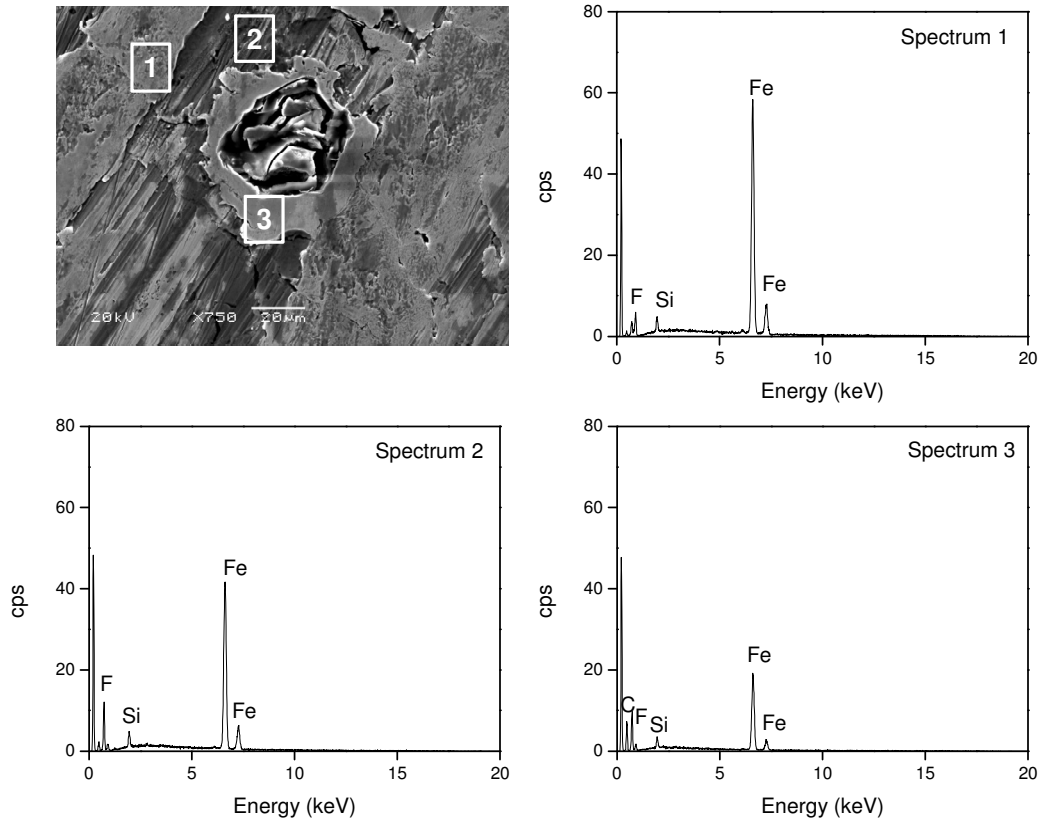

Figure 3.58: EDS spectra at different locations on texture pattern A1 after durability testing

Figure 3.59 shows the EDS spectra at two different locations on the surface of texture pattern C1 tested with Mineral oil. Similar elements were detected at both locations even though they were visually very different suggesting some changes. However, the EDS spectra confirmed that no chemical changes occurred and the surface damaged was only due to the mechanical rubbing action.

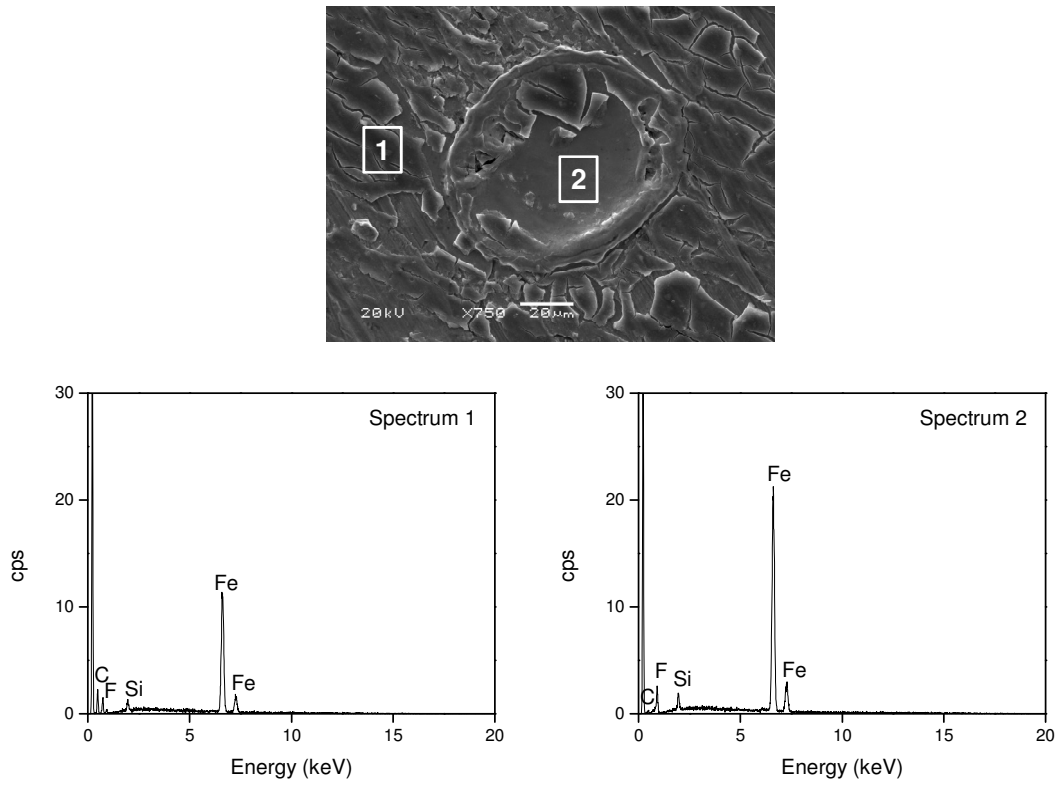

Figure 3.59: EDS spectra at different locations on texture pattern C1 tested with Mineral oil

3.7 Summary and Conclusions

In this chapter, detailed experimental investigations were carried out to answer two main questions:

1. Can surface texturing be used in compressor realistic operating conditions?
2. Can surface texturing provide any tribological benefit compared to the untextured specimen?

From the work done in this chapter, it is clear that surface texturing can indeed be successfully used in compressor realistic operating conditions. Surface texturing was found to significantly improve the performance. While untextured pins were unable to operate for more than approximately 10-20 minutes, textured pins operated successfully under identical conditions with minimal wear for up to three hours of continuous testing.

The wear rate was extremely low and was found to be equivalent to that of different protective surface coatings. Most importantly, all tests were carried out under starved lubrication conditions, which are typically very aggressive test conditions.

From the tests done with different sliding speeds, it was found out that the textured pins had no distinct advantage over the untextured pins at lower speeds, but at higher sliding speeds the benefit was clear. While untextured pin could not survive the test, textured pins ran successfully for the entire duration of testing. The effect of the texture geometry on the tribological performance was also more prevalent at aggressive conditions of higher sliding speeds. The wear performance was almost similar at small speeds as determined from the surface profile measurements.

The tribological advantages derived from the textured pins could be attributed to the lubricant storage and wear debris entrapment ability of the micro-dimples. Tests done in the presence of different types of lubricants proved the case in point. The good tribological behavior was not dependent on the type of lubricant chosen. Similar performance was observed for inexpensive mineral oils versus expensive synthetic compressor lubricants like PAG and POE. However, more polishing or burnishing of the texture pattern was observed for POE compared to PAG and Mineral Oil.

It was also found that the type of refrigerant environment does not have a great influence on the tribological performance of the textured pins. While the friction coefficients of the untextured pins were found to heavily dependent on the refrigerant environment, those for the textured pins had only a weak dependence. Tests done in the presence of R-744, R-134a and R-1234yf also highlighted the importance of the lubricant-refrigerant relationship in a compressor operating condition.

Among the different texture patterns, the difference in the performance though not much, was primarily driven by the geometrical parameters such as diameter, depth and area density of the micro-dimples. Usually the tribological performance got worse as the area density increased. A trade-off between the lubricant storage ability of the micro-dimples and the effect of the material pile-ups or bulges was realized. The effect of the material pile-ups or bulges could be significant as they not only generated wear debris but also provided a wear resistant contact surface. Further experiments, especially with polished textured surfaces to remove the material pile-ups or bulges and nano-mechanical property measurements of the pile-ups could provide insights into the effect of the pile-ups. Some preliminary results are presented in the appendix.

Thus, through the numerous experiments and analysis done in this chapter it can be concluded that surface texturing has a great potential for application in air-conditioning and refrigeration compressors to improve the durability and reliability of critical compressor components.

CHAPTER 4: SCUFFING EXPERIMENTS IN THE PRESENCE OF REFRIGERANT ENVIRONMENT

4.1 Objective

Scuffing refers to instantaneous or sudden failure of the sliding interfaces. It causes catastrophic damage, in particular, to the topmost layers (depths ranging from sub-micron to micron) [50]. This is of major concern for compressor manufactures as unlike other tribological failures it occurs abruptly, leading to complete destruction of the sliding pair, thus rendering the device non-functional [48]. Several factors affect scuffing such as contact pressure, sliding velocity, contact temperature, lubricant and lubrication regime, surface topography, materials etc. [50]. Several physical phenomena occur during the onset of scuffing, such as the collapse of the lubricant films, destruction of physically or chemically absorbed films, and breakdown of any protective oxide layers. Other phenomena like local thermal expansion, plastic flow of asperities, accumulation of wear debris at the sliding interface and failure of subsurface material have also been reported [51, 52].

Scuffing experiments are carried out in a step loading manner at a constant sliding speed where the normal load is increased in steps with specified step duration until failure occurs. The onset of scuffing is typically defined as the instance where a sharp increase in friction coefficient and near contact temperature is observed. This indicates the breakdown of the lubricant film or destruction of any protective surface layer. Such kind of experiments help to identify the maximum load carrying capacity of the sliding

interface and can be used to compare the performance of different materials, lubricants and refrigerants.

4.2 Experimental Procedure

Step-loading scuffing experiments were conducted in a pin-on-disk configuration on a High Pressure Tribometer (HPT), shown in Figure 4.1.

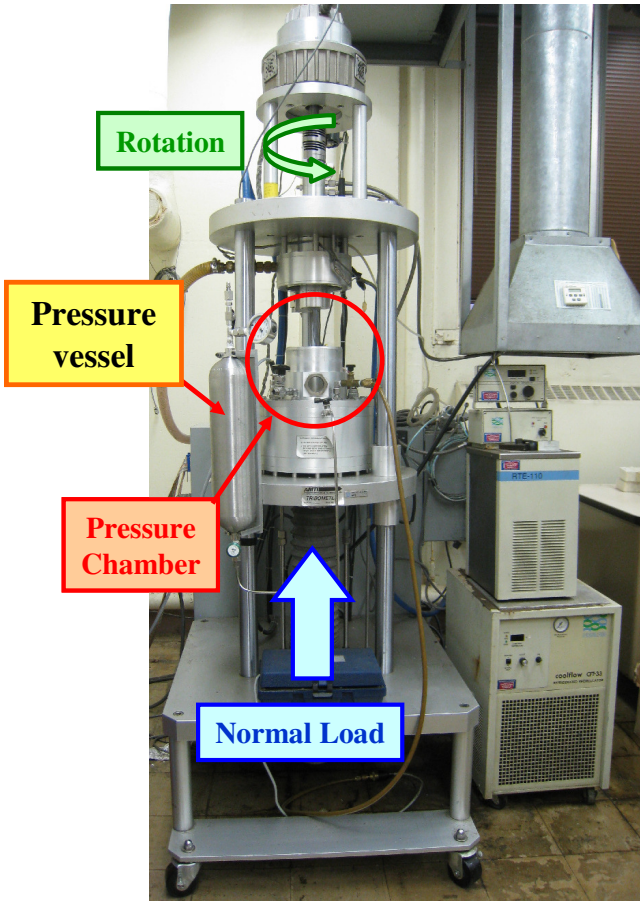

Figure 4.1: High Pressure Tribometer (HPT) showing the different components

The gray cast iron disk is attached to the rotating spindle while the gray cast iron pin is mounted on a holder at the bottom stationary part, which is connected to a six-axis

force transducer capable of measuring normal loads from 45 N to 4450 N and friction forces up to 2225 N using strain gauges. The DC servo motor is used to achieve rotational speeds as high as 2000 rpm. There is also an arrangement to measure the near contact temperature by inserting a thermocouple through miniature hole drilled up to 2 mm below the surface at the back of the pin. In addition, the chamber can be pressurized with a refrigerant up to 1.7 MPa (250 psi) and the temperature can be controlled from 10 °C to 120 °C by re-circulating a heat transfer fluid inside the hollow spindle.

Step loading experiments were performed with gray cast iron untextured and textured pins at a constant sliding speed of 2.4 m/s, ambient laboratory conditions of 20-22 °C and 40-50% RH, and 0.17 MPa of R-744. Normal load was applied in steps of 67 N every 30 seconds. Starved lubrication was simulated by directly applying a small amount of 23 mg of PAG lubricant (approximately one drop) at the interface. Although, the typical operating pressures for R-744 compressors are 3 MPa for the low pressure side and 12 MPa for the high pressure side, a lower pressure of 0.17 MPa (25 psi) was used for the testing because the effect of R-744 pressure on the viscosity of PAG in starved lubrication conditions is relatively small. Similar experiments with different material pairs have been successfully carried out earlier [4]. However, few tests were also conducted at 0.51 MPa (75 psi) of R-744 to investigate if there was any effect of the increased, albeit low, chamber pressure.

Before conducting the experiments, the samples were immersed in a pool of acetone and ultrasonically cleaned for 10 minutes, followed which they were rinsed with propanol and dried using warm air.

4.3 Results and Discussions

4.3.1 Scuffing performance

To establish a baseline, experiments were first conducted with untextured surfaces. Figure 4.2 shows the results of scuffing tests using untextured surfaces. As can be seen, after the brief running-in period, the friction coefficient becomes fairly constant until failure occurs, when the friction coefficient increases sharply. Two tests were done to ensure repeatability.

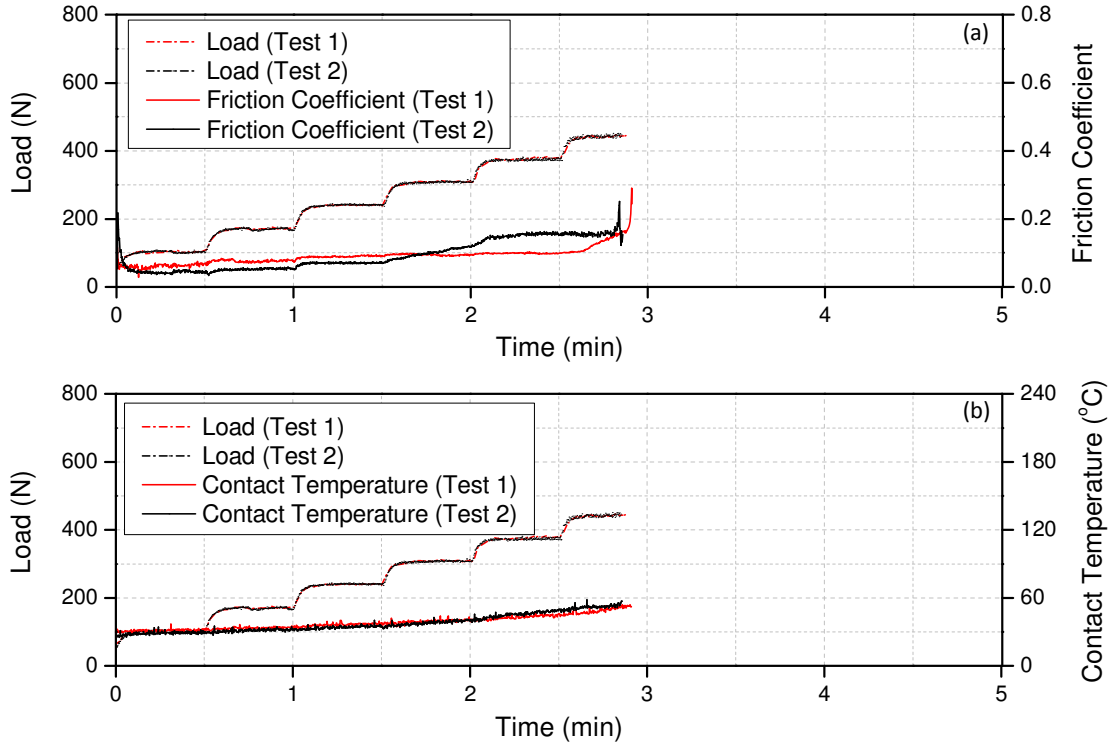

Figure 4.2: Scuffing performance of untextured surface at R-744 chamber pressure of 0.17 MPa (25 psi)

In both cases, the test lasted approximately 3 minutes. Although, such tests are of very short duration, they are useful in providing information about the maximum scuffing resistance of the sliding interface. It should be remembered that these tests were

conducted by directly adding a very small amount of lubricant before initiating the test. As the normal load keeps on increasing, the lubricant at the interface is "squeezed out" till the point where the interface runs out of lubricant resulting in increased metal-to-metal interaction. At the onset of scuffing, the friction coefficient increases sharply due to the adhesive interactions between the disk and pin. The contact temperature showed steady increase throughout the tests. For the untextured surface, scuffing was found to occur at approximately 450 N, compared to 2700 N for the experiments done by Demas et al. [48]. They conducted step loading scuffing experiments with gray cast iron pins and disks of similar geometry at 2.4 m/s sliding speed, R-744 chamber pressure of 1.4 MPa and chamber temperature of 120 °C. PAG lubricant was applied directly to the interface by an absorbing medium which ensured a thin film of lubricant at the interface until failure, unlike in this work where only 23 mg of PAG lubricant was used to simulate starved lubrication conditions. Also, the R-744 chamber pressure of 1.4 MPa, used by Demas et al. [48], is significantly higher than the chamber pressure of 0.17 MPa used in this work which could have a strong influence on the scuffing performance.

Textured pins have an array of micro-dimples on their surface, which increase the lubricant storage ability of the interface. This beneficial effect of the micro-dimples was seen during the constant load wear experiments performed in Chapter 3. Also, for scuffing or seizure resistance of sliding interfaces, deep micro-dimples have been shown to be advantageous under starved lubrication conditions [43] which again points to the lubricant volume available at the interface. Thus, as a start, texture patterns A2, B2 and C2 were tested for their scuffing resistance and compared against an untextured surface under identical conditions. This is because they had larger number of micro-dimples and

so higher lubricant volume at the interface. However, several other factors such as the geometry of the dimples, the area density and the material pile-ups around the micro-dimples could play a significant role and alter the results. So, the other texture patterns A1, B1 and C1 were also tested and the scuffing resistance was compared.

Figures 4.3 shows the results of the scuffing test for pattern A2. Two tests were done to ensure repeatability. In both cases, performance is similar and better than that of the untextured surfaces. The tests lasted about 3.5-4.5 minutes, with the average scuffing load being 610 N. The tests are repeatable and the little difference in the maximum scuffing load and friction coefficient may be explained by the fact that in both cases, the surfaces of the pins including the texture geometries and material pile-ups around the micro-dimples are not identical. In both cases, however, after the initial running-in the friction coefficient remained fairly stable for sometime beyond which it increases steadily until failure occurred. The interface is found to be unstable which may be due to the fact that as the normal loads became higher, lubricant was squeezed out of the interface and more wear debris was generated, particularly because the surface textured samples have material pile-ups around the micro-dimples. However, as the sliding continues, there is an opportunity for the wear debris to accumulate inside the micro-dimples. This would happen until the micro-dimples were clogged and scuffing occurred. This hypothesis is further corroborated through optical and high magnification SEM images which are presented and discussed later.

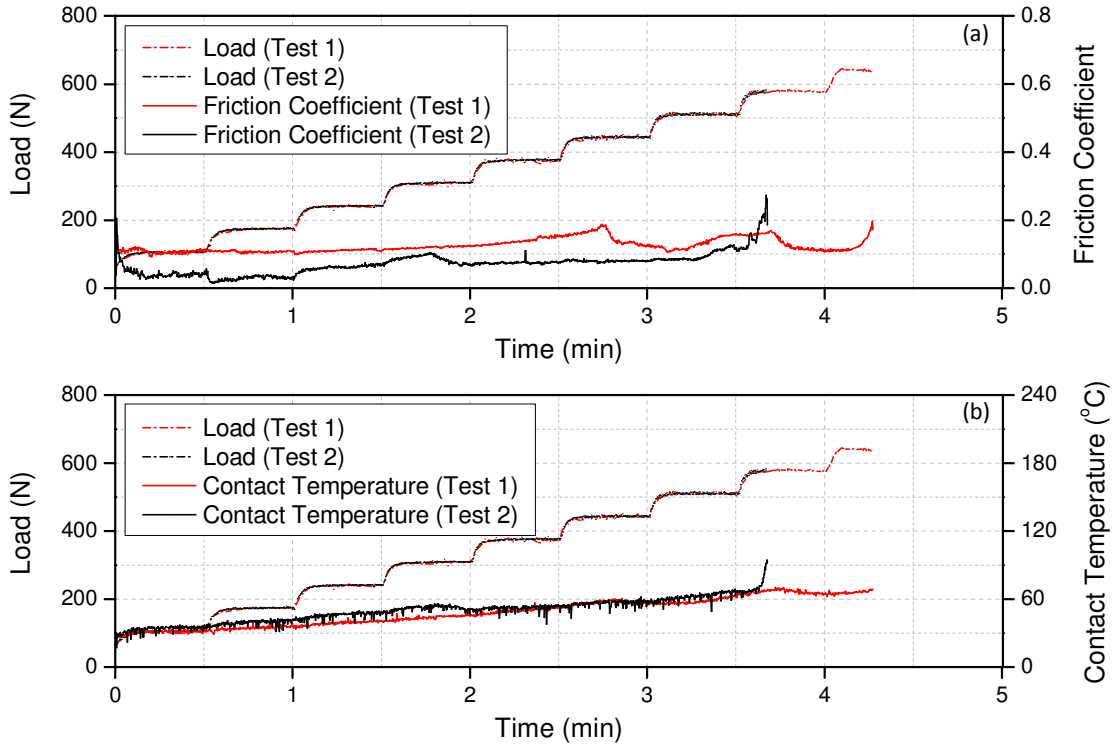

Figure 4.3: Scuffing performance of texture pattern A2 at R-744 chamber pressure of 0.17 MPa (25 psi)

Figure 4.4 shows the results of the scuffing test for pattern B2. The friction coefficient remained fairly constant at approximately 0.1 for about 4 minutes until it increased sharply when failure occurred. The maximum scuffing load for texture pattern was found to be approximately 600 N, which is similar to that of pattern A2. The micro-dimples on pattern A2 have a diameter of 40 µm and depth of 10 µm while those on pattern B2 have a diameter of 60 µm and depth of 7.5 µm. Thus, these two patterns are similar in terms of the lubricant storage volume and the height of the material pile-ups around the micro-dimples and hence, the scuffing load is similar.

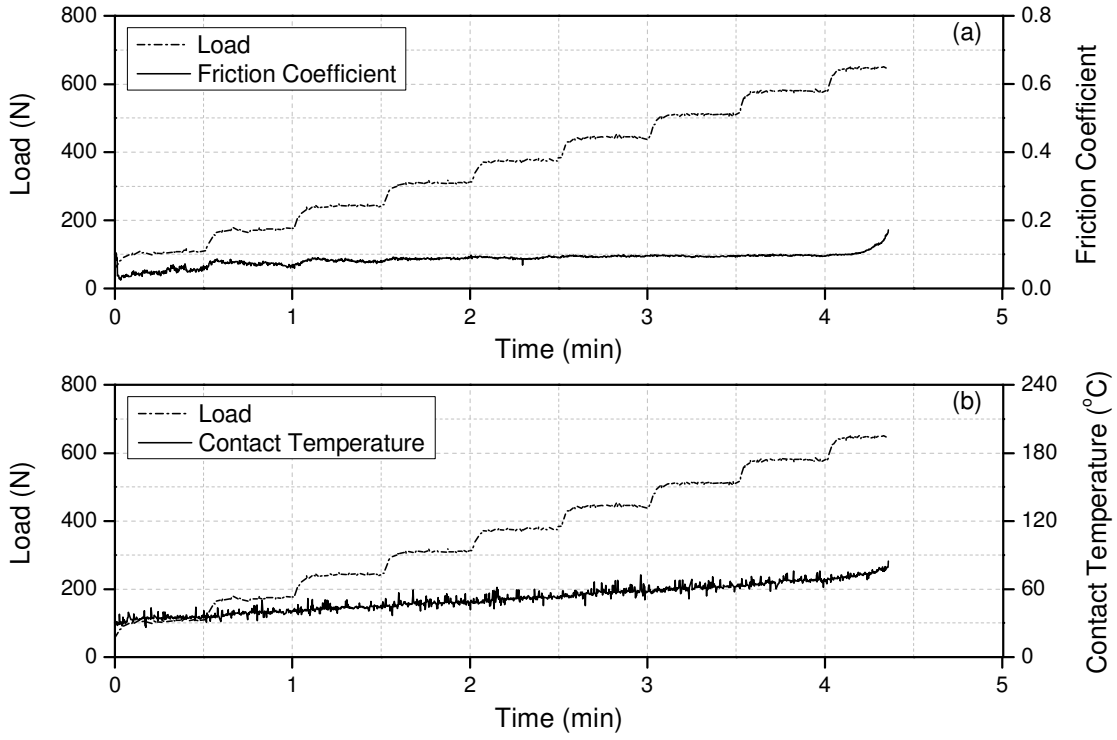

Figure 4.4: Scuffing performance of texture pattern B2 at R-744 chamber pressure of 0.17 MPa (25 psi)

In comparison to the scuffing loads of 610 N for pattern A2 and 600 N for pattern B2, the maximum scuffing load for pattern C2 was only 300 N. Figure 4.5 shows the results of the scuffing experiments using pattern C2. The micro-dimples on pattern C2 have a diameter of 60 µm and depth of 4 µm. Thus, the lubricant storage volume is the least for pattern C2 which means that less amount of lubricant was available at the interface as the load continually increased, finally causing failure at a lower load than other patterns.

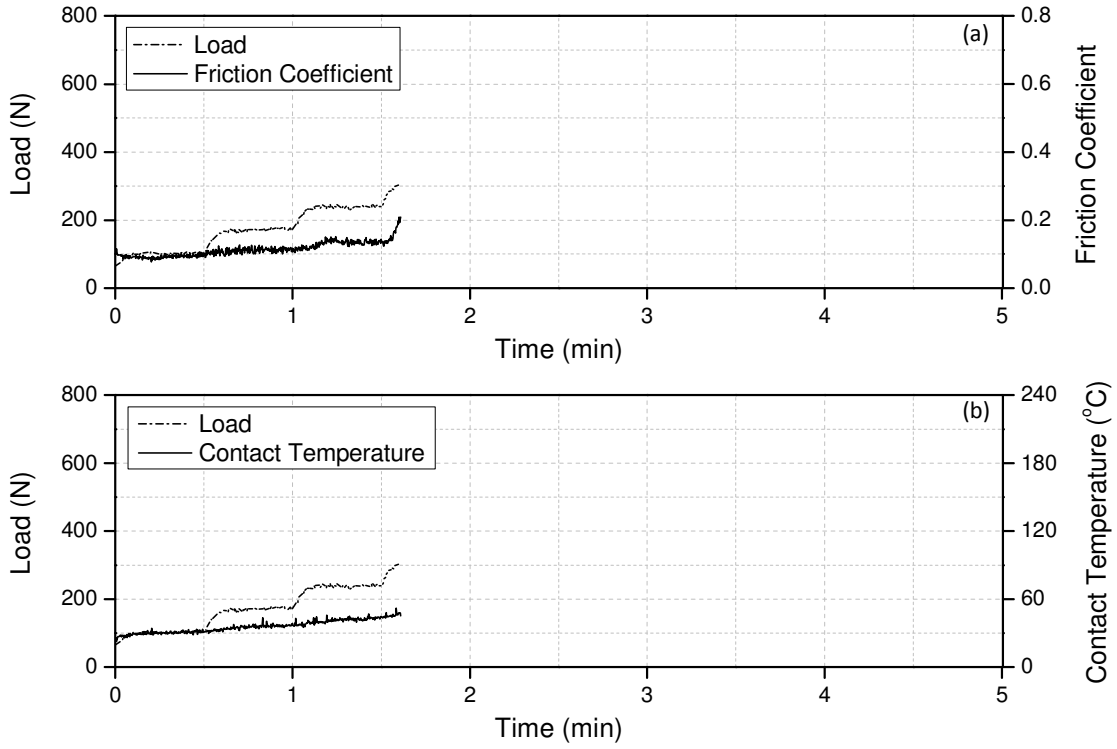

Figure 4.5: Scuffing performance of texture pattern C2 at R-744 chamber pressure of 0.17 MPa (25 psi)

Figure 4.6 shows the optical images of the textured and untextured pins used for the scuffing tests. Scuffing by definition is instantaneous failure due to solid phase welding without any local melting. From the optical pictures, it can be seen clearly that adhesive type failure occurred at the interface. It is interesting to note that the failure is localized on the pin surface and in the case of textured pins many micro-dimples are still intact.

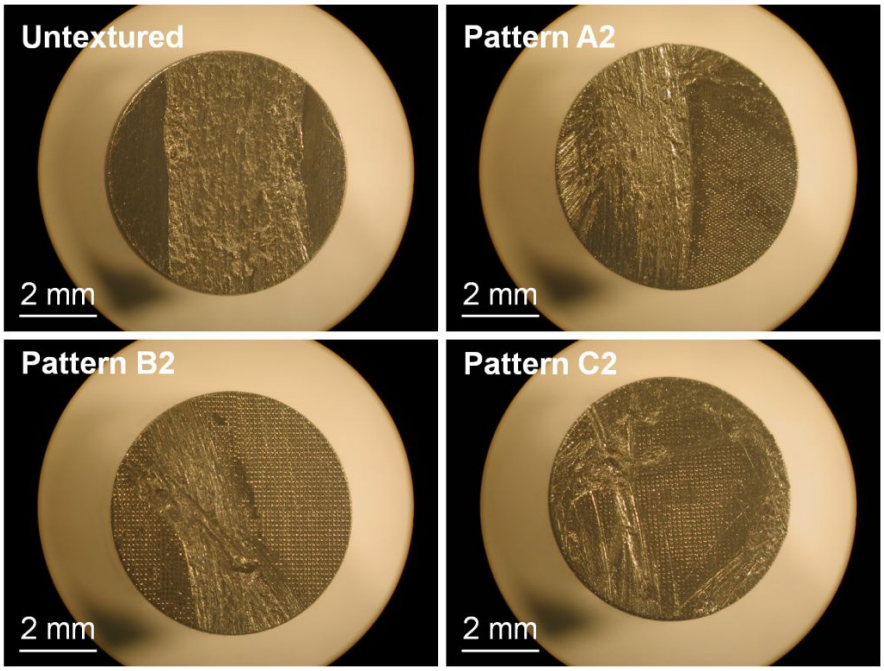

Figure 4.6: Optical images of the textured and untextured pins showing the scuffed surfaces

Figures 4.7 and 4.8 show higher magnification SEM images of the untextured surface and texture pattern A2. For the untextured surface, localized adhesive failure led to instantaneous scuffing. For the texture pattern A2, it can be noted that even though scuffing occurred, not all the micro-dimples were removed. The mechanism by which micro-dimples act under starved lubrication condition is also clear from the SEM image of the texture pattern A2 (Figure 4.8). As the test continues, wear debris generated due to the polishing of the material pile-ups under the action of the continually increasing step loading fills up the micro-dimples until they are fully clogged. At that point, the micro-dimples can no longer act as lubricant reservoirs and under the action of further loading eventually severe adhesive failure occurred.

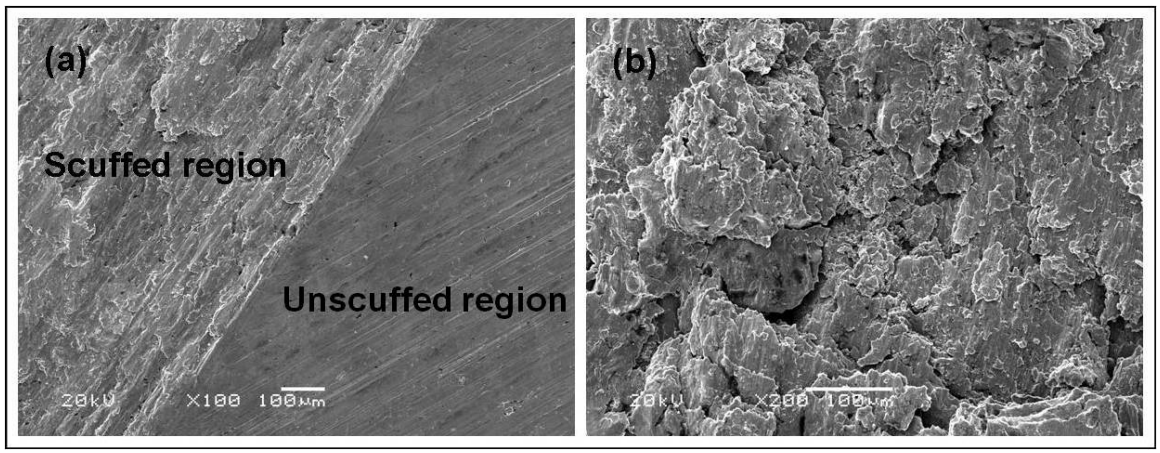

Figure 4.7: SEM images of the untextured surface showing the (a) transition between the scuffed and unscuffed region and (b) higher magnification image of the scuffed region

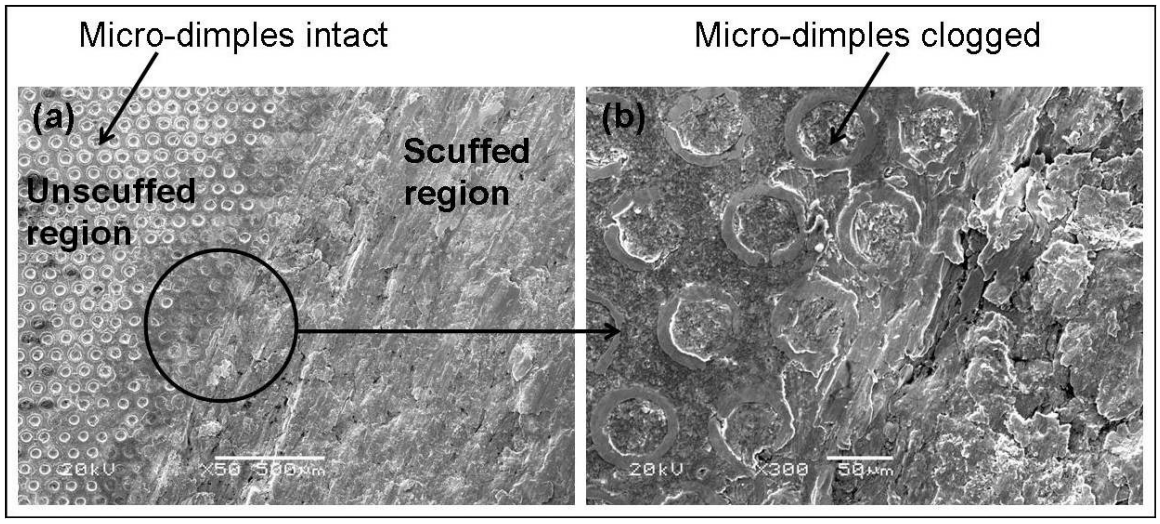

Figure 4.8: SEM images of the texture pattern A2 showing the (a) transition between the scuffed and unscuffed region and (b) higher magnification image of the scuffed region

To evaluate the damage on the counter surface gray cast iron disk, optical images were taken and surface profile measurements of the wear tracks were carried out. 1-D line scans were done across the wear tracks with the help of Tencor P-15 Surface Profilometer. 1-D line scans are a quick way to estimate the extent of damage by measuring the depth of the wear track. Figure 4.9 shows the optical images and Figure

4.10 shows the surface profile measurements of the wear tracks on the gray cast iron disks used for the testing.

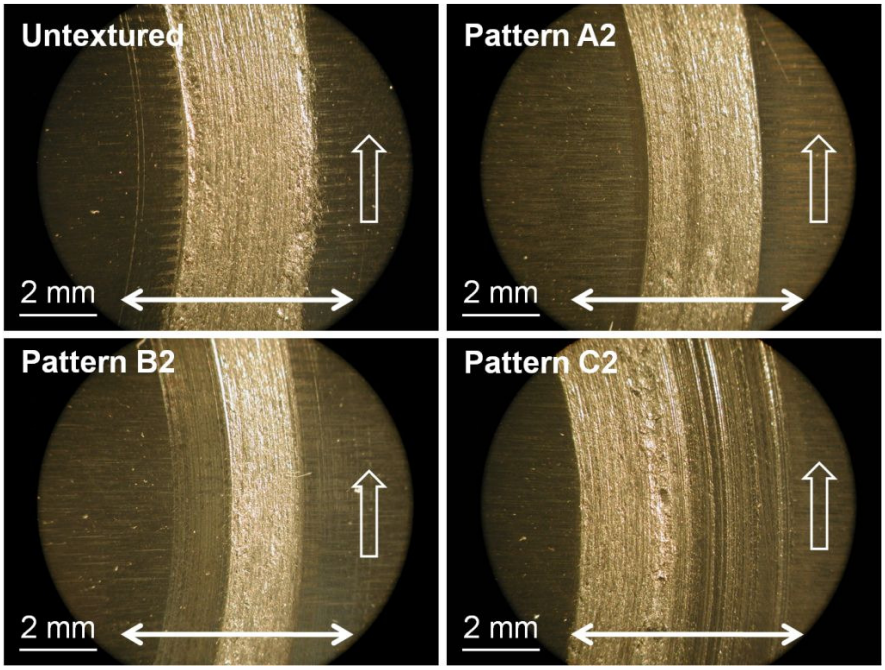

Figure 4.9: Optical images of the disks tested with the textured and untextured pins showing the wear tracks (Solid arrow indicates direction of machining marks and hollow arrow indicates sliding direction)

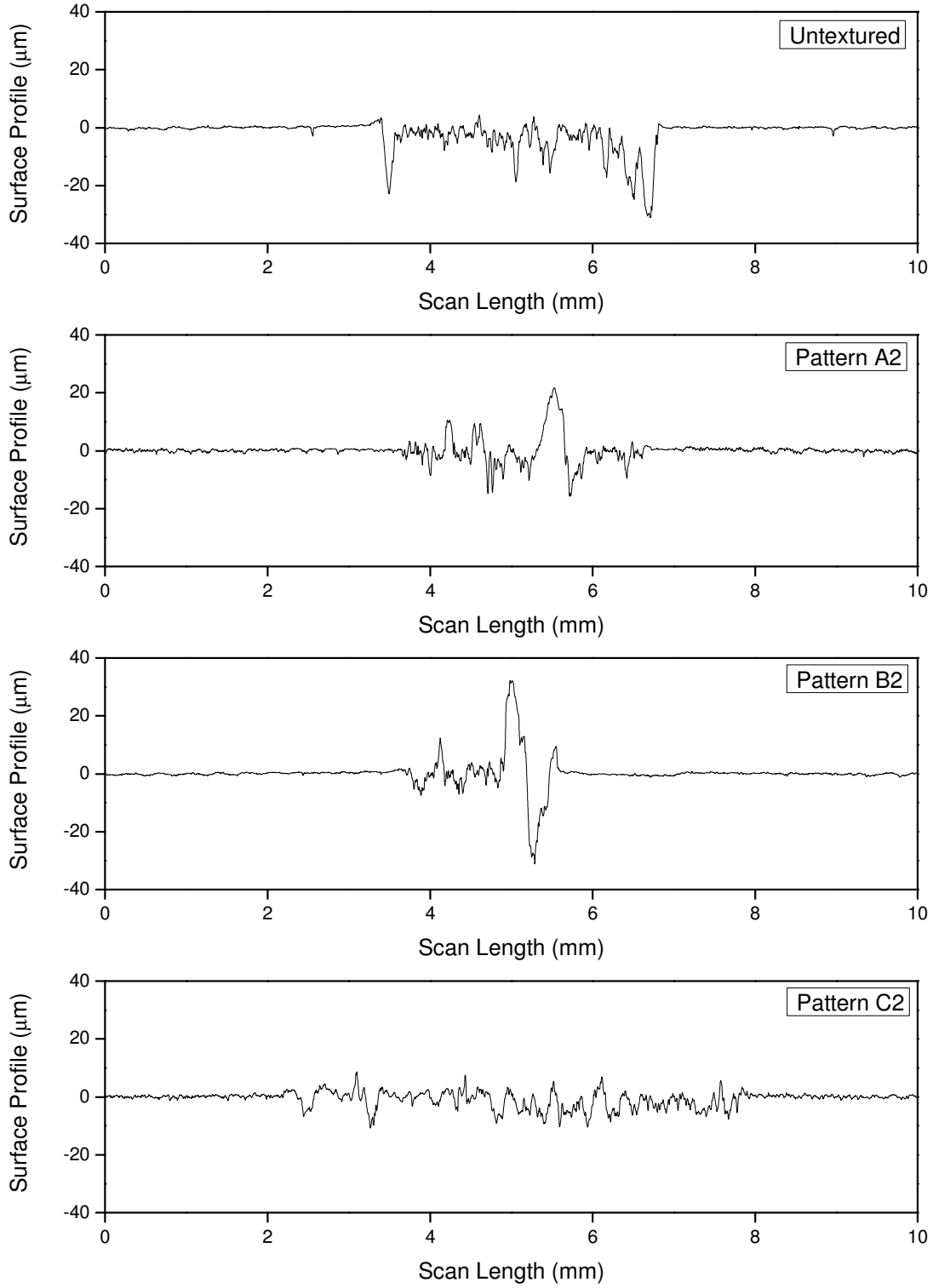

Figure 4.10: Surface profiles of the disk wear tracks after the scuffing tests at R-744 chamber pressure of 0.17 MPa (25 psi)

From the optical images and 1-D wear profile measurements it is clear that significant wear occurred which is expected since scuffing is a catastrophic failure. From Figure 4.10, it is clear that in some cases material transfer also occurred from the pin to the disk. All these again point to the adhesive nature of scuffing failure.

To further understand the role of the texture geometries and area density, scuffing experiments were also done on patterns A1, B1 and C1 which had the same geometrical features but reduced area density of 5 % than the earlier patterns. Figure 4.11 shows the results of the scuffing tests with texture pattern A1. The conditions were identical under which pattern A2 was tested.

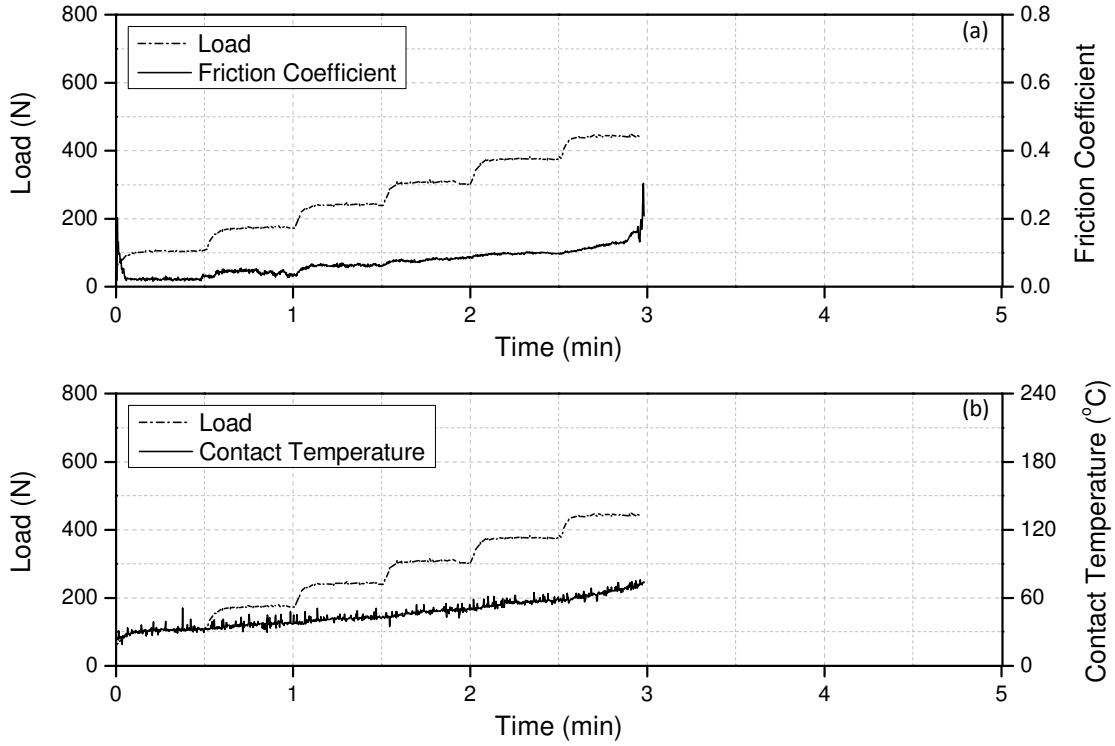

Figure 4.11: Scuffing performance of texture pattern A1 at R-744 chamber pressure of 0.17 MPa (25 psi)

Compared to pattern A2 which scuffed at 600 N, pattern A1 scuffed at 450 N. The difference between the two patterns is the area density. A1 has the lower area density of 5% which means that the number of material pile-ups and the lubricant storage volume for A1 is less than that of A2. Thus, this combined effect leads to a lower scuffing load for A1.

Figures 4.12 and 4.13 show the scuffing performance of pattern B1 and C1 tested under identical conditions as B2 and C2. Surprisingly, pattern B1 scuffed at approximately 200 N while pattern C1 scuffed at approximately 400 N. Pattern C1 having lower lubricant storage volume than A1 was expected to have a lower scuffing resistance and was indeed the case. However, the scuffing load of pattern B1 was expected to be more than C1 and closer to that of A1 due to similarity of the micro-dimples geometries. Thus, for clarity the experiments with pattern B1 should be repeated to establish conclusively the comparative scuffing performance.

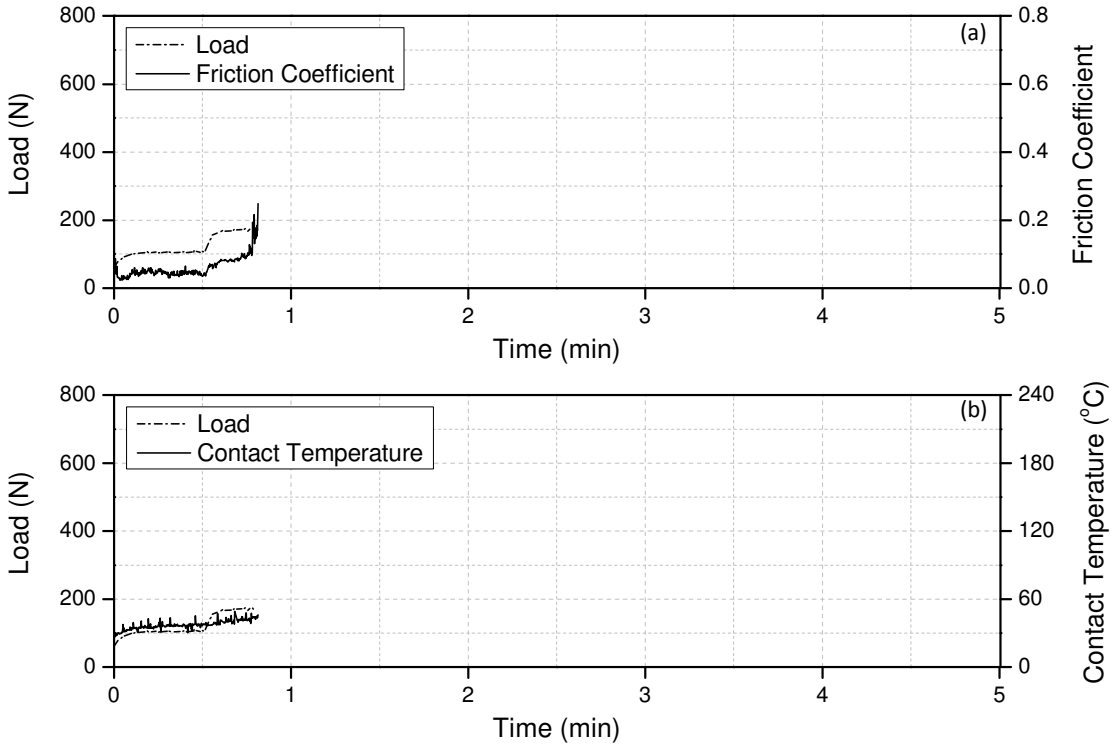

Figure 4.12: Scuffing performance of texture pattern B1 at R-744 chamber pressure of 0.17 MPa (25 psi)

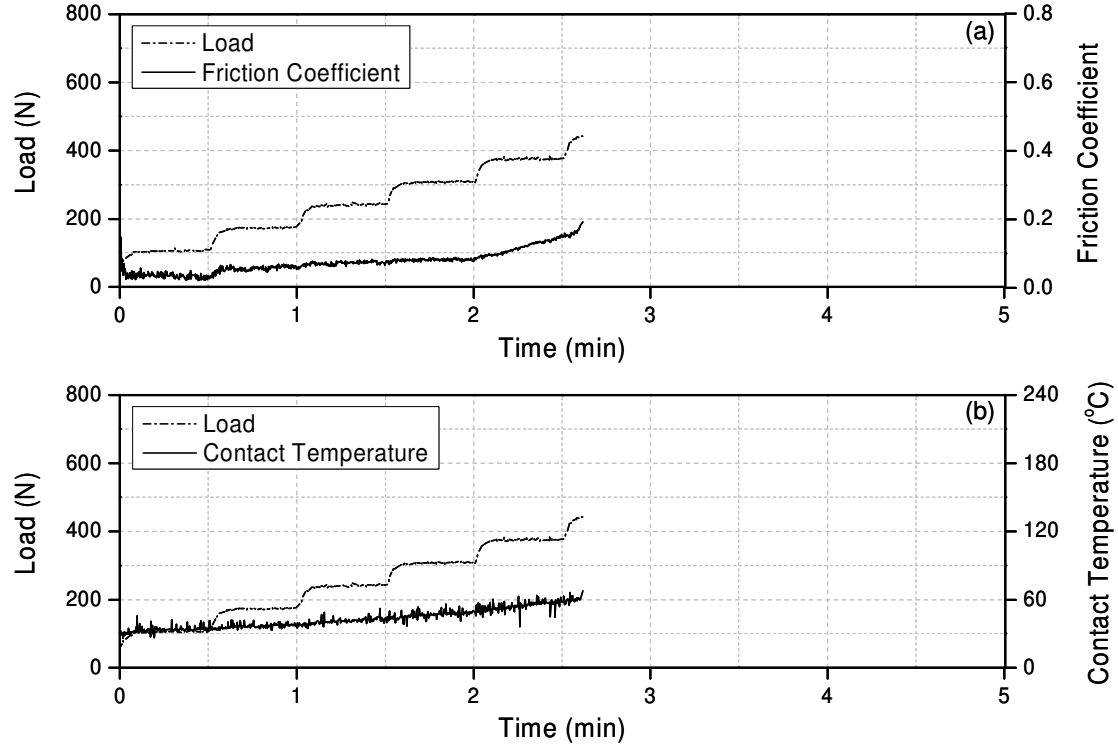

Figure 4.13: Scuffing performance of texture pattern C1 at R-744 chamber pressure of 0.17 MPa (25 psi)

Figure 4.14 shows the comparison of the scuffing load of the different untextured and texture patterns tested under identical conditions. From the figure, it is clear that texturing does not always help in improving the scuffing resistance. This is in contrast to the results from the wear and durability experiments, where texturing always proved to be beneficial. Except for pattern B1, the trend is similar between the two sets of texture patterns. Textures with deeper micro-dimples such as pattern A1 and A2 have a higher scuffing resistance than textures with shallow micro-dimples such as pattern C1 and C2. Thus, it can be concluded with fair degree of confidence that the lubricant storage ability of the micro-dimples manifested in the form of the volume of the micro-dimples play a more significant role than the material pile-ups of bulges in determining the scuffing resistance of the texture patterns. However, additional experiments should be performed to fully understand the role of material pile-ups or bulges and area density of the micro-dimples on the scuffing resistance.

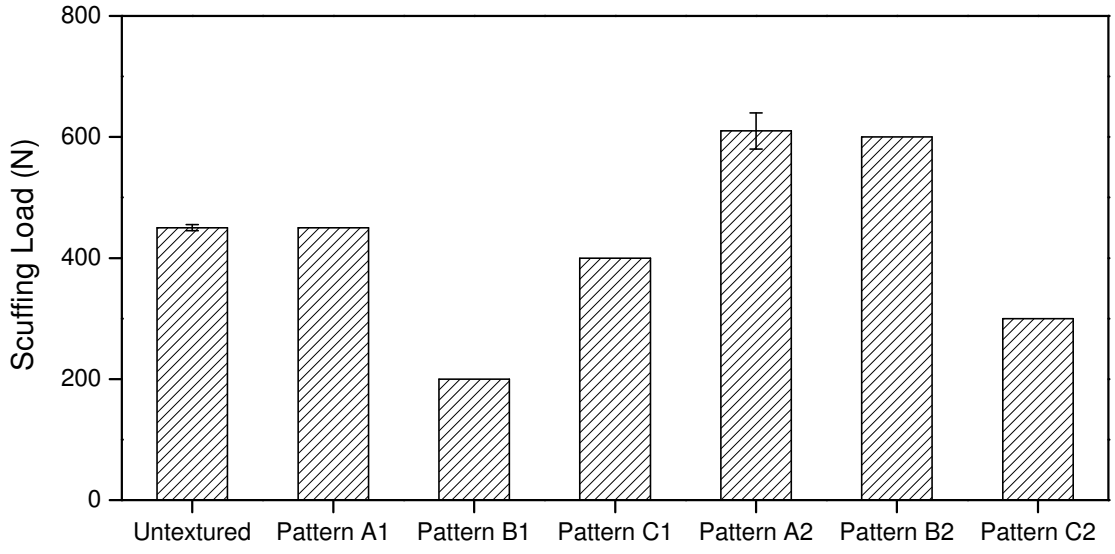

Figure 4.14: Comparison of the scuffing load of the different texture patterns with an untextured surface tested under identical conditions

4.3.2 Effect of R-744 pressure

To understand the effect of the chamber pressure on the scuffing performance, few tests were conducted at a higher chamber pressure of 0.51 MPa. Although only one test was done per sample, such step loading tests have been earlier shown to be repeatable when the untextured surface and texture pattern A2 were tested twice under identical conditions at 0.17 MPa of R-744 chamber pressure yielding similar scuffing loads. Figure 4.15 shows the results of the scuffing test for the untextured surface at 0.51 MPa chamber pressure of R-744.

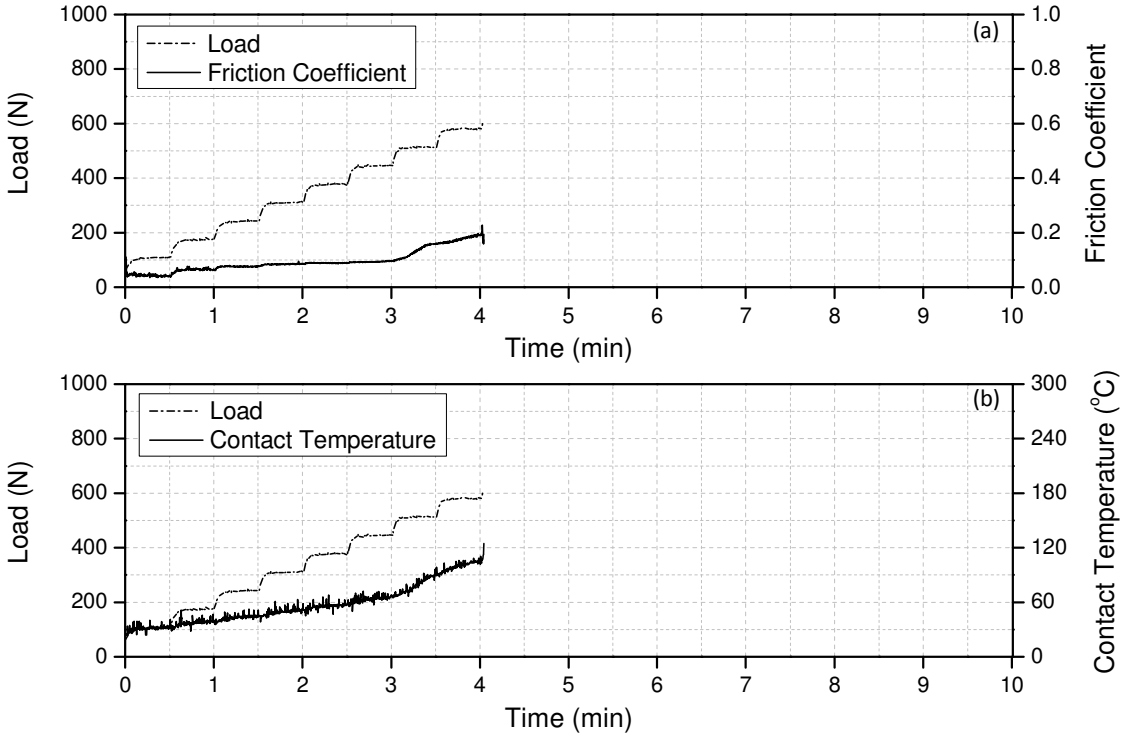

Figure 4.15: Scuffing performance of an untextured surface at R-744 chamber pressure of 0.51 MPa (75 psi)

For the untextured pin, the scuffing load is observed to increase when the pressure was increased three folds to 0.51 MPa. At a chamber pressure of 0.51 MPa, scuffing

occurred at 600 N compared to 450 N at 0.17 MPa (Figure 4.2). Thus, the pressure of R-744 seems to play a critical role in altering the tribological behavior. As can be seen in Figure 4.16, similar results were also observed when texture pattern A2 was tested at 0.51 MPa of R-744. Compared to a scuffing load of approximately 610 N at 0.17 MPa, scuffing occurred at 900 N.

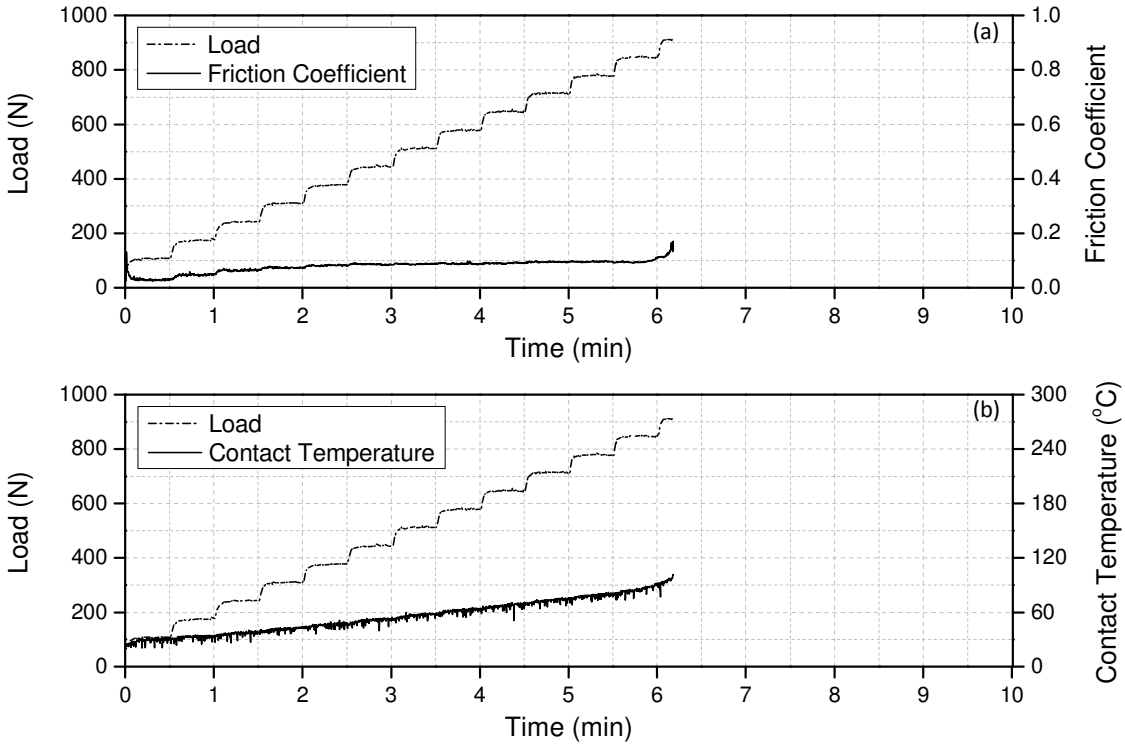

Figure 4.16: Scuffing performance of texture pattern A2 at R-744 chamber pressure of 0.51 MPa (75 psi)

Figure 4.17 summarizes the scuffing loads of the untextured surface and texture pattern A2 at two difference chamber pressures of refrigerant R-744. As can be clearly observed there is a positive trend of increased scuffing load with increased chamber pressure. Demas et al. [48] carried out similar scuffing experiments with untextured gray cast iron pins and reported the scuffing load to be 2700 N at 1.4 MPa of R-744 chamber

pressure. However, to conclusively establish this relationship additional experiments need to be performed in the future at higher chamber pressures of refrigerant R-744.

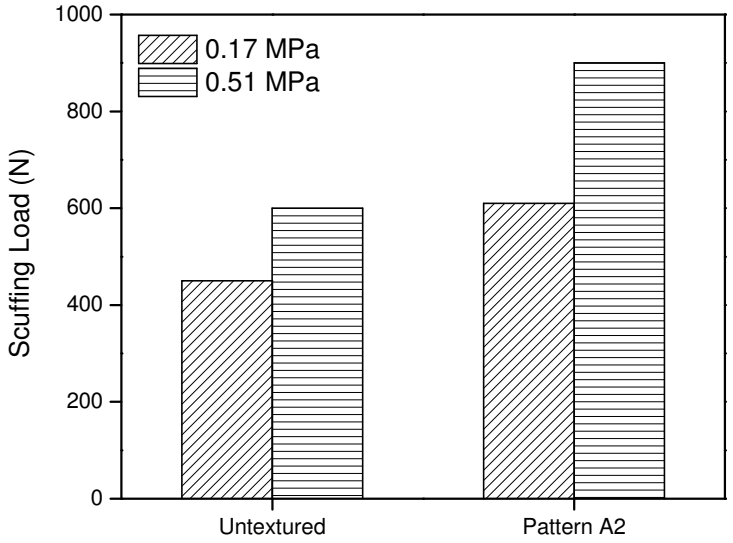

Figure 4.17: Comparison of the scuffing load between an untextured surface and texture pattern under starved lubrication conditions in presence of R-744 at chamber pressures of 0.17 MPa and 0.51 MPa

4.3.3 Effect of different refrigerants

The effect of different refrigerants namely, R-134a and R-1234yf on the scuffing resistance was also investigated. Texture pattern A2 was the best performing in the presence of R-744. So, it was selected for these tests. Step loading tests were performed at a constant sliding speed of 2.4 m/s, ambient laboratory conditions of 20-22 °C and 40-50% RH, and 0.17 MPa of chamber pressure. Normal load was applied in steps of 67 N every 30 seconds. Starved lubrication was simulated by directly applying small amount of 23 mg of PAG lubricant (approximately one drop) at the interface.

Figure 4.18 shows the scuffing performance in the presence of R-134a at 0.17 MPa chamber pressure. The friction coefficient was somewhat erratic until failure occurred at approximately 400 N. It might be recalled that under identical conditions,

pattern A2 failed at 600 N which points to the significance of the refrigerant environment.

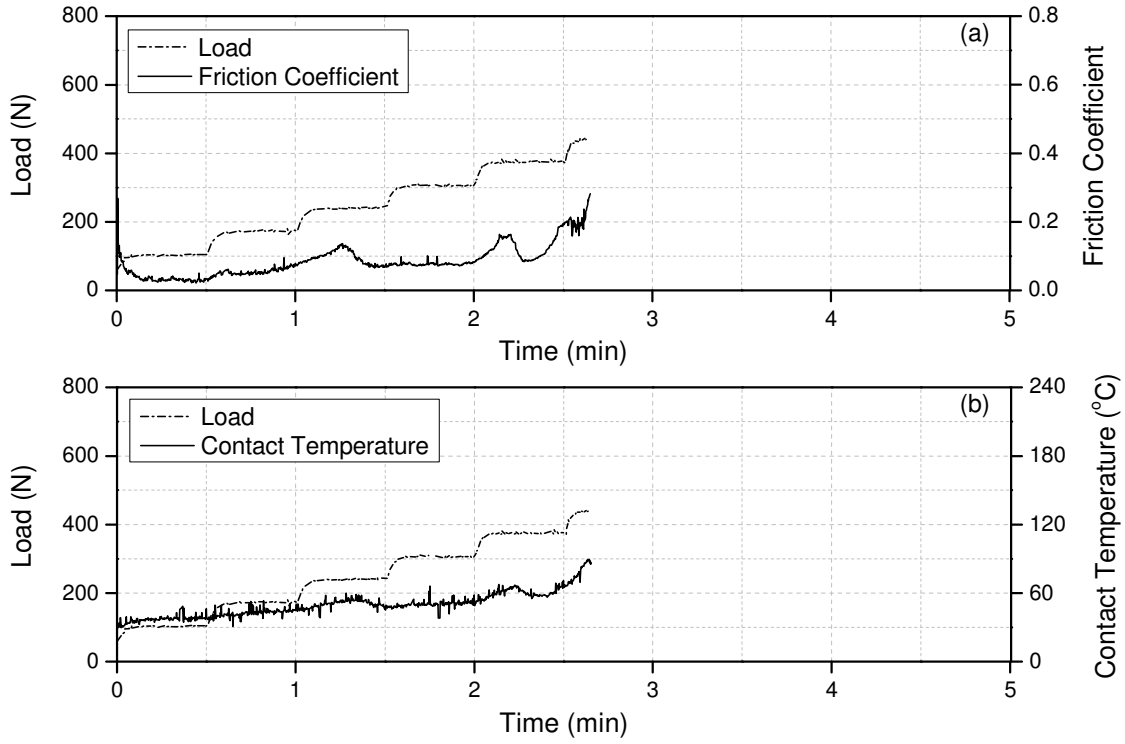

Figure 4.18: Scuffing performance of texture pattern A2 at R-134a chamber pressure of 0.17 MPa (25 psi)

In comparison to scuffing resistance of 400 N in R-134a, texture pattern A2 failed at 600 N in the presence of R-1234 yf, as shown in Figure 4.19. The performance is similar to that of R-744 where the friction coefficient remained at 0.1 for most part until failure occurred at 600 N. R-1234yf is a new environmentally friendly refrigerant being introduced into the market. Compared to R-134a which is widely used these days, the performance of R-1234yf is better. Table 4.1 summarizes the scuffing resistance of texture pattern A2 in the presence of different refrigerants.

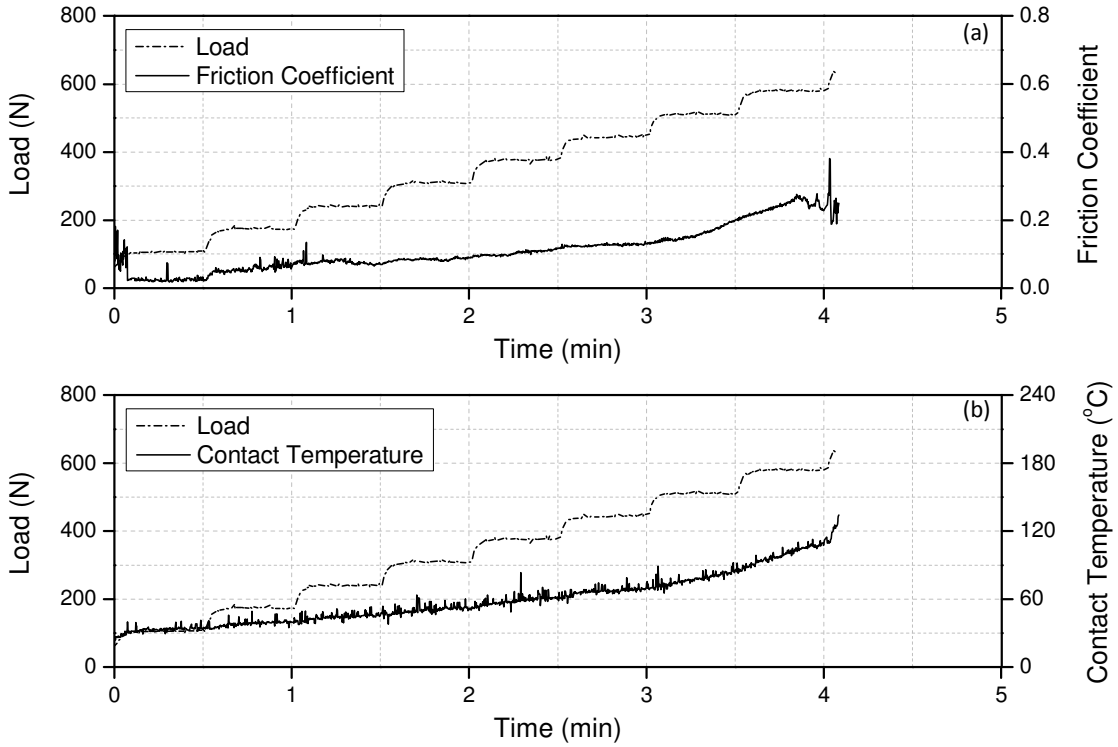

Figure 4.19: Scuffing performance of texture pattern A2 at R-1234yf chamber pressure of 0.17 MPa (25 psi)

Table 4.1: Scuffing resistance of texture pattern A2 in the presence of different refrigerants

Refrigerant	Scuffing Load (N)
R-744	600
R-134a	400
R-1234yf	600

4.4 Summary and Conclusions

Step-loading tests gave an indication of the maximum load carrying capacity of the different interfaces under specific testing conditions. It is important to remember that all the tests were conducted in starved lubrication condition, which was achieved by adding a very small of lubricant, PAG in this case, directly at the interface. The scuffing

performance was determined by the lubricant storage ability of the micro-dimples and also by the material pile-ups around the micro-dimples. The material pile-ups or bulges got polished during the course of testing to generate wear debris. As the test continued, the interface ran out of lubricant pushing the interface to more aggressive conditions. The mode of failure was strongly adhesive in nature as determined by the optical images of the pins and disks and by the surface profile measurements of the disks after the testing. For the textured surfaces, it was a case of clogging the micro-dimples by the wear debris which eventually led to the scuffing failure.

Few tests were done by increasing the chamber pressure of R-744 and results were positive. Tests conducted with different refrigerants highlighted the importance of the refrigerant type. Since R-1234yf is being touted as a replacement to R-134a, it was encouraging to find that its performance was better than R-134a. More comprehensive tests need to be done to fully understand the various parameters such as texture geometry, area density, chamber pressure and refrigerant type on the scuffing performance.

CHAPTER 5: CONCLUSION AND FUTURE WORK

5.1 Summary of Thesis

To remain competitive, compressor manufacturers have to ensure that their compressors become more energy efficient and durable. With the environmental regulations getting stricter, new refrigerants are being introduced which are environmentally friendly such as R-744 (CO_2). There is a need to fully understand the characteristics of these new refrigerants and their impact, not only on the thermodynamic performance of the compressors but also on the durability of the compressor components. In a compressor, several critical interfaces exist and the mechanical performance of the compressor depends on how good the interfaces are. Thus, there is a need to investigate and understand the tribological aspects of compressors. Compressor tribology consists of investigations in friction, wear, lubrication and scuffing of critical compressor components. Several approaches exist and one of them is laboratory scale tribo-testing by simulating realistic compressor operating conditions. The Tribology Laboratory at the University of Illinois has been actively involved in this area.

With the introduction of new materials, refrigerants and lubricants, the immediate impact is on the load limit, friction and wear performance of critical tribo-contacts inside the compressor. In the past, numerous studies have been conducted by the Tribology Laboratory at the University of Illinois, including in the area of surface engineering. In particular, different types of hard coatings such as DLC, WC/C and soft coatings such as PEEK/PTFE based polymeric coatings have been extensively worked on. In this thesis, an attempt has been made to apply a well known surface engineering approach called

surface texturing, for use in compressor surfaces. Surface texturing has been extensively used in other mechanical systems such as piston/cylinder liners in engines, mechanical face seals, hydrodynamic bearings etc. Surface texturing has been found to be successful in different lubrication regimes and different operating conditions of loads and speeds. However, till date, surface texturing has not been realized for use in compressor surfaces with an aim to improve the tribological performance of critical tribo-contacts inside the compressor.

The three key parameters of textured surfaces are the diameter, depth and the area density of the micro-dimples. Texturing was performed by an external company, MLPC Inc. by the process of laser surface texturing (LST). LST is the most popular and widely used method to prepare the textures on the surface as it is versatile and easily controllable. Three type of texture geometries and two types of area density were selected for this study. Since, no other work on texturing has been reported in the open literature for compressor applications, the choice of these texture patterns was mainly based on literature review on surface textures for other mechanical systems and cost considerations for preparing these textures. The "as-received" texture patterns were characterized both qualitatively and quantitatively. Qualitative characterization was done by means of optical images and high magnification SEM images. Quantitative characterization involved measuring the surface profiles of the texture patterns using a contact surface profilometer. Material pile-ups or bulges were observed around the micro-dimples which were a result of the melting of the material and solidification. Using the contact surface profilometer, the profiles of the material pile-ups were also measured.

Unlubricated experiments were performed first, and texturing was found to be much worse than the baseline untextured surfaces, failing instantly as the test was initiated. Moving forward, all other experiments were done with a very small amount of lubricant applied directly at the interface before the test started. Three types of experiments were conducted: Wear experiments, Durability experiments and Scuffing experiments.

Wear experiments were designed to understand the feasibility of using textures on compressor surfaces under realistic operating conditions, through experimental protocols established by the Tribology Laboratory at the University of Illinois. All the texture patterns were tested in the presence of refrigerant R-744 and small amount of lubricant at the interface. To further understand the role of operating parameters such as sliding speeds, lubricant type and refrigerants, representative wear experiments were also conducted with selected texture patterns. Three types of sliding speeds, three types of lubricants namely PAG, POE and Mineral oil and three types of refrigerants namely R-744, R-134a and R-1234yf were investigated.

The role of the durability experiments was to investigate the long term performance of the textured surfaces under extended periods of operation. A typical durability experiment lasted three hours (or 25,920 meters of sliding distance) in comparison to the wear experiments which were run for one hour (or 8,640 meters of sliding distance). All durability experiments were conducted in the presence of refrigerant R-744.

Scuffing experiments with step-loading were also done under starved lubrication conditions to understand the effect of texturing on the maximum load carrying capacity

of the interfaces. All the texture patterns were tested and compared against an untextured surface. Scuffing experiments were carried out in the presence of refrigerant R-744 at two different chamber pressures to study the effect of chamber pressure.

To better understand the tribological performance, characterization of the pins and disks were done after the tribo-testing. Optical images of the pins and disks served as a quick way to ascertain the extent of wear. High magnification SEM images were also taken to get a better idea of the morphological changes during the course of testing. Quantification of the extent of the wear was done by measuring the surface profiles of the micro-dimples of the various texture patterns and comparing against those before the test. The wear depth on the counter gray cast iron disk was also measured with the help of a surface contact profilometer. In a compressor environment, the lubricant-refrigerant relationship is very significant and in many cases leads to chemical changes such as formation of beneficial compounds at the interface. Thus, chemical changes at the interface were also investigated using EDS.

5.2 Primary Conclusions

Based on the research on surface texturing for use in compressor surfaces carried out in this work, several conclusions can be made. They have been itemized as below:

(1) Surface textures can be successfully applied to compressor surfaces, as shown through pin-on-disk testing at realistic compressor operating conditions in the presence of R-744. In comparison to the baseline untextured surfaces, significant improvement in performance was achieved under starved lubrication conditions.

While untextured surfaces failed early, textured surfaces could be successfully operated under identical conditions for extended periods of time without failure. However, textured surfaces failed instantly under unlubricated conditions and the failure was attributed to the material pile-ups or bulges around the micro-dimples causing an increase in localized pressure and generation of wear debris during the testing.

(2) Surface texturing was found to provide advantages under different operating conditions, as detailed below:

(a) At lower sliding speeds, the untextured surfaces did not fail and displayed similar friction performance as textured surfaces while at higher sliding speeds, the difference in performance was clear with the textured surfaces operating successfully compared to the untextured surfaces which failed.

(b) The tribological benefits were found to be largely dependent on the textures and not on the type of lubricant used for the study. An inexpensive mineral oil showed similar performance as advanced specialized compressor lubricants such as PAG and POE.

(c) The performance was linked to the refrigerant environment used. The refrigerant environment had a strong influence on the performance of the untextured surfaces, while the performance of the textured surfaces was largely independent of the refrigerant. However, the presence of refrigerant environment was found to be significant. Tests done in ambient air that although the textured surfaces

survived the testing longer than the untextured surfaces, the overall performance was poorer as compared to that in the presence of refrigerant environment.

(3) Wear on the pins and disks were not significant. For the texture patterns, the mass loss of the pins was negligible and only polishing/flattening of the material pile-ups around the micro-dimples was observed through optical and high magnification SEM images. Thus, wear quantification of the texture patterns was done by means of a simple geometric wear calculation model and the wear rate was found to be extremely small ($< 10^{-8}$ mm^3/Nm). The wear track on the counter gray cast iron disks was also not measurable and only mild burnishing was noticed.

(4) The EDS spectra of some of the textured surfaces were compared to that of untested textured surfaces. The results showed that no chemical changes occurred at the interface, thus confirming mechanical rubbing action as the only mechanism of the polishing/flattening of the material pile-ups around the micro-dimples. SEM images further highlighted the role of micro-dimples in trapping of wear debris.

(5) Scuffing experiments established the role of micro-dimples as reservoirs of lubricants. Deeper micro-dimples could carry larger volume of lubricant and helped in increasing the scuffing resistance of the interfaces. SEM images showed the clogging of the micro-dimples leading to adhesive failure of the interfaces.

5.3 Future Work

The work done in this thesis is a first of its kind study in investigating the feasibility of using surface texturing for compressor surfaces. Based on the research conducted, the tribological benefits of textured surfaces compared to untextured surfaces in compressor realistic operating conditions have been realized. However, it is only a starting point and many useful research investigations could possibly stem out from the work presented in this thesis. Some ideas and directions for future work in this area are presented below:

(1) In this work, the critical role of the material pile-ups around the micro-dimples has been observed. Even under extended periods of testing, the pile-ups did not completely wear out and supported the load. However, more studies such as nano-mechanical properties measurements need to be done to clearly identify and understand their effect on the tribological behavior. It is particularly significant if laser surface texturing (LST) is used as the texturing method. Laser texturing causes sublimation, melting and vaporization of the material resulting in the textures. Thus it is possible that the microstructure of the material near the micro-dimples is altered causing a change in the mechanical properties such as hardness and elastic modulus, which can have an effect on the tribological behavior. Some preliminary nano-indentation measurements were done (see Appendix) on the as-received gray cast iron texture pattern C1. The hardness and reduced elastic modulus of the flat area between the micro-dimples was 9 GPa and 153 GPa respectively. In comparison, measurements were done on the top of the material pile-ups and yielded values of 13

GPa and 175 GPa. The effect on laser surface texturing in altering the surface nano-mechanical properties is evident. However, more detailed analysis needs to be done to establish clearly the changes in the nano-mechanical properties and their subsequent impact on the tribological performance.

(2) Although the increased nano-mechanical properties of the material pile-ups would mean that the surfaces are more difficult to wear out, the role of the pile-ups in wear debris generation is also critical. In literature, to avoid this issue, most researchers polish the surfaces after texturing to remove the material pile-ups. In this work, our focus was on as-received textured surfaces without polishing. This is because polishing adds another process step and hence additional cost for the compressor manufacturer when they scale up this technology and also because of an interest to understand the role of these material pile-ups on the tribological behavior. Additionally, if the micro-dimples are shallow then the polishing process, if not controllable, could well remove the micro-dimples. However, some preliminary tests were conducted with some polished texture patterns (see Appendix). The main hindrance was to be able to produce a polished surface without inducing curvature during manual polishing. Although the results were not comprehensive, they indicate that under compressor realistic operating conditions of starved lubrication, polished textured patterns performed similarly to untextured surfaces. This encourages further understanding of the tribological performance with polished textured surfaces in the future. Prior to the tribo-testing, a robust method for polishing the surface without inducing any curvature should be established.

(3) It is now established that textured surfaces can be successfully used under realistic compressor operating conditions. Typically, compressors operate under boundary/mixed/starved lubrication. Under such starved lubrication conditions, it is difficult to model the tribological behavior and most researchers rely on experimental approach. The next step should be optimization of the texture geometries to improve the tribological performance by a careful design of experiments.

(4) Preliminary studies indicated the positive effect of R-744 chamber pressure on the scuffing resistance. More extensive research needs to be done to conclusively establish this behavior.

(5) As surface texturing technology is getting popular, more innovative applications including combination with other existing surface engineering methods are being explored by many researchers. Tribological performance can be investigated by applying a thin layer of hard coating such as DLC or WC/C on top of the textures and/or by filling the micro-dimples with powders with good tribological properties such as MoS_2, graphite or polymeric powders.

BIBLIOGRAPHY

[1] E.E.Nunez "Scuffing and wear of engineering materials under different lubrication regimes in the presence of environmentally friendly refrigerants" PhD Thesis, University of Illinois at Urbana Champaign 2010

[2] T.A.Solzak and A.A.Polycarpou (2010) "Tribology of hard protective coatings under realistic operating conditions for use in oilless piston-type and swash-plate compressors" Tribology Transactions, 53, 3 pp 319-328

[3] J.M.Calm (2008) "The next generation of refrigerants – historical review, considerations, and outlook" International Journal of Refrigeration, 31, pp 1123-1133

[4] E.E.Nunez, N.G.Demas, K.Polychronopoulou and A.A.Polycarpou (2010) "Comparative scuffing performance and chemical analysis of metallic surfaces for air-conditioning compressors in the presence of environmentally friendly CO2 refrigerant" Wear, 268, pp 668-676

[5] E.E.Nunez, K.Polychronopoulou and A.A.Polycarpou (2010) "Lubricity effect of carbon dioxide used as an environmentally friendly refrigerant in air-conditioning and refrigeration compressors" Wear, 270, pp 46-56

[6] T.Fannin (1989) "Compressor lubrication" Proceedings of the Institute of Refrigeration, 86, pp 41-46

[7] B. Hubacher, and E. Groll (2002) "Measurement of performance of carbon dioxide compressors" Air Conditioning Refrigeration and Technology Institute, ARTI-21 R/611-10070-01

[8] M.H.Kim, J.Pettersen, and C.W.Bullard (2004) "Fundamental process and systems design issues in CO2 vapor compression systems" Progress in Energy and Combustion Science, 30, pp 119-174

[9] A.Yokoseki (2006) "Solubility correlation and phase behaviors of carbon dioxide and lubricant oil mixtures" Applied Energy, 84, No. 2, pp 159-175

[10] T.A.Solzak and A.A.Polycarpou (2006) “Triboogy of WC/C coatings for use in oil-less piston-type compressors” Surface and Coatings Technology, 201, pp 4260-4265

[11] E.E.Nunez, N.G.Demas, K.Polychronopoulou and A.A.Polycarpou (2008) “Tribological study comparing PAG and POE lubricants used in air-conditioning compressors under the presence of CO_2” Tribology Transactions, 51, pp 790-797

[12] J.D.B.De Mello, R.Binder, N.G.Demas and A.A.Polycarpou (2009) “Effect of the actual environment present in hermetic compressors on the tribological behavior of a Si-rich multifunctional DLC coating” Wear, 267, pp 907-915

[13] N.G.Demas and A.A.Polycarpou (2008) “Tribological performance of PTFE-based coatings for air-conditioning compressors” Surface and Coatings Technology, 203, pp 307-316

[14] E.E.Nunez, S.M.Yeo, K.Polychronopoulou and A.A.Polycarpou (2011) “Tribological study of high bearing blended polymer-based coatings for air-conditioning and refrigeration compressors” Surface and Coatings Technology, 205, pp 2994-3005

[15] D.Dascalescu, K.Polychronopoulou and A.A.Polycarpou (2009) “The significance of tribochemistry on the performance of PTFE-based coatings in CO_2 refrigerant environment” Surface and Coatings Technology, 204, pp 319-329

[16] I.Etsion (2004) “Improving tribological performance of mechanical components by laser surface texturing” Tribology Letters, 17, pp 733-737

[17] L.M.Vilhena, M.Sedlacek, B.Podgornik, J.Vizintin, A.Babnik and J.Mozina (2009) “Surface texturing by pulsed Nd:YAG laser” Tribology International, 42, pp 1496-1504

[18] Y.Kligerman, I.Etsion and A.Shinkarenko (2005) “Improving tribological performance of piston rings by partial surface texturing” ASME Journal of Tribology, 127, pp 632-638

[19] D.Yan, N.Qu, H.Li and X.Wang (2010) “Significance of dimple parameters on the friction of sliding surfaces investigated by orthogonal experiments” Tribology Transactions, 53, pp 703-712

[20] T.Nanbu, N.Ren, Y.Yasuda, D.Zhu and Q.J.Wang (2008) “Micro-textures in concentrated conformal-contact lubrication - effects of texture bottom shape and surface relative motion” Tribology Letters, 29, pp 241-252

[21] K.Dou, E.T.Knobbe, R.L.Parkhill and Y.Wang (2000) “Surface texturing of aluminum alloy 2024-T73 via femto- and nanosecond pulse excimer laser irradiation” IEEE Journal of Selected Topics in Quantum Electronics, 6, pp 689-695

[22] C.Vincent, G.Monteil, T.Barriere and J.C.Gelin (2008) “Control of quality of laser surface texturing” Microsystems Technologies, 14, pp 1553-1557

[23] A.Greco, S.Raphaelson, K.Ehmann, Q.J.Wang and C.Lin (2009) “Surface texturing of tribological interfaces using the vibromechanical texturing method” Journal of Manufacturing Science and Engineering, 131

[24] U.Pettersson and S.Jacobson (2006) “Tribological texturing of steel surfaces with a novel diamond embossing tool technique” Tribology International, 39, pp 695-700

[25] A.H.Cannon and W.P.King (2009) “Casting metal microstructures from a flexible and reusable mold” Journal of Micromechanics and Microengineering, 19

[26] A.H.Cannon and W.P.King (2010) “Microstructured metal molds fabricated via investment casting” Journal of Micromechanics and Microengineering, 20

[27] A.Moshkovith, V.Perfiliev, D.Gindin, N.Parkansky, R.Boxman and L.Rapoport (2007) “Surface texturing using pulsed air arc treatment” Wear, 263, pp 1467-1469

[28] D.B.Hamilton, A.J.Walowit and C.M.Allen (1966) “A theory of lubrication by microasperities” ASME Journal of Basic Engineering, 88, pp 177-185

[29] I.Etsion and L.Burstein (1996) “A model for mechanical seals with regular microsurface structure” Tribology Transactions, 39, pp 677-683

[30] I.Etsion, G.Halperin and Y.Greenberg (1997) “Increasing mechanical seal life with laser-textured seal faces” 15th International Conference on Fluid Sealing BHR Group, Maastricht

[31] I.Etsion, Y.Kligerman and G.Halperin (1999) “Analytical and experimental investigations of laser-textured mechanical seal faces” Tribology Transactions, 42, pp 511-516

[32] I.Etsion (2000) “Improving tribological performance of mechanical seals by laser surface texturing” Proceedings of the 17th International Pump Users Symposium

[33] I.Etsion (2005) “State of art in laser surface texturing” ASME Journal of Tribology,127

[34] A.Ronen, I.Etsion and Y.Kligerman (2001) “Friction reducing surface texturing in reciprocating automotive components” Tribology Transactions, 44, pp 359-366

[35] G.Ryk, Y.Kligerman and I.Etsion (2002) “Experimental investigation of laser surface texturing for reciprocating automotive components” Tribology Transactions, 45, pp 444-449

[36] G.Ryk and I.Etsion (2006) “Testing piston rings with partial laser surface texturing for friction reduction” Wear, 261, pp 792-796

[37] M.Nakano, A.Korenaga, A.Korenaga, K.Miyake, T.Murakami, Y.Ando, H.Usami and S.Sasaki (2007) “Applying micro-texture to cast iron surfaces to reduce the friction coefficient under lubricated conditions” Tribology Letters, 28, pp 131-137

[38] W.Yi and X.Dang-Sheng (2008) “The effect of laser surface texturing on frictional performance of face seal” Journal of Materials Processing Technology, 197, pp 96-100

[39] M.Wakuda, Y.Yamauchi, S.Kanzaki and Y.Yasuda (2003) “Effect of surface texturing on friction reduction between ceramic and steel materials under lubricated sliding contact” Wear, 254, pp 356-363

[40] A.Borghi, E.Gualtieri, D.Marchetto, L.Moretti and S.Valeri (2008) “Tribological effects of surface texturing on nitriding steel for high-performance engine applications” Wear, 265, pp 1046-1051

[41] S.J.Hupp and D.P.Hart (2006) “Defining the mechanisms by which surface texturing reduces friction” Proceedings of the International Joint Tribology Conference, San Antonio, TX, USA

[42] A.Kovalchenko, O.Ajayi, A.Erdemir, G.Fenske and I.Etsion (2005) “The effect of laser surface texturing on transitions in lubrication regimes during unidirectional sliding contact” Tribology International, 38, pp 219-225

[43] W.Koszela, L.Galda, A.Dzierwa and P.Pawlus (2010) “The effect of surface texturing on seizure resistance of steel-bronze assembly” Tribology International, 43, pp 1933-1942

[44] L.Galda, A.Dzierwa, J.Sep and P.Pawlus (2010) “The effects of oil pockets shape and distribution on seizure resistance in lubricated sliding” Tribology Letters, 37, pp 301-311

[45] M.Varenberg, G.Halperin and I.Etsion (2002) “Different aspects of the role of the wear debris in fretting wear” Wear, 252, pp 902-910

[46] A.Volchok, G.Halperin and I.Etsion (2002) “The effect of surface regular micro-topography on fretting fatigue life” Wear, 253, pp 509-515

[47] N.G.Demas and A.A.Polycarpou (2006) “Ultra high pressure tribometer for testing CO_2 refrigerant at chamber pressures up to 2000 psi to simulate compressor conditions” Tribology Transactions, 49, pp 291-296

[48] N.G.Demas, A.A.Polycarpou and T.F.Conry (2005) “Tribological studies on scuffing due to the influence of CO_2 used as a refrigerant in compressors” Tribology Transactions, 48, pp 336-342

[49] N.G.Demas, J.Zhang, A.A.Polycarpou and J. Economy (2008) “Tribological characterization of aromatic thermosetting copolyster-PTFE blends in air conditioning compressor environment” Tribology Letters, 29, pp 253-258

[50] A.Y.Suh, J.J.Patel, A.A.Polycarpou and T.F.Conry (2006) “Scuffing of cast iron and Al390-T6 materials used in compressor applications” Wear, 260, pp 735-744

[51] T.K.Sheiretov, H.K.Yoon and C.Cusano (1998) “Scuffing under dry sliding conditions. Part I: experimental studies” Tribology Transactions, 41 No. 4, pp 435–446

[52] T.K.Sheiretov, H.K.Yoon and C.Cusano (1998) “Scuffing under dry sliding conditions. Part II: experimental studies” Tribology Transactions, 41 No. 4, pp 447–458

APPENDIX A: PRELIMINARY EXPERIMENTS WITH POLISHED TEXTURE PATTERNS

A.1 Polishing process

The texture patterns were polished using grit paper P2400 for 1 minute followed by P4000 grit paper for 1 minute with the application of water. This was done at the sample preparation room at the Materials Research Laboratory (MRL) at UIUC. Figure A.1 shows the surface profile measurements performed on texture pattern A1 after the polishing process. Measurements were done along and perpendicular to the original machining marks on the pin surface. It should be noted that the polishing was done manually and so it was extremely difficult to control issues such as flatness of the texture pattern surface. As can be seen in Figure A.1, the manual polishing resulted in slight curvature towards the outside edges of the pin surface. The inaccuracy in the flatness of the pin surface is of the order of 4 - 5 μm. This is particularly significant for shallow micro-dimples, such as texture pattern C1 which has micro-dimples of depth 4 μm, as such a manual polishing could possibly remove them.

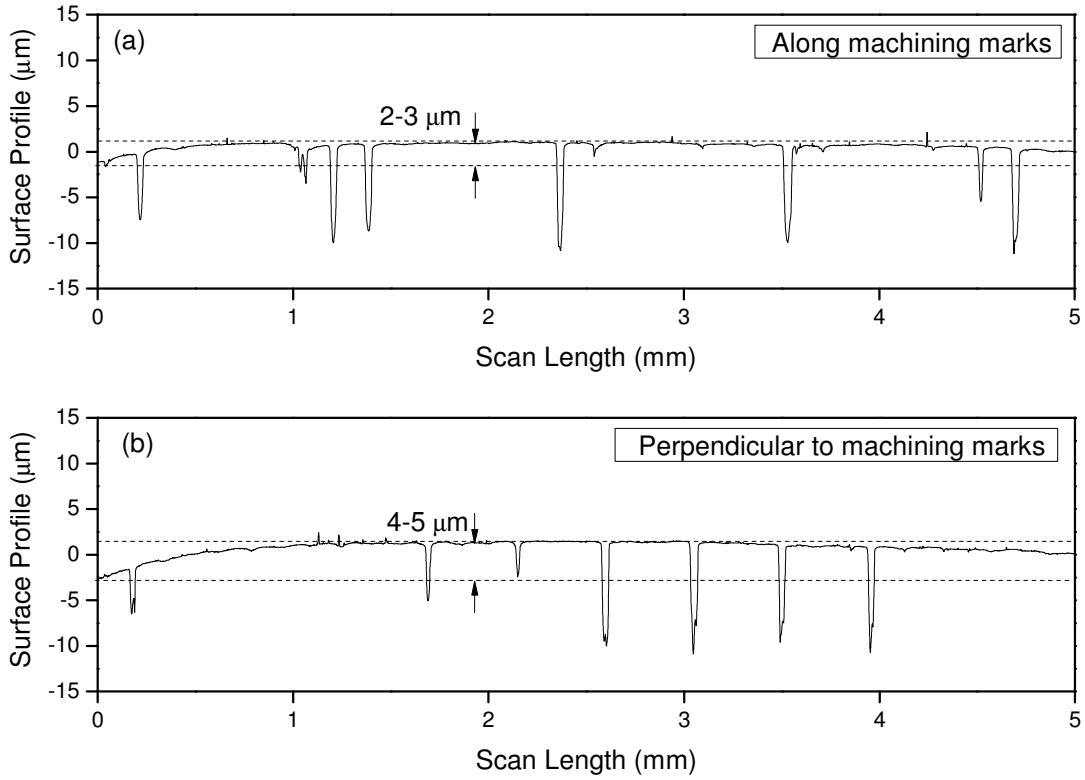

Figure A.1: Surface profile measurements of texture pattern A1 (a) along machining marks and (b) perpendicular to machining marks

A.2 Preliminary results

Figure A.2 compares the performance between an untextured surface and texture pattern A1 (as received and polished). All tests were conducted at a normal load of 89 N, sliding speed of 2.4 m/s with 23 mg of PAG lubricant directly applied at the interface in the presence of refrigerant R-744 at a chamber pressure of 1.93 MPa.

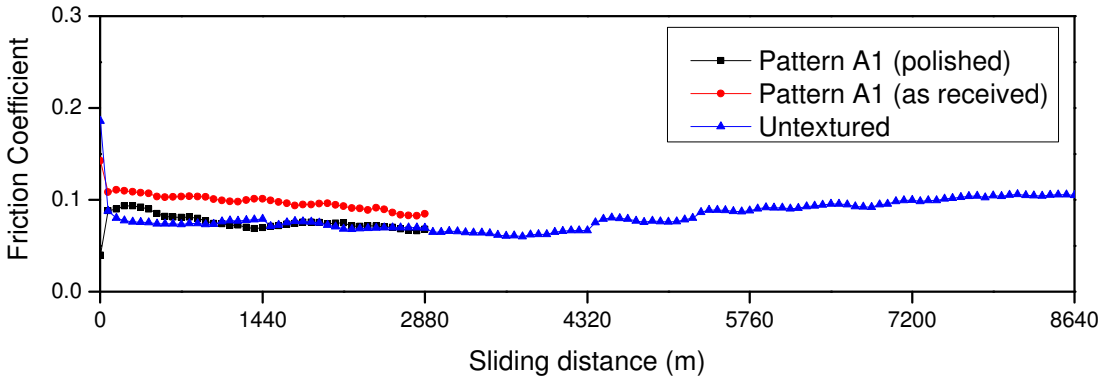

Figure A.2: Comparison of friction coefficient between an untextured surface and texture pattern A1 (polished and as received) tested a normal load of 89 N, sliding speed of 2.4 m/s with 23 mg of PAG lubricant applied directly at the interface in the presence of R-744 at a chamber pressure of 1.93 MPa

The texture pattern A1 was tested for only 20 minutes which corresponds to a sliding distance of 2,880 meters. The friction coefficient of the polished texture pattern is similar to the untextured surface and lower than that of the as-received texture pattern A1. Figure A.3 shows the optical images of as-received and polished texture pattern A1 and the counter surface disks after the test. Clearly, the disk tested with the as-received suffered more burnishing because of the material pile-ups or bulges around the micro-dimples. In the absence of those pile-ups, the disk suffered minimum damage. Note the patchy region on the surface of the polished texture pattern A1. This is possibly because the surface of the texture pattern was not flat after the polishing process and the patchy region indicates the area where contact occurred.

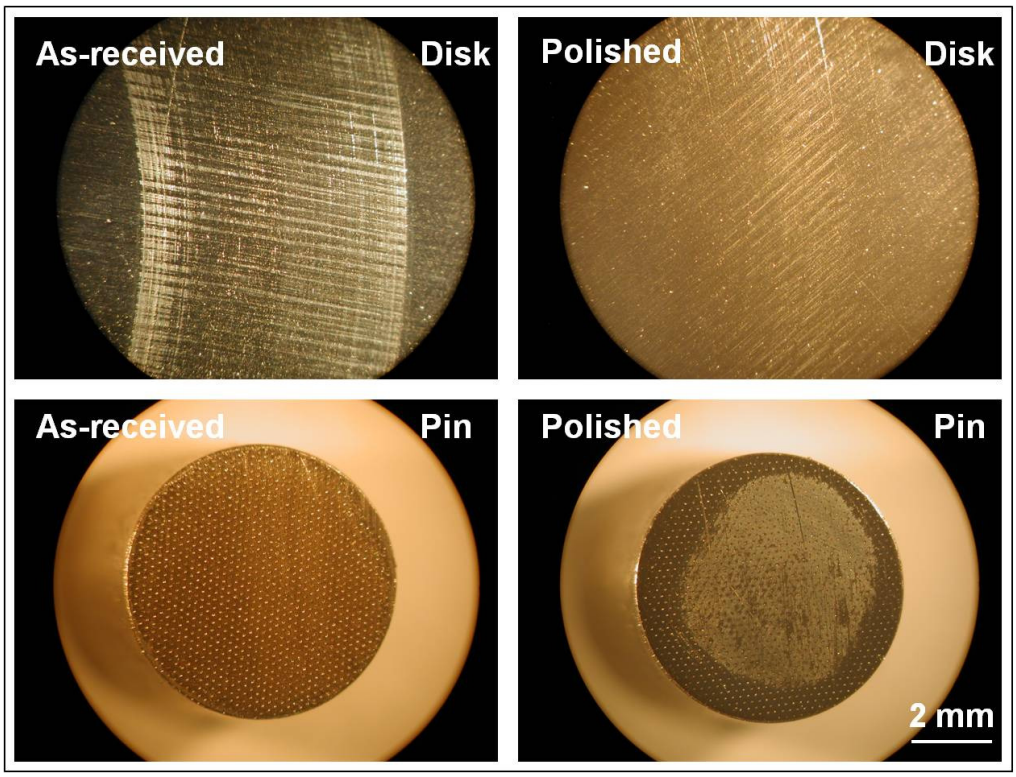

Figure A.3: Optical images of the as-received and polished texture pattern A1 and the counter surface disks after testing at a normal load of 89 N, sliding speed of 2.4 m/s with 23 mg of PAG lubricant applied directly at the interface in the presence of R-744 at a chamber pressure of 1.93 MPa

Figure A.4 compares the performance between an untextured surface and texture pattern B1 (as received and polished). All tests were conducted at a normal load of 178 N, sliding speed of 2.4 m/s with 23 mg of PAG lubricant directly applied at the interface in the presence of refrigerant R-744 at a chamber pressure of 1.93 MPa. Only the as-received texture pattern B1 survived the entire duration of testing of 60 mins, which corresponded to a sliding distance of 8,640 meters. It is interesting to note that the polished texture pattern B1 performed similar to the untextured surface, in that both surfaces failed early and could not survive the entire duration of testing.

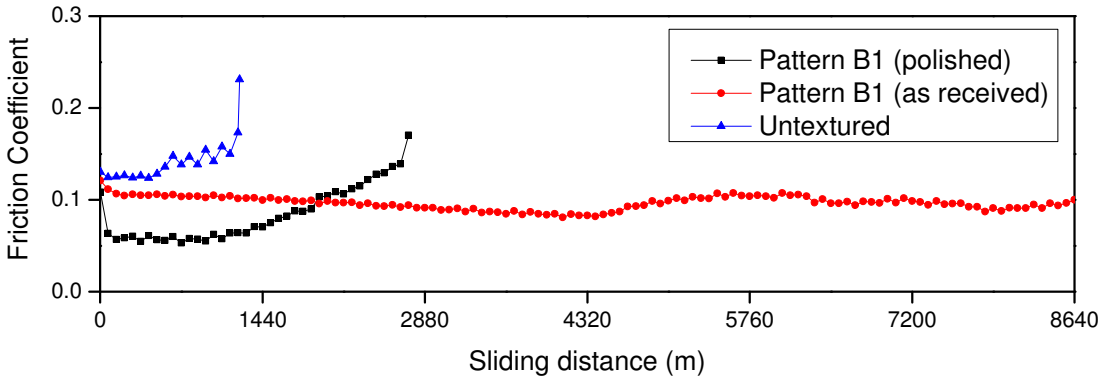

Figure A.4: Comparison of friction coefficient between an untextured surface and texture pattern B1 (polished and as received) tested a normal load of 178 N, sliding speed of 2.4 m/s with 23 mg of PAG lubricant applied directly at the interface in the presence of R-744 at a chamber pressure of 1.93 MPa

A.3 Future work

Preliminary results show that at lower loading conditions, polishing is beneficial. However, as the load is increased, polished texture pattern behaves similar to the untextured surface. This might be due to the fact that polishing removes the material pile-ups or bulges around the micro-dimples and thus the lubricant storage ability of the micro-dimples is reduced. The positive behavior of micro-dimples under starved lubrication conditions could also be due to the stable tribo-contact between the possibly harder material pile-ups on the pin and the disk. Thus, the removal of the pile-ups results in an overall poor tribological performance.

However, to be certain and conclusively identify the effect of the pile-ups additional experiments need to be performed. The pre-requisite of that, however, is to establish a robust polishing process without any issues of flatness.

APPENDIX B: PRELIMINARY STUDIES ON POLYMERIC COATINGS AT ELEVATED TEMPERATURES FOR COMPRESSOR APPLICATIONS

B.1 Introduction

Compressor manufacturers are investigating ways to make compressors more energy efficient and environmentally friendly while still pursuing longer life. The use of lubricant has been known to affect the thermodynamic performance. In the absence of liquid lubrication, the contacting and sliding interfaces would experience extreme conditions and thus new materials, surface treatments and coatings are being developed. In recent years, work has been done by the Tribology Laboratory at the University of Illinois on polymeric coatings for oil-less compressor applications. In order to increase efficiency, the operating temperatures of the compressors are being constantly pushed to higher values. In light of these developments, it is necessary to develop an understanding of the tribological behavior of these polymeric coatings at elevated temperatures.

B.2 Experimental

B.2.1 High Temperature Tribometer

Preliminary studies were conducted on PEEK based polymeric coatings using a High Temperature Tribometer (HTT), shown in Figure B.1. The HTT is a ball-on-disk tribometer capable of testing specimens up to 1000 °C. The HTT consists of a rotating/oscillating lower spindle on which the disk is mounted and an upper top holder which holds the ball by the help of a specially designed ball holder. Normal load is applied using the top holder in a closed loop manner via an electromagnet, which also

measures the in-situ normal and friction forces. The spindle assembly is a DC servo motor drive and is cooled by a re-circulating coolant system. Rotary speeds up to 1000 rpm can be achieved on the lower spindle. The output of the HTT is fed into a LabView® program which records the friction and normal load values. The test chamber consists of a gold reflecting insulating furnace which provides testing temperatures up to 1000 °C. The furnace is wound with an Inconel heating element and has a low thermal mass, rapid response and operates cleanly.

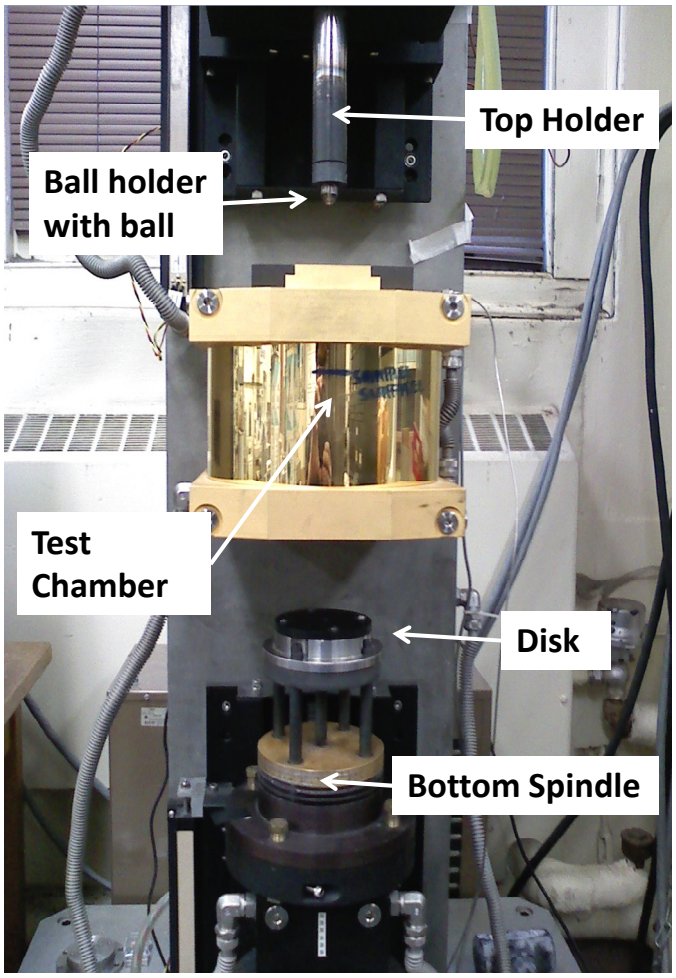

Figure B.1: High Temperature Tribometer for controlled tribological experiments up to 1000 °C

B.2.2 PEEK based polymeric coatings

For the purpose of this study PEEK/Ceramic coatings were used. The disks were coated with these coatings. Figure B.2 shows the SEM cross-section image of the coating and Table B.1 gives some relevant information about it.

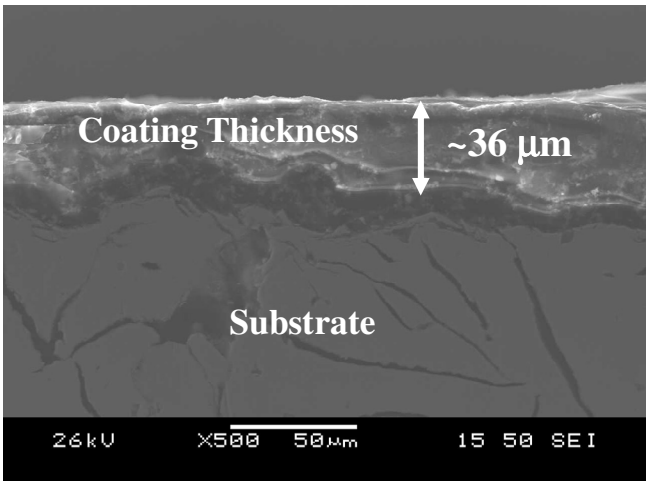

Figure B.2: SEM cross-section image of PEEK/Ceramic coating [14]

Table B.1: Some relevant information about the PEEK/Ceramic coating [14]

Standard Film Thickness (µm)	25-38
Reduced Modulus (GPa)	9.92 ± 1.91
In-use Temperature (°C)	260
Color	Beige Tan

B.2.3 Test Conditions

Experiments were conducted at a sliding speed of 0.4 m/s in a ball-on-disk configuration using coated disks and SAE 52100 steel balls of diameter 6.25 mm. A normal load of 10 N was used, which corresponds to a maximum hertzian contact pressure of 0.17 GPa. Tests were conducted at 25 °C and 100 °C. Test at each

temperature was done twice: one for 15 minutes duration and other for 30 minutes duration.

B.3 Results and Discussions

The purpose of conducting the tests at the same temperature but for two different durations was to understand the evolution of friction coefficient and wear performance over time. Figure B.3 and B.4 shows the friction coefficient values for tests conducted at 25°C for 15 mins and 30 mins respectively. The friction coefficient values in both cases were fairly stable and constant over the entire period of testing, indicating a stable sliding contact. It also suggests that no or little wear of the coating occurred.

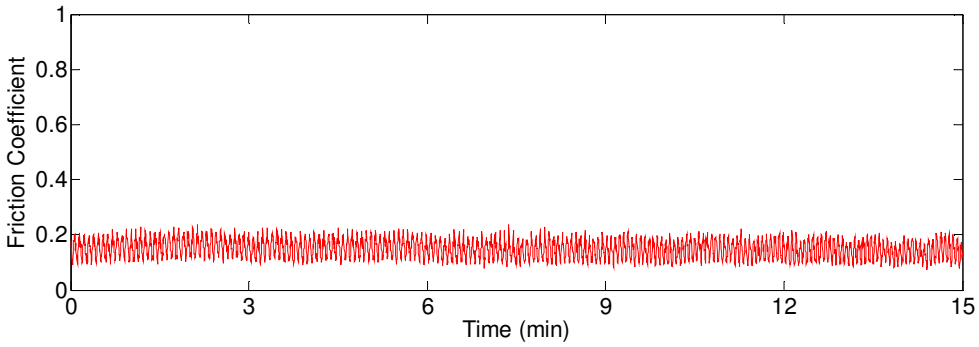

Figure B.3: Friction coefficient result for test done at 25 °C for a duration of 15 minutes

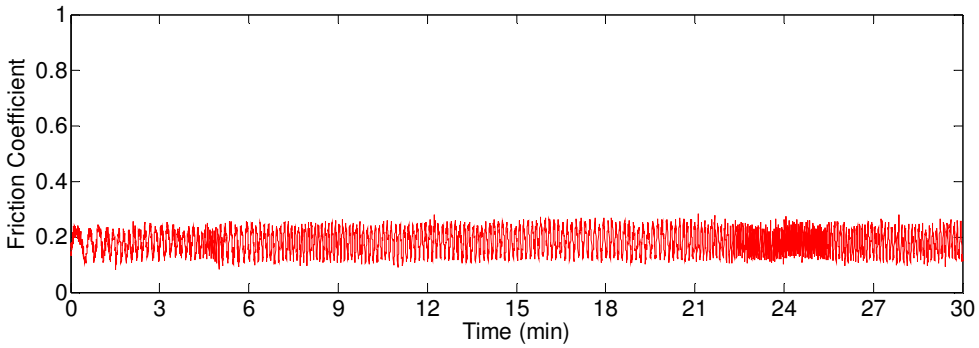

Figure B.4: Friction coefficient result for test done at 25 °C for a duration of 30 minutes

Figure B.5 shows the optical images of the coated disks after 15 mins and 30 mins of testing at 25 °C. It is clear that no significant wear occurred in case of the test done for 15 mins, while the wear track is more prominent for the test done at 30 mins. However, in both cases the wear is not significant and the coating is still intact.

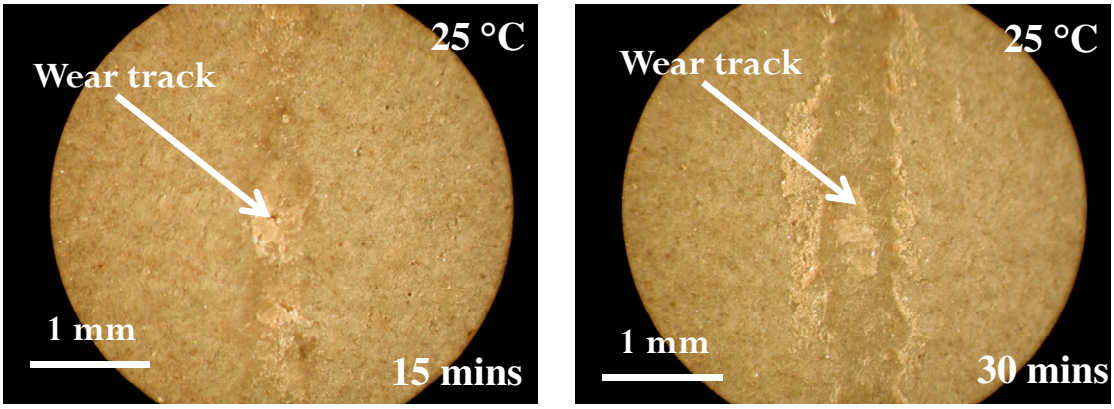

Figure B.5: Optical images of the coated disks showing the wear tracks after testing at 25° C

To quantify the wear depth, surface profile measurements were done with the help of Tencor® P-15 contact surface profilometer. Figure B.6 shows the surface profile measurements of the PEEK/Ceramic coated disks. No significant wear is seen, and only polishing of the surfaces is observed from the surface profile measurements. This is because, the coated disk itself is very rough and so it gets polished under the sliding action of the steel ball.

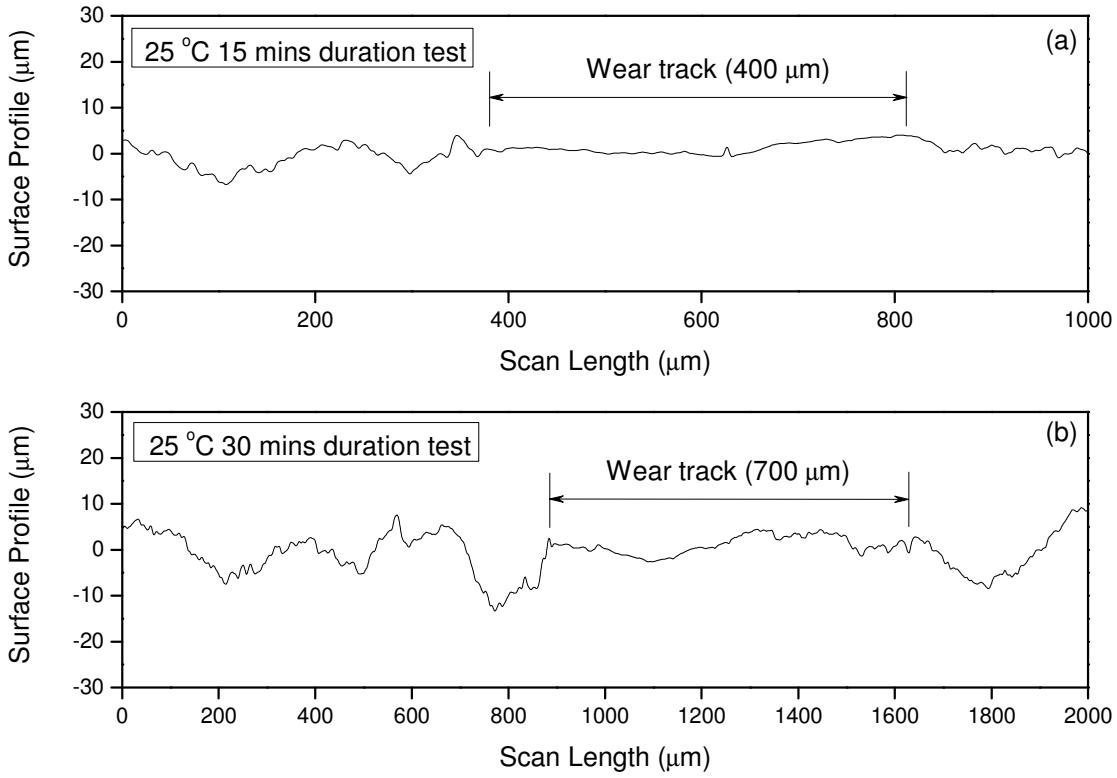

Figure B.6: Surface profile measurements of the coated disks after tests at 25 °C

Figure B.7 and B.8 shows the friction coefficient values for tests conducted at 100°C for 15 mins and 30 mins respectively. It can be seen from Figure B.7 that after roughly 6 minutes, the friction coefficient becomes erratic, suggesting significant wear of the coating. For the tests done for 30 minutes, the same event happens at around 9 minutes, although the overall friction behavior is more uniform.

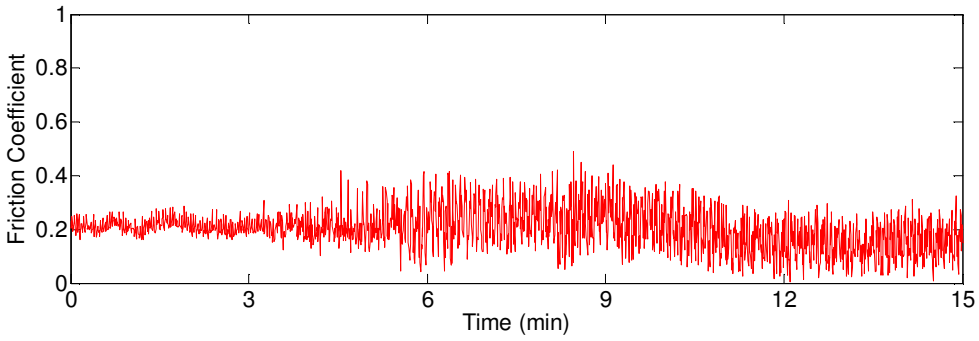

Figure B.7: Friction coefficient result for test done at 100 °C for a duration of 15 minutes

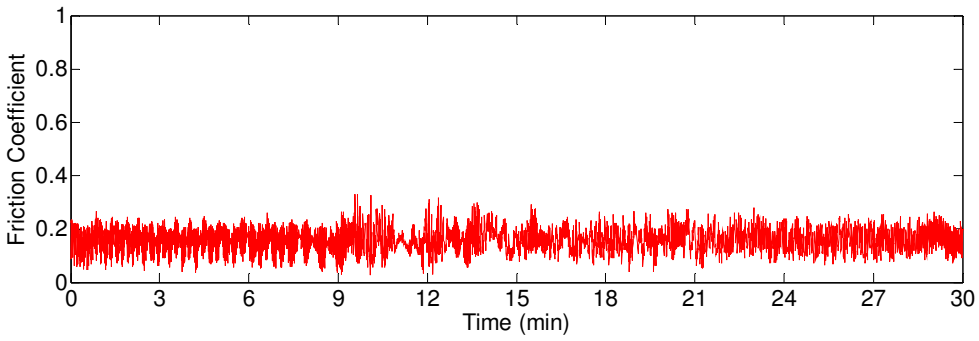

Figure B.8: Friction coefficient result for test done at 100 °C for a duration of 30 minutes

Figure B.9 shows the optical images of the coated disks after 15 mins and 30 mins of testing at 100 °C. It is evident that significant wear occurred. The difference in color of the wear track and the coating suggests that perhaps coating penetration occurred. This was further verified by surface profile measurements.

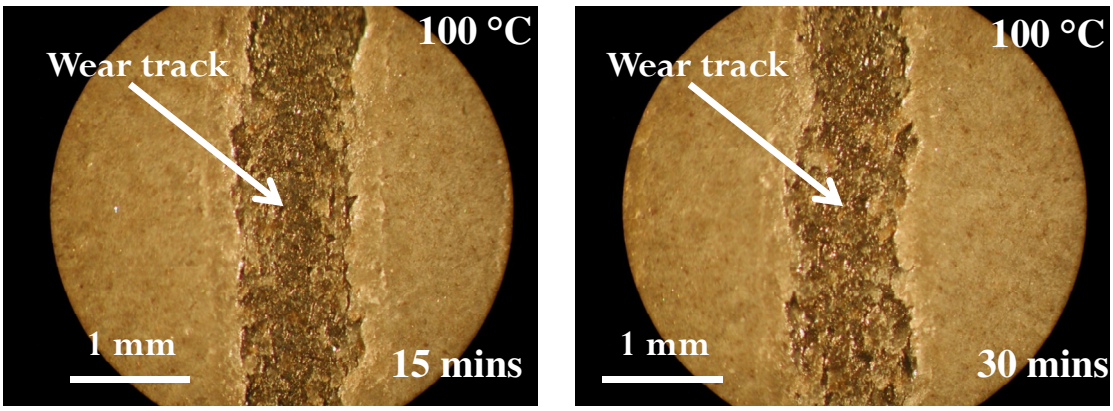

Figure B.9: Optical images of the coated disks showing the wear tracks after testing at 100° C

Figure B.10 shows the surface profile measurements of the PEEK/Ceramic coated disks. Significant wear is observed in both cases with wear depths approximately 45 µm. The thickness of the coating is typically 36 µm as shown in Figure B.2. This confirms that coating penetration occurred when tests were carried out at 100 °C.

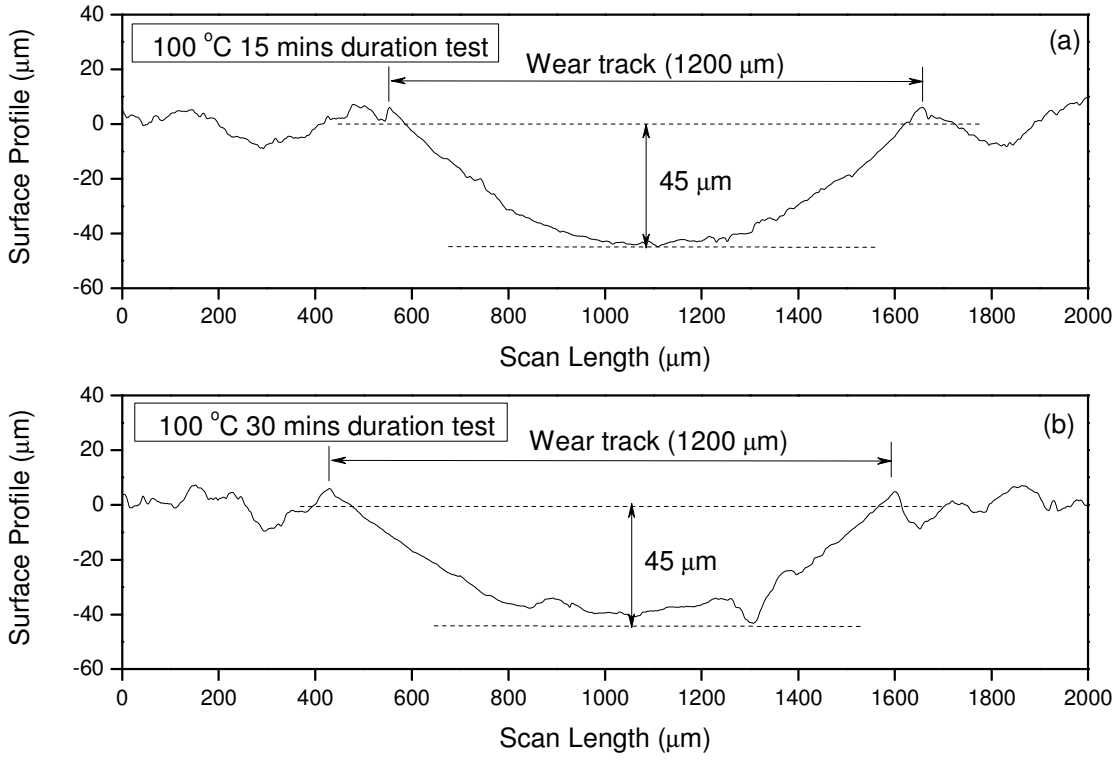

Figure B.10: Surface profile measurements of the coated disks after tests at 100 °C

It is interesting to note, however, that the wear track width and depth are similar when tests were done for 15 mins and 30 mins duration. It implies that most of the wear of the PEEK/Ceramic coating occurred during the initial period when tested at elevated temperatures. Also, the average friction coefficient for 30 mins test was slightly lower than that for the 15 mins test at 100 °C. This could be due to the beneficial effect of the wear debris, which has been shown to have the potential to act as a third-body solid lubricant [13], and needs further investigation.

B.4 Summary and Future Work

Preliminary tests were conducted on PEEK/Ceramic coated disks at two different temperatures. Two tests of different duration were done at each temperature to

understand the evolution of friction and wear performance with time. Figure B.11 compares the average friction coefficient for the two tests done at each temperature. In general, there is a trend of increase of friction coefficient with temperature.

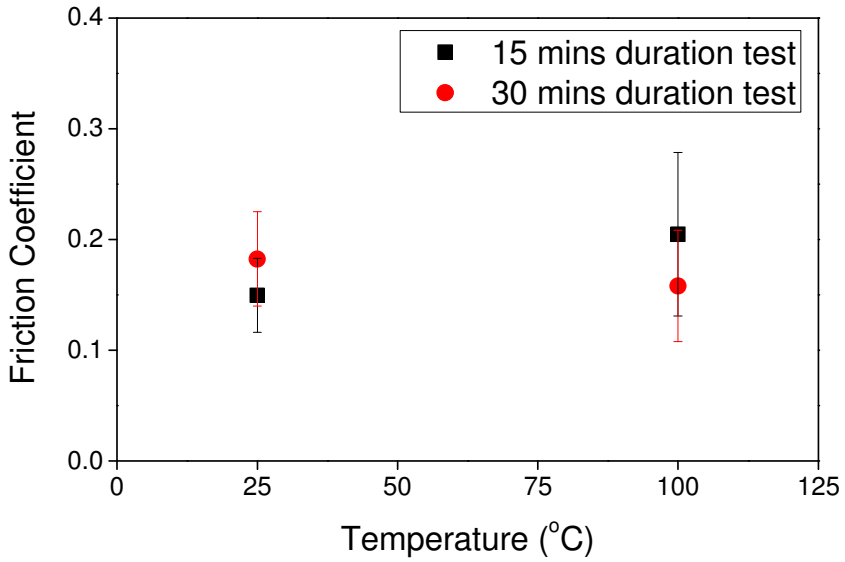

Figure B.11: Comparison of friction coefficient at two different temperatures

However, as can be seen, the friction coefficient for 30 mins test at 100 °C is lower than for the 15 mins test. Also, the wear performance was similar for both test durations. Thus, this tribological behavior needs further understanding.

The glass transition temperature of PEEK is 144 °C. So, to fully understand the behavior of these coatings at elevated temperatures, additional experiments are needed at higher temperatures such as 150 °C, 200 °C and 300 °C to. Also, to further characterize the morphological/chemical changes at the interface, SEM and EDS studies are necessary.